PHOTOCATALYTIC DESTRUCTION OF VOLATILE ORGANIC COMPOUNDS FROM THE OIL AND GAS INDUSTRY

OLUWATOSIN TOKODE

A thesis submitted in partial fulfilment of the requirements of the Robert Gordon University for the degree of Doctor of Philosophy.

April, 2014

DECLARATION

I declare that the work presented herein is mine except where otherwise acknowledged, and has not been submitted in any form for another degree or qualification at any other academic institution.

ACKNOWLEDGEMENT

My sincere appreciation goes to;

My loving and supportive parents for funding this PhD.

My supervisors: Prof. Linda A. Lawton, Prof. Peter K. J. Robertson and Dr Radhakrishna Prabhu for their supervision.

Allan MacPherson and Andy Ross for their technical expertise.

TABLE OF CONTENTS

GLOSSARY

List of Abbreviations

AOPs	Advanced Oxidation Processes
BTEX	Benzene, Toluene, Ethylbenzene, Xylene
CAD	Computer Aided Design/Drafting
CdS	Cadmium sulphide
CFC	Chlorofluorocarbons
CFD	Computational Fluid Dynamics
CH_4	Methane
CSTR	Continuous Stirred-Tank Reactor
CPI	Controlled Periodic Illumination
DEFRA	Department for Environment, Food and Rural Affairs
EED	Energetic Efficiency of Degradation
E_{EO}	Electrical Energy per Order
E_{EM}	Electrical Energy per Unit Mass
Eg	Energy gap
EHQ	European headquarters
EU	European Union
HCl	Hydrochloric acid
HQ	Headquarters
HNO_3	Nitric acid
IPPC	Integrated Pollution Prevention and Control

IR	Infrared
LED	Light Emitting Diode
meq	Monolayer Equivalent
MO	Methyl orange
NAEI	National Atmospheric Emissions Inventory
N_2O	Nitrous oxide
NMVOC	Non-Methane Volatile Organic Compound
NO_x	Oxides of Nitrogen
NPS	Nonpoint sources
O_3	Ozone
PID	Photo-ionization Detector
PIR	Photocatalytic Impeller Reactor
PMMA	Poly(methyl methacrylate)
PPM	Parts per Million
R&D	Research and Development
RB	Rose bengal
RNG	Renormalization Group
RPM	Revolutions per minute
SEM	Scanning Electron Microscopy
SEPA	Scottish Environment Protection Agency
SO_2	Sulphur dioxide
SOA	Secondary Organic Aerosol

SO_x	Oxides of Sulphur
SS	Steady State
TCE	Trichloroethene
TFA	Trifluoroacetic acid
TiO_2	Titanium dioxide
TOC	Total Organic Carbon
TTIP	Titanium(IV)isopropoxide
UK	United Kingdom
UV	Ultraviolet
VOCs	Volatile Organic Compounds
ZnO	Zinc oxide

List of Symbols

Å	Angstrom
β	Mass Transfer Coefficient
C	Concentration
C_e	Initial concentration
D_s	Diffusivity
Da_{II}	Dimensionless Damköhler number
e^-	Electron concentration
E_{bg}	Bandgap
e_{cb}^-	Conduction band electron
h^+	Hole concentration
$OH^\bullet$	Hydroxyl radical
hv	Photon energy
h_{vb}^+	Valence band hole
I_{avg}	Average intensity
I_{max}	Maximum intensity
k_1	Oxidation reaction rate constant
K_{ads}	Langmuir adsorption coefficient
k_r	Reaction rate constant
K_{CT}	Interfacial charge transfer rate
K_g	Light absorption rate constant
K_R	Electron-Hole recombination rate

k_t	Electron transfer rate constant
I	Incident light intensity
m	Order of light intensity
n	Order of reaction
n_A	Number of surface sites for MO
r_0	Initial reaction rate
r	Reaction rate
Re	Dimensionless Reynolds Number
Sc	Dimensionless Schmidt Number
Sh	Dimensionless Sherwood Number
t	Time
T_{off}	Dark Time
T_{on}	Light Time
T_{total}	Total time
n_A	Number of surface sites for hydroxyl/formate
ζ	Photonic efficiency
φ	Quantum yield
Ω_A	Surface fractional coverage by hydroxyl/formate ion
γ	Duty cycle

LIST OF FIGURES

LIST OF TABLES

SCIENTIFIC OUTPUT

Journal publications

O. Tokode, R. Prabhu, L.A. Lawton, P.K.J. Robertson. "*Effect of controlled periodic-based illumination on the photonic efficiency of photocatalytic degradation of methyl orange".* - Journal of Catalysis, 290 (2012), 138–142.

O. Tokode, R. Prabhu, L.A. Lawton, P.K.J. Robertson. "*The effect of pH on the photonic efficiency of the destruction of methyl orange under controlled under periodic illumination with UV-LED sources".* – Chemical Engineering Journal, 246 (2014) 337-342.

O. Tokode, R. Prabhu, L.A. Lawton, P.K.J. Robertson. "*Mathematical modelling of quantum yield enhancements of methyl orange photo-oxidation in aqueous TiO_2 suspensions under controlled periodic UV-LED illumination".* – Applied Catalysis B: Environmental. 156-157 (2014), 398-403.

O. Tokode, R. Prabhu, L.A. Lawton, P.K.J. Robertson. "*A photocatalytic impeller reactor for gas phase heterogeneous photocatalysis".* – Submitted for publication (Environ. Sci. Technol.)

O. Tokode, R. Prabhu, L.A. Lawton, P.K.J. Robertson. "*UV-LED sources for heterogeneous photocatalysis".* – Draft

Oral presentations

O. Tokode, R. Prabhu, L.A. Lawton, P.K.J. Robertson. "*Quantum yield enhancement for the photocatalytic treatment of wastewater using titanium dioxide"* presented at *Aberdeen Association of Civil Engineers (AACE)*, 2012.

O. Tokode, R. Prabhu, L.A. Lawton, P.K.J. Robertson. "*Effect of controlled periodic UV-LED illumination on the photo-oxidation of methyl orange"* presented at *Symposium on Fundamentals and Applications of Semiconductor Photocatalysis for Environmental Remediation,* Robert Gordon University, 2012.

P.K.J. Robertson, **O. Tokode**, R. Prabhu, L.A. Lawton. "*Photonic efficiency of UV-LED based photocatalytic purification of produced water from the oil and gas industry"* presented at *Optoelectronic Technologies for the Oil and Gas Industry Technical Meeting,* Hilton Tree Tops Hotel, Aberdeen, 2013.

Poster presentations

O. Tokode, R. Prabhu, L.A. Lawton, P.K.J. Robertson. "*Photochemical degradation of environmental pollutants under periodic UV illumination."* Presented at *5th Scottish Postgraduate Symposium on Environmental Analytical Chemistry*, University of Aberdeen, 2012.

O. Tokode, R. Prabhu, L.A. Lawton, P.K.J. Robertson. *"pH effects on photonic efficiency of TiO_2 photocatalysis under periodic UV-LED illumination"* Presented at *4th International Conference on Semiconductor Photochemistry (SP4),* Institute of Chemical Technology, Prague, 2013.

ABSTRACT

Heterogeneous photocatalysis is an advanced oxidation technology widely applied in environmental remediation processes. It is a relatively safe and affordable technology with a low impact on the environment and has found applications in a number of fields from chemical engineering, construction and microbiology to medicine. It is not catalysis in the real sense of the word as the photons which initiate the desired photocatalytic reaction are consumed in the process. The cost of these photons is by far the limiting economic factor in its application. From a technical standpoint, the inefficient use of the aforementioned photons during the photocatalytic reaction is responsible for the limited adoption of its application in industry. This inefficiency is characterised by low quantum yields or photonic efficiencies during its application. The mechanism of the technique of controlled periodic illumination which was previously proposed as a way of enhancing the low photonic efficiency of TiO_2 photocatalysis has been investigated using a novel controlled experimental approach; the results showed no advantage of periodic illumination over continuous illumination at equivalent photon flux. When the technique of controlled periodic illumination is applied in a photocatalytic reaction where attraction between substrate molecules and catalyst surface is maximum and photo-oxidation by surface-trapped holes, $\{Ti^{IV}OH^{\bullet}\}^{+}_{ads}$ is predominant, photonic efficiency is significantly improved. For immobilized reactors which usually have a lower illuminated surface area per unit volume compared to suspended catalyst and mass transfer limitations, the photonic efficiency is even lower. A novel photocatalytic impeller reactor was designed to investigate photonic efficiency in gas–solid photocatalysis of aromatic volatile organic compounds. The results indicate photonic efficiency is a function of mass transfer and catalyst deactivation rate. The development of future reactors which can optimise the use of photons and maximize photonic efficiency is important for the widespread adoption of heterogeneous photocatalysis by industry.

Titanium dioxide, Photocatalysis, Advanced oxidation process, Mass transfer, Mathematical modelling, Photonic efficiency, UV-LED, UV-VIS spectroscopy, Reactor engineering, Methyl orange.

CHAPTER I

1. ENVIRONMENTAL POLLUTION AND REMEDIATION

1.1. Introduction

Environmental pollution is the introduction of substances (pollutants) having anthropogenic or natural origins into the environment in amounts high enough to adversely affect the usefulness of a resource and cause harm to ecological systems and living resources[1, 2]. The pollutants can be physical or chemical in nature and are therefore measured less accurately when released into the environment. About five million different chemicals have been synthesized in the last 46 years and over 40,000 of these chemicals are used extensively in a variety of products often with limited toxicological information on them[3]. The expansion and growth of the chemical manufacture and process industries as a result of surging global demand for their products, has led to public concern and consciousness of the presence of chemicals in the environment. The continuous introduction of contaminants into the natural environment; air, land/soil and water has rightly heightened concerns about environmental pollution and elevated its status to that of a clear and present danger to biodiversity, habitats and climate. As the world's population exceeds seven billion[4], increased demand for energy/fuel, land and water resources, mostly in urban areas[5], will lead to greater amounts of waste released into the environment. Some of the contaminants released into the environment quickly diffuse in the wind or are easily diluted by water reducing their concentrations while in some cases they remain intact and through gradual build-up, reach levels where remediation actions are required for their removal and the restoration of polluted areas[6].

Chemical pollutants are discharged into the environment through point sources or nonpoint sources (NPS)/diffuse. The Scottish Environment Protection Agency (SEPA) defines point source discharge as the release of pollutants or effluents into the natural environment via an outlet, pipe,

fixed installation or otherwise[7]. Point sources are usually identifiable and discernable and the term derives from its use in mathematical modelling where the sources can be approximated to a mathematical point for simplification of analysis. Non-point sources on the other hand refers to the release of effluents and potential pollutants from different activities which individually are not likely to have an effect on the environment, but the release is at a scale large enough to have a significant impact[7]. The pollutants might originate from a point source, but the distance travelled and multiple sources make it non-point/diffuse pollution and hence very difficult to regulate.

1.2. Pollution of Soil, Water and Air

The components of the natural environment; soil, water and air are generally susceptible to pollution. This pollution can have natural or anthropogenic sources and affect these components in different ways.

1.2.1. Soil

Soil/land naturally is a heterogeneous assembly of materials which form a porous media; it consists of degrading organic matter and mineral particles having different shapes and sizes. Soil pollution occurs when pollutants of any origin accumulate in the soil medium, thereby altering the natural soil equilibrium usually as a result of human activity[8]. Materials that pollute the soil are majorly of four types[9]:

- Inorganic toxic compounds – Industrial activity is a major source of toxic wastes such as arsenic, lead and cadmium.
- Organic wastes – Organic wastes are usually from domestic sources, industrial waste and municipal sewage which are improperly disposed.
- Organic pesticides – Pesticides used in agricultural activities which do not decompose rapidly can accumulate to high concentrations which are toxic, these eventually get washed by erosion and run-off and find their way into aquatic organisms which are taken in as food.

- Radionuclide – Radioactive wastes are the primary sources of radionuclide, these wastes usually come from nuclear power plants, mining plants of radioactive minerals, hospitals and medical research laboratories.

1.2.2. Water

Approximately 75 per cent of water/marine pollution globally, is a direct consequence of human activities on land; most effluents, sediments, pesticides, thermal pollution and nutrients discharged into water bodies come from land-based sources and activities such as farming, sewage, forestry and mining[3]. Sources of water pollution usually contain a range of compounds, leading to complex effects on ecosystem processes. Some types of water pollution include:

- Organic pollution – This results from large amounts of organic matter being discharged into a watercourse or water body. A major source of organic pollution is sewage from sewage treatment plants.
- Eutrophication – This refers to the addition of nutrients to a water body during the breakdown of organic matter, burning of fossil fuels or agricultural run-off. Excessive amount of nutrients can lead to algal blooms, dense growth of weeds and changes in fish species[10].
- Acidification – Acids find their way into waterbodies usually as a result of precipitation as acid rain, burning of fossil fuels or run-off from soil within the catchment area[2].
- Thermal pollution – The major source of thermal pollution of water bodies is the discharge of cooling water from power plants. The temperature increase alters the water body in terms of oxygen concentration, density and metabolism of organisms[2].

Other pollutants include oil from spills, radioactivity from radioactive waste and toxic chemicals from industries.

1.2.3. Air

Air pollution is caused by the presence in ambient atmosphere, of pollutants that exist either in the particulate or gaseous form, in sufficient concentration to reduce air quality and cause harm to living organisms[11, 12]. Examples of pollutants in the gaseous form include ozone and carbon dioxide; their concentrations are usually expressed as volume mixing ratio (parts per million or billion) or mass per unit volume of air (μg m^{-3}). Pollutants in the particulate form vary in composition and size, ranging from nanometres to micrometres in diameter, they include liquid droplets and solid particles and their concentrations are also determined in mass per unit volume (μg m^{-3}). When these pollutants are released into the atmosphere, they are referred to as primary air pollutants; when they are formed within the atmosphere, they are referred to as secondary air pollutants[13].

Sources of air pollution can be natural or anthropogenic, while sulphur dioxide can be released into the atmosphere through the combustion of coal, oil or sulphur ores by man, it can also be released naturally through volcanoes. In the UK, road transportation, agricultural waste and power generation are major sources of air pollutants (fig. 1.1).

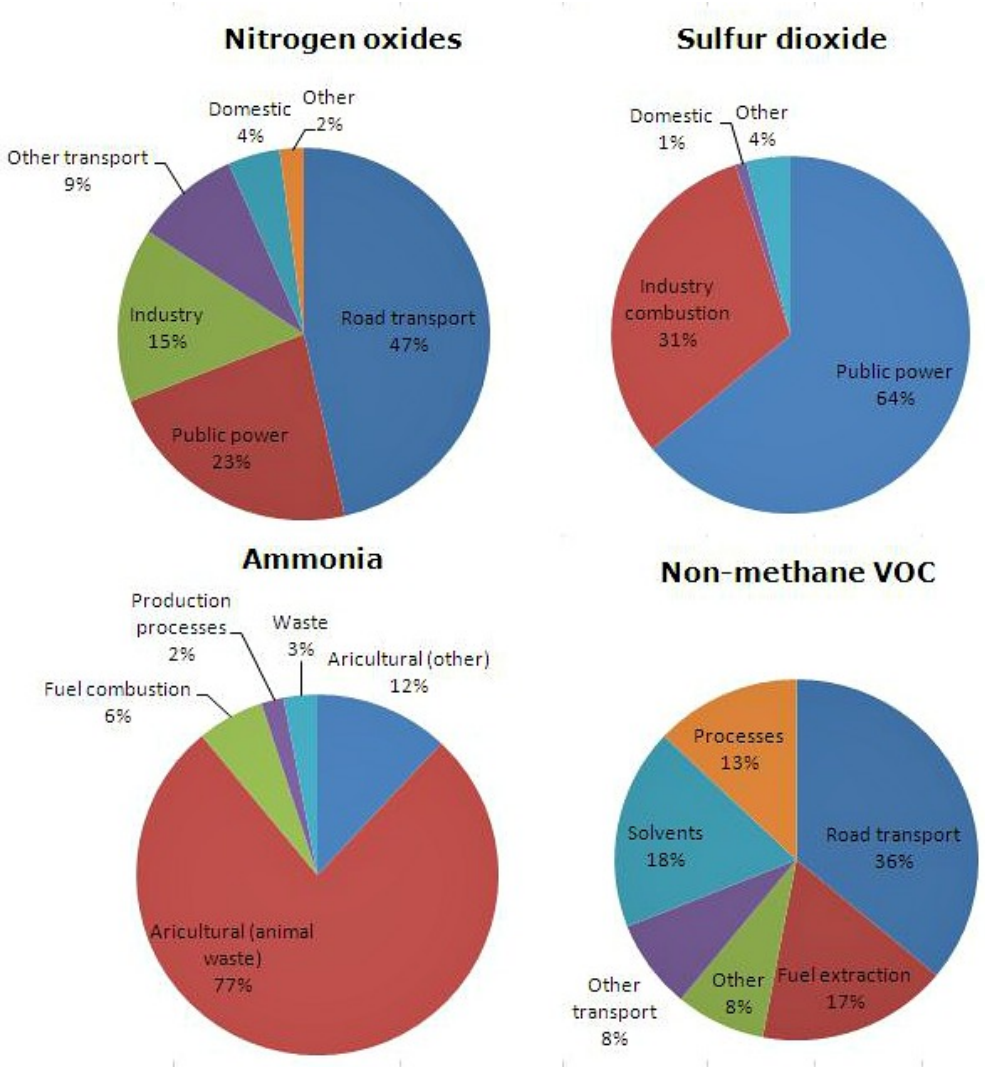

Figure 1.1: Anthropogenic sources of common air pollutants in the UK by sector (2001)[13].

Apart from volcanoes, natural emissions can fluctuate significantly within a year, but not from year to year and are rarely concentrated within a geographical location. Anthropogenic emissions on the other hand have been on a steady increase as a result of population growth and industrial expansion, they cause pollution problems not because of the magnitude of emission but because of the concentration in urban areas with large population sizes[12]. To understand the sources of primary air pollutants, it is important to know how they are formed and released into the environment (Table 1.1).

Table 1.1: Sources of primary air pollutants and their mode of formation[12], [13].

POLLUTANT	ANTHROPOGENIC SOURCE	NATURAL SOURCE
Sulphur dioxide (SO_2)	Combustion of coal, oil, roasting of sulphide ores	Volcanoes
Hydrogen sulphide (H_2S)	Chemical processes, Sewage treatment	Volcanoes, bioactions in swamps
Carbon monoxide (CO)	Automobile exhausts, incomplete combustion of fossil fuels	Forest fires, terpene reaction
Nitrogen dioxides (NO_2)	Combustion	Bacterial action in soils, electrical storms
Ammonia	Waste decay	Biological decay
Nitrous oxide (N_2O)	Indirectly from use of nitrogenous fertilizers	Biological action in soils
Carbon dioxide (CO_2)	Combustion	Biological decay, ocean release
Volatile organic compounds (VOCs)	Combustion of fuels, chemical processes, evaporation of liquid fuels, incineration processes	Vegetation, forests fires, volcanoes
Particulates	Combustion of fuels, quarrying, construction and demolition	Volcanoes

1.3. Atmospheric pollution from the oil and gas industry

The oil and gas industry is a multi-billion pound sector responsible for exploration, extraction, refining, distribution and marketing of oil and gas products. These products are vital to many industries and the sector is a major source of revenue to many countries where it is heavily subsidized [14, 15]. The UK oil and gas industry is particularly important because of its advancement in the areas of design engineering, project management, R&D, asset management and financial services. As a result, a number of operators have moved their European headquarters (EHQ) and headquarters (HQ) to the UK[16]. Oil production in the North Sea is expected to continue for another 30 to 40 years with a potential for about £25 billion in investments still to come and $10 billion in oil and gas services and equipment being exported yearly[16]. This industry

however has come under intense scrutiny for its contribution to environmental pollution. The atmospheric pollutants emitted by the activities of the oil and gas industry include but are not limited to VOCs, SO_2 and CH_4 but the most important of these emissions are NO_X and CO_2.

1.4. Impacts of atmospheric pollution on the environment

Among the many problems caused by atmospheric pollution, three are of great significance:

i) Acid precipitation

The emission of SO_2 and NO_x from the combustion of fossil fuels is the primary cause of acid precipitation. When emitted, these emissions can be transported over great distances in the atmosphere resulting in precipitation (dew, rain or snow) that is unusually high in nitric and sulphuric acid[17]. Some of the well known effects of acid precipitation include acidification of streams, rivers, lakes and groundwater leading to damage of agricultural crops/forests, death of marine life and deterioration of building materials. The awareness of the effects of these compounds particularly with regard to regional and trans-boundary effects has brought about growing concern and interests in the contribution other atmospheric pollutants such as volatile organic compounds (VOCs), chlorides and ozone may be having in acid precipitation[18].

ii) Greenhouse effect

The greenhouse effect is a major cause of global warming, continued increase in concentration of greenhouse gases such as CH_4, ozone, CO_2, CFC and NO_X in the atmosphere result in more heat being trapped and this leads to the increase in average temperature of the earth. The aforementioned greenhouse gases are particularly dangerous because they do not undergo condensation and precipitation in the atmosphere[19]. VOCs are not directly responsible for the greenhouse effect, but contribute indirectly by taking part in photochemical reactions which lead to ozone formation in the troposphere and they also prolong the

residence time of CH_4 in the atmosphere. The eventual consequence of increasing concentrations of greenhouse gases is climate change, consequences of which include changes in rainfall patterns, extreme weather events and global warming.

iii) Stratospheric ozone depletion

The presence of a layer of ozone between altitudes 12 and 25 km helps to prevent excessive solar radiation from the sun reaching the earth. The ozone layer plays an equilibrium-maintaining role by absorbing ultraviolet (UV) and infrared (IR) radiation from the sun[20]. One of the environmental impacts of atmospheric pollution from the oil and gas industry is the depletion of the stratospheric ozone layer by CFCs and NO_x emissions. A depleted stratospheric ozone layer will lead to increased UV radiation reaching the earth and this can cause increased rates of eye damage and skin cancer to humans and also harm other biological species.

1.5. Volatile organic compound (VOC) emissions from the oil and gas industry

The oil and gas industry plays a major role in atmospheric pollution through the emission of volatile organic compounds (VOCs). VOCs are an empirically defined group of carbon compounds excluding metallic carbides or carbonates, carbon monoxide, ammonium carbonate, carbon dioxide, and carbonic acid; VOCs generally have the following characteristics[21, 22]:

- Have small specific gravity, low molecular weight, water solubility and boiling point.
- Include aromatic and aliphatic hydrocarbons, alcohols, ketones, halocarbons and aldehydes.
- Their analysis usually involves the use of mass spectrometry and gas chromatography.

The UK Department for Environment, Food and Rural Affairs (DEFRA) lists over 60 non-methane volatile organic compounds (NMVOC) from oil refineries alone in the UK National Atmospheric Emissions Inventory

(NAEI)[23]. In 2001, the amount of VOCs generated onshore and offshore in the UK industry alone reached a total of 190,461 tonnes and the trend shows a yearly increase[24]. Prominent among the VOCs emitted by the oil and gas industry are benzene, toluene, ethylbenzene and xylene (BTEX).

1.5.1. Sources of VOC emission

The primary sources of VOC emissions in the oil and gas industry include; venting and flaring of gases from production facilities, vapour displacement during the loading and unloading of oil tankers, fugitive emissions from flanges, pumps and valves, particulates from burning during well testing and the storage of volatile materials[25]. From an environmental standpoint, the destruction and elimination of VOCs is important for many reasons, many VOCs are toxic with some having mutagenic and carcinogenic health effects at certain levels of exposure[26, 27]. The greatest problem associated with VOCs is their direct involvement in the formation of ground-level ozone, the primary constituent of smog when they react with oxides of nitrogen (NO_x) in the presence of sunlight[26, 28]. They also take part directly or indirectly in the formation of organic particulate matter.

1.5.2. Benzene, toluene, Ethylbenzene and Xylene (BTEX) volatile organic compounds

BTEX is a generic term used to describe a group of compounds (Benzene, Toluene, Ethylbenzene and Xylene) which are all related to benzene including benzene itself. They are sweet-smelling, colourless liquids which vapourise easily at room temperature. These compounds are soluble in organic solvents but have limited solubility in water. Their volatile properties ensures any release into the environment ends up in the atmosphere where they react with other air pollutants such as NO_x resulting in the formation of photochemical smog or ground level ozone. At normal concentrations, the BTEX compounds pose no environmental risk but become moderately toxic to aquatic life at higher concentrations[29]. Human exposure to BTEX at normal environmental concentrations pose no health risks, at higher concentrations for short

exposure, health risks are also unlikely. Long-term exposure to BTEX at high concentration however, can pose serious risks to human health such as headaches, dizziness, liver and kidney damage, irritation of the eyes and nose, exacerbation of respiratory conditions like asthma and brain damage. Benzene is the most hazardous of the four compounds; it is a known carcinogen which has been identified as a cause of leukaemia [30] and as a result benzene is listed as a "priority substance" for the proposed Water Framework Directive in the EU.

1.5.3. Beneficial uses of BTEX compounds

The BTEX group of compounds are very important petrochemical materials and therefore have beneficial uses. Demand for benzene which is the building block of the BTEX compounds was estimated at more than 40 million tonnes in 2010[31]. In the oil and gas sector, they are used in processing refined petroleum products, toluene and xylene are used as solvents in blending petrol while drilling companies regularly employ these compounds in their hydraulic fracturing treatments. Outside the oil and gas industry, toluene is used in fingernail polish, paint, paint thinners, adhesives, lacquers and leather tanning processes. Ethylbenzene is primarily used as an intermediate in manufacturing styrene monomer and as a diluent in paint. Xylene is used in the printing ink industry, polyester fibre, perfumes, as a cleaning agent and in pesticide formulations.

As a result of the hazardous effects of the BTEX compounds, there is an ongoing effort by operators in the oil and gas industry to move their operations away from the use of BTEX compounds to less hazardous compounds such as terpenes.

1.5.4. Role of VOCs in the formation of photochemical smog

In the 19th century, the combustion of large amounts of coal within a city led to the formation of smog having SO_x and particulate components. In recent times, activities of the oil and gas industry, vehicular emissions from internal combustion engines and other industrial fumes are mostly responsible. There now exists qualitative and quantitative understanding

of the atmospheric chemistry of VOCs in the formation of ground-level ozone and eventually photochemical smog.

The essential precursors of ground-level ozone (O_3) are VOCs and NO_x. VOCs in the atmosphere are transformed by photolysis, reaction with NO_x or reaction with OH radical. Cardelino and Chameides[32] developed an observation-based model which showed the sensitivity of local O_3 production to the concentration of VOCs and NO_x emissions in the environment. In the presence of sunlight, reaction with NO_x leaves behind airborne particles, converts NO to NO_2 and the formation of ground-level ozone, this combination is referred to as photochemical smog[33].

1.5.5. Removal of VOCs from the atmosphere

Eventually, VOCs will be removed from the atmosphere through the natural processes of wet and dry deposition, conversion to secondary organic aerosols (SOA) or oxidation to CO/CO_2(fig. 1.2)[34].

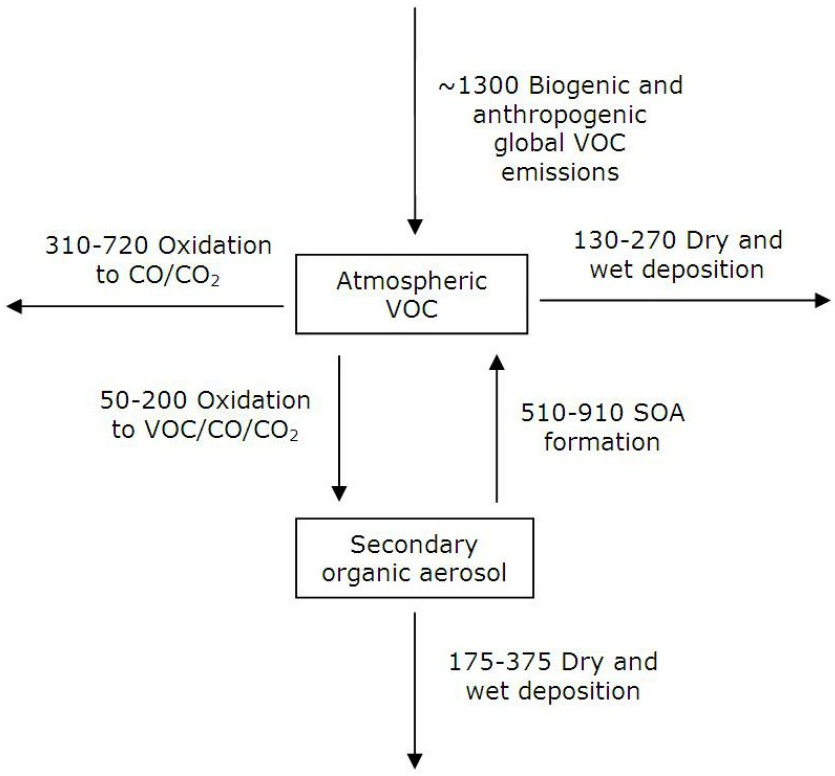

Figure 1.2: Mass-balance estimate of global budget of atmospheric VOCs. (Arrows indicate fluxes, units = Tg C/yr)[34].

This removal can follow two pathways; oxidation leads to the formation of CO_2 usually through CO or the production of highly soluble compounds that are transformed into SOAs and removed through wet and dry deposition.

1.5.6. Regulation to control VOC emission

The quality of air in a country or region is affected by the emission of air pollutants into the atmosphere, their dispersion, reaction and deposition. These substances can have direct impacts or impacts as a result of reacting together. For the adequate protection of ambient air quality in the UK, a number of policy instruments have been introduced at the European (EU) level and the national level (UK)[35]. At the European level, there are currently twenty directives on protecting the environment[36], the Integrated Pollution Prevention and Control (IPPC) Directive aims to reduce, eliminate and prevent pollution from industrial and agricultural activities[37, 38]. This is implemented by regulating how the industrial sites operate, the kind of technology used, emissions to air, land and water, and how any waste produced is managed[36]. The Air Quality Framework Directive was adopted to set a common strategy for member nations by identifying a number of air quality objectives for specific pollutants[39], the "stage one" directive covers the control of VOC emissions during transportation to retail outlets and at major terminals, this will be further extended to cover other sources from the oil and gas industry[39].

1.5.7. Techniques and Technologies for VOC destruction

The focus of this research is on the destruction and elimination of VOCs through TiO_2 heterogeneous photocatalysis and how it can be improved to a level where it is applicable in industry, but it is important to be aware of other available techniques for VOC destruction. Destruction of VOCs by industry is done in two major ways; oxidation and bio-filtration. VOCs can be oxidized in a number of ways including thermal oxidation, reverse flow reactor in which flow direction is periodically reversed for energy savings and catalytic oxidation[40]. Thermal oxidation systems are also known as fume oxidation systems, they can achieve 95% to 99% destruction of virtually all VOCs by combusting these VOCs at

temperatures as high as 704 °C – 982 °C[40]. Catalytic oxidation systems combust VOCs in a similar manner to thermal oxidation, but the catalytic system is operated at a lower temperature between 371 °C – 482 °C[40]. Oxidation is achievable at this low temperature because of the lowering of the activation energy required for the reaction by the catalysts. These two systems though effective, consume a lot of energy. Reverse flow reactors on the other hand can oxidize VOCs through an auto thermal process without an external energy supply, the disadvantage however, is the complexity in design and high initial investment and maintenance cost. Bio-filtration on the other hand involves the conversion of organic pollutants, under aerobic conditions, to water, bio-mass and carbon dioxide[40]. It is mostly effective when the organic pollutant is in low concentration.

The use of photocatalytic oxidation; an advanced oxidation process is an alternative oxidation process currently receiving a lot of attention in the remediation of pollutants including VOCs, and it involves heterogeneous photocatalysis using semiconductors as photocatalysts. Heterogeneous photocatalysis does not require the high energy input thermal and catalytic oxidation requires, but it requires some energy to provide the light which initiates the oxidation reaction.

1.6. Advanced Oxidation Processes (AOPs)

Over the years, it has been observed that certain pollutants cannot be treated by biological and conventional treatment methods because of their high chemical stability or strong resistance to mineralization; in such cases, it is necessary to adopt a more reactive system. A special class of oxidation processes defined as advanced oxidation processes which operate at ambient temperature and pressure have gained prominence as alternative treatment methods. Advanced oxidation processes are characterized by a unique chemical feature common to them: the production and exploitation of highly reactive OH radicals which drive the oxidation process by attacking most organic molecules with rate constants in the range 10^6-10^9 M^{-1} s^{-1} [41, 42]. They are also characterized by the selectivity of attack and versatility in the variety of

ways OH radicals are produced[43]. The several possibilities of advanced oxidation processes are shown in the list below[22]:

H_2O_2/Fe^{2+}	(Fenton)
TiO_2/UV	(Photocatalysis)
$O_3/UV/H_2O_2$	
H_2O_2/UV	

Heterogeneous photocatalysis is one of the advanced oxidation processes, it involves processes in which reactions or molecular transformations which are photo-induced, take place on the surface of photocatalysts[44]. Semiconductors are suitable as photocatalysts because they do not possess a continuum of electron states like metals instead, they have a void region called the band gap, with no energy levels that extends from the top of the valence band to the bottom of the conduction band[44]. Heterogeneous photocatalysis is said to have taken place if after excitation, the semiconductor remains unchanged while the charge transfer to any adsorbed species is exothermic and continuous[44]. Photocatalysis can be divided into two types with respect to where the initial excitation takes place; when photoexcitation first occurs in the adsorbate molecule which then interacts with the catalyst substrate in the ground state, it is called a catalyzed photoreaction; when the catalyst substrate is photoexcited and then transfers an electron to a molecule in the ground state, it is referred to as a sensitized photoreaction[44]. However, most heterogeneous photocatalytic reactions involving TiO_2 as a catalyst are sensitized reactions.

1.6.1. Titanium dioxide (TiO_2) photocatalysis

There are earlier reports on TiO_2 photocatalysis before 1972 however, scientific research in this field was popularised over three decades ago with photo-electrochemical conversion of solar energy for hydrogen production but later shifted into the environmental remediation of pollutants[45, 46]. In 1972, a study by Fujishima and Honda[47] reported the photocatalytic decomposition of water by UV-VIS light into oxygen and hydrogen using TiO_2 and platinum electrodes without any externally

applied voltage. The water splitting was sustained by keeping the TiO_2 and platinum electrodes apart and the equation for the reaction is as follows:

$$TiO_2 + 2hv \rightarrow 2e^- + 2h^+ \quad (1.1)$$

$$H_2O + 2h^+ \rightarrow \frac{1}{2}O_2 + 2H^+ \text{ (at } TiO_2 \text{ electrode)} \quad (1.2)$$

$$2H^+ + 2e^- \rightarrow H_2 \text{ (at Pt electrode)} \quad (1.3)$$

The overall reaction is

$$H_2O + 2hv \rightarrow \frac{1}{2}O_2 + H_2 \quad (1.4)$$

Heterogeneous photocatalysis has received a great deal of interest over the years, since the discovery of the Honda-Fujishima effect, with the most cited review paper[48] having over 12600 citations since 1995 and the total literature in heterogeneous photocatalysis exceeding 5000 papers[49] as at 2005 now more than doubles that figure. This field (fig 1.3) has now experienced an increase in the number of citations and patents and this growing number of papers and patents is as a result of a high level of engineering and commercial interest in its applications.

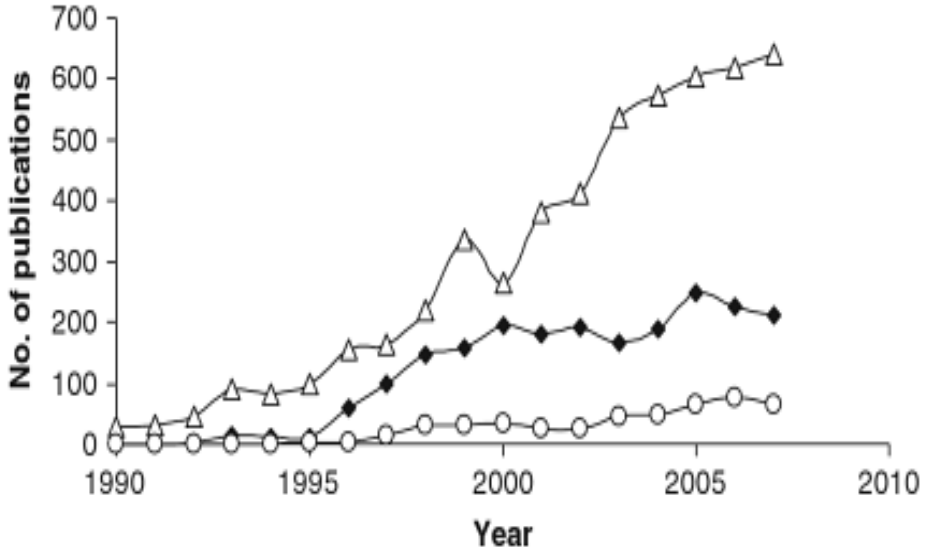

Figure 1.3: Estimated number of TiO_2 photocatalysis manuscript per year according to: water treatment (△); air treatment (◆); self cleaning surfaces (○)[50].

Extensive research has been conducted to understand its fundamental processes and applications with several reviews by Hoffman *et al*.[48], Linsebigler *et al*.[44], Fox and Dulay[51], McCullagh *et al*.[52], and Fujishima *et al*.[45, 53]. Some other applications of TiO_2 photocatalysis include disinfection, prevention of metal corrosion and lithography.

1.6.2. Titanium dioxide catalysts

Titanium dioxide is an oxide of titanium which is naturally occurring. It is one of the most widely studied and used photocatalyst alongside cadmium sulphide (CdS) and Zinc oxide (ZnO) because it has a high photocatalytic activity which is now used as a benchmark for other photocatalysts[51]. Despite its high photocatalytic activity, one of the drawbacks to the use of TiO_2 is its wide band-gap which makes it absorb photons in the UV range alone and therefore unable to utilize visible light for photocatalysis[54-56]. Small band gap photocatalysts like CdS are able to utilize visible light but are unstable and photodegrade over time, self-oxidation in CdS and ZnO causes photocorrosion of the semiconductor, a phenomenon which TiO_2 is resistant to[51, 57].

Generally, TiO_2 exists in three forms; rutile, anatase and brookite with rutile being the most stable and common form (fig. 1.4). Degussa (Evonik) P25 TiO_2 catalyst, a commercially available TiO_2 produced from high temperature flame hydrolysis of $TiCl_4$ is a mixture of anatase and rutile in the ratio 70:30 has been widely investigated as a photocatalyst. It exhibits a high activity in photocatalytic reactions, is commonly used in photocatalysis research and has been accepted as the de-facto standard by the research community[58-60]. It is nonporous, has a crystal size of 30 nm in 0.1 μm diameter aggregates and has a surface area of about 55 $m^2 g^{-1}$.

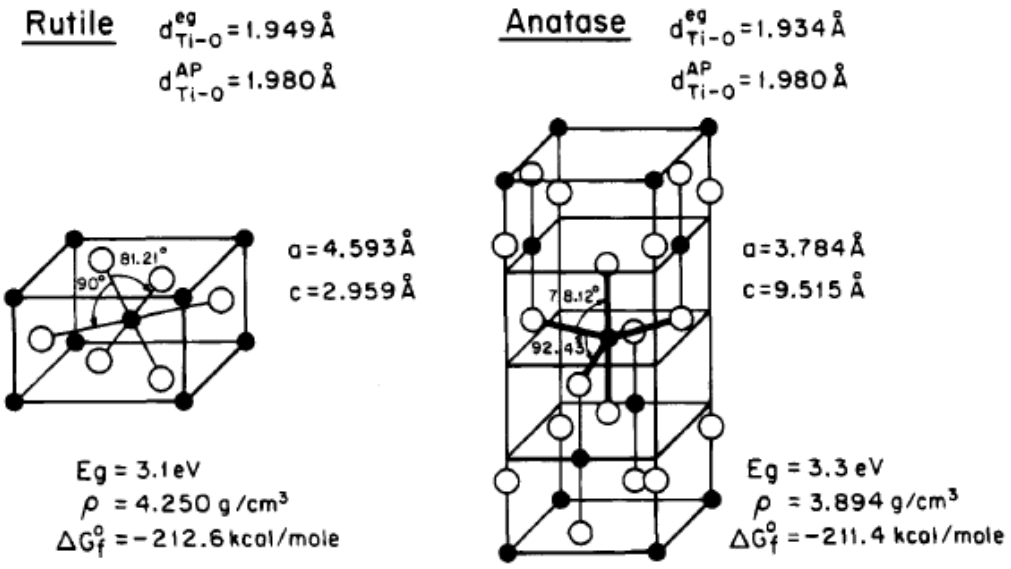

Figure 1.4: Structure of rutile and anatase TiO_2. Used with permission from[44]. Copyright (1995) American Chemical Society.

TiO_2 is ideal for photocatalysis for several reasons; it is inexpensive, chemically and biologically inert, photo-stable, non-toxic and produces highly oxidizing photogenerated holes and highly reducing photogenerated electrons which can reduce dioxygen to superoxide[53].

1.6.3. Mechanism of semiconductor photocatalysis

The band structure of a semiconductor exists as a series of energetic, tightly packed energy levels associated with atoms exhibiting covalent bonding which make up the valence band and another series of similar energetic levels which are spatially diffuse and at a higher energy,

associated with conduction in the conduction band[51]. The size of the energy gap (E_{bg}) (fig. 1.5) between the valence and the conduction band is responsible for the electrical conductivity of the semiconductor in its undoped state and its wavelength sensitivity to irradiance[51].

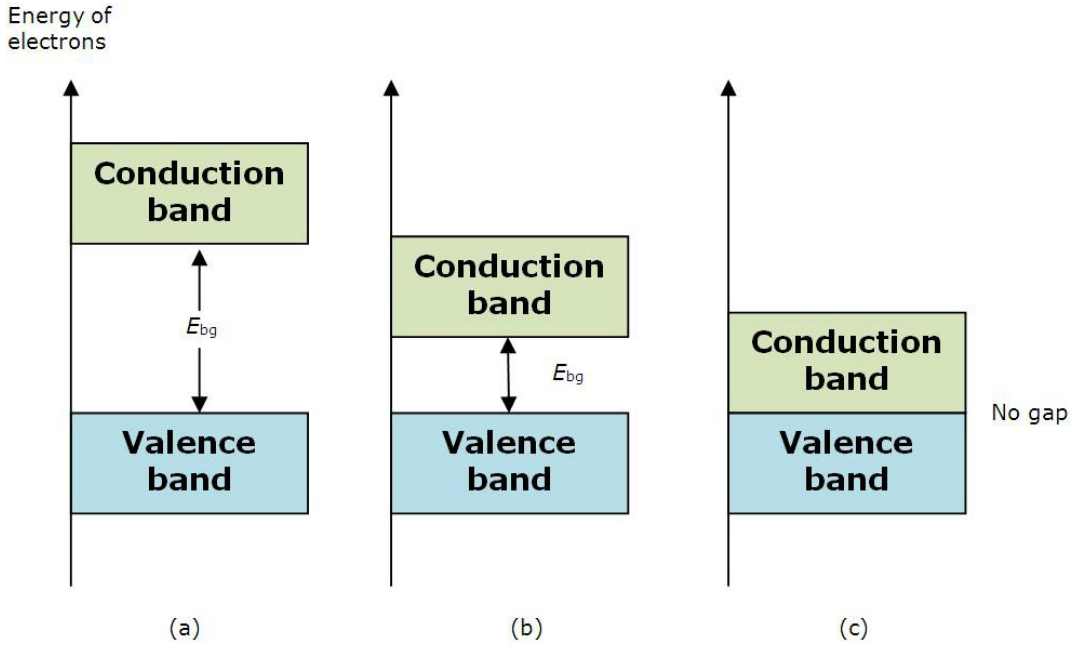

Figure 1.5: Energy bands in solids: (a) insulator; (b) semiconductor; (c) conductor.

When light of energy greater than or equal to the band gap is incident on the semiconductor, photo-excitation occurs, promoting an electron from the valence to the conduction band leaving behind a hole (h^+) i.e. an electron vacancy[51, 61]. Figure 1.6 (a) shows the pathways of the photogenerated electron and hole which can either recombine dissipating energy as heat, become trapped in a metastable state or take part in reduction and oxidation of surface-adsorbed and bulk substrates[51, 61]. Figure 1.6 (b) shows oxidation process of VOCs using TiO_2. Since photo-oxidation is by far, the most typical of photocatalytic reactions (because conduction band electrons have significantly lower reducing powers relative to oxidizing powers of valence band holes), photo-degradation of organic compounds usually employ the oxidizing power of holes (h^+) or hydroxyl radical ($OH^\bullet$), build-up of negative charge should be prevented by the provision of reducible species the electrons can react with[48].

(a)

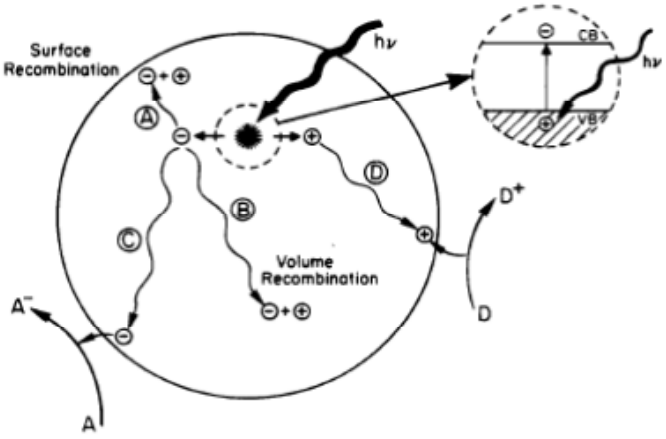

(b)

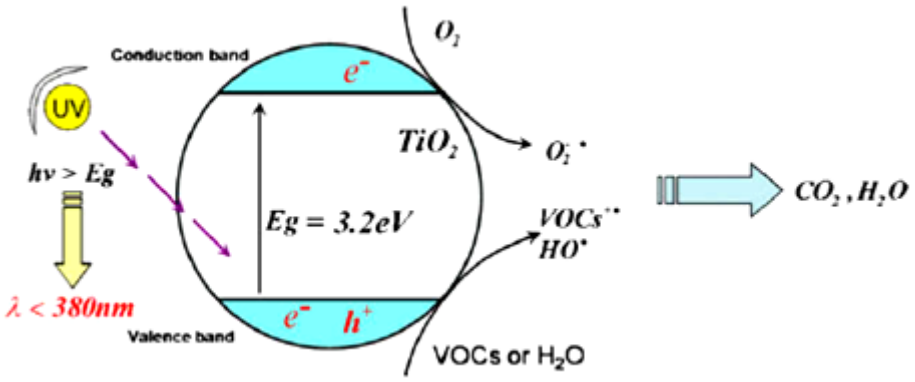

Figure 1.6: (a) Charge-carrier pathways. Used with permission from[45]. Copyright (1995) American Chemical Society. (b) Schematic of TiO_2 UV photocatalytic oxidation process of VOCs[73].

Hoffmann *et al.*[48] have proposed characteristic times for the primary processes of heterogeneous photocatalysis on TiO_2 based on measurements of laser flash photolysis, the characteristic times for the primary processes are shown in table 1.2.

Table 1.2: Characteristic times of primary processes in heterogeneous photocatalysis of TiO_2[48].

PRIMARY PROCESS	CHARACTERISTIC TIMES
Charge-carrier generation	
$\mathbf{TiO_2} + h_\nu \rightarrow \mathbf{h_{vb}^+} + \mathbf{e_{cb}^-}$	Very fast (fs)
Charge-carrier trapping	
$\mathbf{h_{vb}^+} + > \mathbf{Ti^{IV}OH} \rightarrow \{\mathbf{Ti^{IV}OH^\bullet}\}^+$	Fast (10 ns)
$\mathbf{e_{cb}^-} + \mathbf{Ti^{IV}OH} \leftrightarrow \{\mathbf{Ti^{III}OH}\}$	Shallow trap (100 ps)(dynamic equilibrium)
$\mathbf{e_{cb}^-} + > \mathbf{Ti^{IV}} \rightarrow \mathbf{Ti^{III}}$	Deep trap (10 ns) (irreversible)
Charge-carrier recombination	
$\mathbf{e_{cb}^-} + \{> \mathbf{Ti^{IV}OH^\bullet}\}^+ \rightarrow \mathbf{Ti^{IV}OH}$	Slow (100 ns)
$\mathbf{h_{vb}^+} + \{> \mathbf{Ti^{III}OH}\} \rightarrow \mathbf{Ti^{IV}OH}$	Fast (10 ns)
Interfacial charge transfer	
$\{> \mathbf{Ti^{IV}OH^\bullet}\}^+ + \mathbf{Red} \rightarrow > \mathbf{Ti^{IV}OH} + \mathbf{Red^{\bullet+}}$	Slow (100 ns)
$\mathbf{e_{tr}^-} + \mathbf{Ox} \rightarrow \mathbf{Ti^{IV}OH} + \mathbf{Ox^{\bullet-}}$	Very slow (ms)

In Table 1.2, $Ti^{IV}OH$ is the hydrated surface TiO_2, e_{cb}^- is the conduction-band electron, e_{tr}^- is the trapped conduction-band electron, h_{vb}^+ is the valence-band hole, Red is the reductant (electron donor), Ox is the oxidant (electron acceptor), $\{>Ti^{III}OH\}$ is a surface-trapped conduction-band electron and $\{>Ti^{IV}OH^\bullet\}^+$ is the valence-band hole trapped at the surface or surface-bound hydroxyl radical.

1.7. Overview of gas phase photocatalysis

The photocatalytic degradation of pollutants in the gas phase has been widely reported in the literature for a wide variety of organic compounds which include aromatics, aliphatics, phenols, dyes, pesticides, surfactants[48, 59, 62-64]. Gas phase photocatalysis research however, has received less attention when compared to the aqueous phase up until 2009. A number of reasons could be responsible for this, notably the fact that the pioneer researchers were from the electrochemistry community, a common feeling that air is a free resource which has no cost and is readily available[50] and also the complexity of gas phase experiments/reactor design. Interest in gas phase photocatalysis began to grow around 1996 with the most activity coming from the industrial and commercial community with the annual number of patents in

photocatalytic air treatment surpassing that from water treatment in 1997(fig. 1.7) while the scientific community continued to focus on and produce more scientific publications on water treatment (fig. 1.3)[50].

(a)

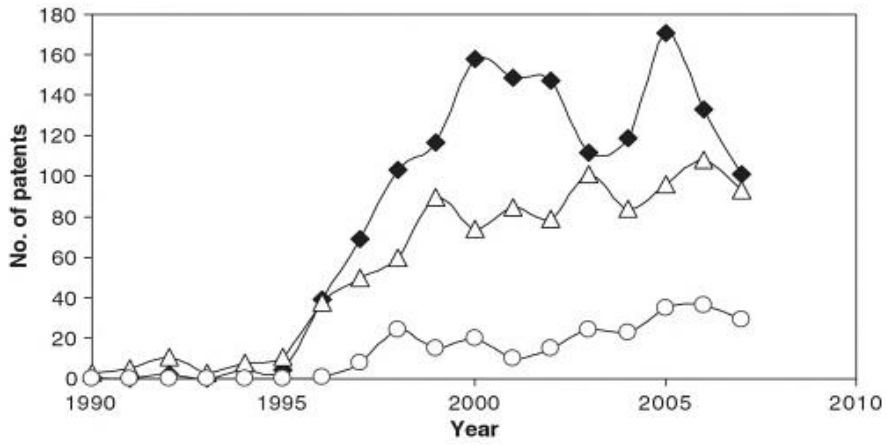

(b)

Figure 1.7: (a) Estimated number of patents on TiO_2 photocatalysis per year according to: water treatment (△), air treatment (♦), self cleaning surfaces (○); (b) distribution of patents according to: water treatment, air treatment and self cleaning surfaces[50].

1.7.1. Photocatalytic oxidation of gas phase aromatic contaminants

The complete oxidation of organic pollutants to produce CO_2 and H_2O is one of the important advantages of photocatalytic oxidation using TiO_2[62, 65], this can however, be hindered by the low photocatalytic reactivity and

photocatalyst deactivation by aromatic contaminants concentrations as low as 10 ppm. Research into the improvement of the yield and selectivity of the oxidation of aromatic compounds has increased over the years; one area of improvement has been in the design of photoreactors with the aim to obtain the greatest yield possible by providing strictly controlled conditions for the photocatalytic oxidation of pollutants. Another area of improvement has been advancement in the understanding of photocatalyst deactivation. It is now known that this phenomenon which is caused by the poisoning effects of strongly adsorbed oxidized intermediates[66, 67], does not occur when contaminants are present in trace amount and is prominent in single-pass fixed-bed photoreactors[68].

1.7.2. Reactor development for gas phase heterogeneous photocatalysis

The removal of volatile organic compounds using heterogeneous photocatalysis is a surface reaction which must proceed in the following manner; first, the VOC molecule must be transported to the catalyst surface. Secondly, redox reactions taking place on the surface of the catalyst degrade the VOC molecule. For the required photocatalytic reaction to proceed in this manner, an environment/enclosure known as a photocatalytic reactor must be provided. Thus, for gas phase photocatalysis, the most important parameters for a reactor are the illuminated surface area of catalyst, convective mass transfer rate of gaseous molecule and the kinetic rate of reaction.

1.7.3. History of photoreactor design

The first contribution to photoreactor design can be traced to Bhagwat and Dhar[69] who studied the effects of stirring on reaction rate. They applied Lambert's law with a constant attenuation coefficient to a flat plate reactor and obtained an expression for light absorption, I_a;

$$I_a = I_w(1 - e^{-\mu s}) \qquad (1.5)$$

If Ω which is the reaction rate is proportional to *n*-power of light

$$\Omega = k_1\{\frac{I_w(1-e^{-\mu s})}{s}\}^n \quad (1.6)$$

The above equation holds for the reaction if it is completely mixed, the authors proposed an equation for incomplete mixing where;

$$\Omega' = \frac{k_1}{ns} I_w^n \mu^{n-1}(1 - e^{-\mu n s}) \quad (1.7)$$

If the absorption of light is very high, $e^{-\mu s} \rightarrow 0$, and the ratio of the rates is:

$$\frac{\Omega}{\Omega'} = n(\mu s)^{1-n} \quad (1.8)$$

If light absorption is low, $e^{-\mu s} \rightarrow (1 - \mu s)$, and

$$\frac{\Omega}{\Omega'} = 1 \quad (1.9)$$

where I_a is the volumetric rate of light absorption, n is order of reaction, Ω is the local reaction rate, k_1 is a kinetic constant, s is the path length of light, μ is the attenuation coefficient and w is the reactor wall

The above equations and experimental observations have led to the following conclusions which are still valid eighty years after;

- If the rate is first order with respect to light absorption (n=1), then stirring has no effect on the rate (compare 1.6 and 1.7).
- If n < 1, stirring increases the average rate.
- For high light absorption media, an increase in the speed of stirring results in a decrease in apparent activation energy for n ≠ 1.
- For low light absorption media or nearly transparent media, there is no effect of stirring on the activation energy.

The second generation of design studies commenced with a review by Doede and Walker[70], opening the door for complementary studies and research activity centred on photoreactor analysis and design. Reactor design and analysis was approached from the point of view that the point values of reaction rates are not intrinsically uniform and are different from the global ones in most cases.

1.7.4. Reactor configurations for VOC treatment

A highly efficient gas phase reactor should have a high specific surface in order to have a large reaction area, uniform irradiation from UV light source and low air velocity for high mass transfer. The structure of the reactor usually consists of the UV source and the reaction structure which supports the catalyst and air flow channels. However, in most reactor design configurations reported in the literature (fig.1.8), the UV source and reaction structure are not designed as a single unit. This leads to reactive or diffusive limitations, incomplete reaction and low VOC removal efficiency in the desired photocatalytic oxidation reaction[71].

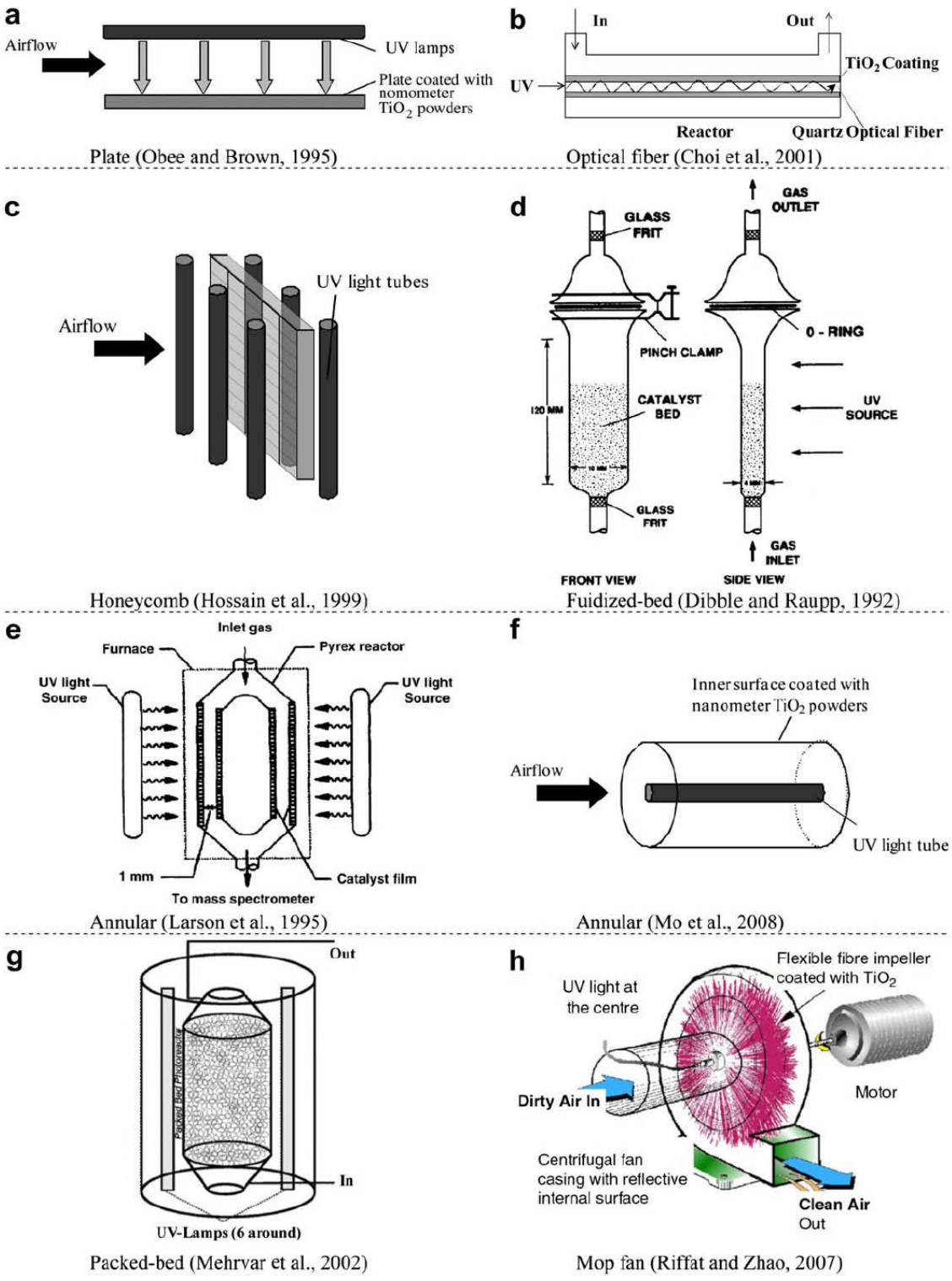

Figure 1.8: Gas phase reactor configurations reported in the literature[72].

Despite the many advantages of photocatalysis for destroying VOCs, it has not been widely adopted in industrial practice for reasons including (i) a lack of suitable design procedures and reactor models, (ii) insufficient information on the physical and chemical parameters[73].

Cassano *et al*.[74] identified other important reasons that point to reactor design, these include (i) limitations in size, (ii) operation of the lamp and maintenance difficulties, (iii) difficulties in construction, (iv) deposits on the reactor wall which affect light penetration (v) configuration, behaviour and lifetime of light source. For gas-solid heterogeneous photocatalysis, the four most widely reported configurations in the literature are monoliths, packed bed, catalytic walls and fluidised bed photoreactors[75]. For batch reactors however, a fixed bed configuration may not provide adequate interaction between the reactants of the gas-solid system, that is; photocatalyst, pollutant and photons in particular because of the reduction of light intensity as it passes through the bed.

1.7.5. Aromatic contaminants of interest

Some of the most widely used and simplest group of aromatic compounds are benzene (C_6H_6), toluene ($C_6H_5CH_3$), ethylbenzene ($C_6H_5C_2H_5$), and xylene; [*o*-xylene, *p*-xylene and *m*-xylene ($C_6H_4(CH_3)_2$)]. Collectively, they are known as the BTEX compounds and are common air pollutants because of their widespread use in adhesives, industrial solvents, chemical manufacture, paints[76, 77]. The four compounds are classified as hazardous substances with benzene being a known carcinogen therefore having the lowest permissible exposure limit of 1 ppm.

Studies by Boulamanti *et al*.[78] have shown that the molecular structure of the BTEX compounds plays a significant role in their photo-oxidation reaction rates. All six compounds were treated with Degussa P25 and while toluene had the highest adsorption rate and ethylbenzene the least, toluene had a lower reaction rate than ethylbenzene meaning a higher adsorption rate does not always translate to higher reaction rate. Overall, the compounds were stable under direct photolysis, benzene had the least photo-oxidation rate while *m*-xylene was the easiest to oxidize and all six compounds showed a substantial deactivation of the photocatalyst.

1.8. Research overview

The reason for limited application of heterogeneous photocatalysis in industry is due to the low efficiency of the process in both aqueous and gas phase photocatalysis. This research will involve aqueous and gas phase studies of heterogeneous photocatalytic reactions. The various parameters affecting the photocatalytic photonic efficiency will be investigated under varying conditions. The research methodology will include experimental and theoretical studies, engineering design and analysis of a reactor and the organic synthesis of catalysts.

1.8.1. Research aim

The central theme of this thesis is the photonic efficiency of heterogeneous photocatalytic reactions. The aim of this research is to study all the parameters that affect photonic efficiency in both aqueous and gas phase photocatalysis under both continuous and intermittent illumination; the photonic efficiency gives an indication of how efficiently incident photons which initiate the photocatalytic process are utilized and ways to enhance and optimize it will be studied.

1.8.2. Research objectives

The objectives of the research are as follows;

First, heterogeneous photocatalysis under Controlled Periodic Illumination (CPI) will be studied extensively in the aqueous phase using a dye compound and the designed photoreactor. This study will provide an understanding of the mechanism of the CPI effect that has been reported as a means of enhancing photonic efficiency.

Secondly, the results of the first objective will provide information on how to optimize the photonic efficiency. This possibility will be investigated in the aqueous phase and provide a deeper understanding of factors affecting photonic efficiency.

The third objective involves theoretical studies of photocatalytic efficiency; theoretical models will be employed in studying and

comparing photonic efficiency and quantum yields. This objective will also validate the results from the experimental study.

The fourth objective is the design and construction of a novel photoreactor for gas phase photocatalysis, this photoreactor will have an immobilized configuration as well as some features of the initial prototype such as the use of UV-LEDs as source of illumination.

The last objective is the operation and evaluation of the designed photoreactor in the photo-oxidation of an aromatic BTEX VOC; an investigation of several factors affecting the performance of this reactor will be carried out and their influence on photonic efficiency will be investigated.

1.8.3. Organisation of the thesis

The thesis consists of a total of five chapters which explore the research title and provide detailed results and discussion of how the set objectives were achieved. The chapters include an introduction and conclusion.

Chapter one is the introductory chapter, it gives an overview of the research by putting it in the context of environmental pollution, its sources, the various types and legislative control by national and regional governments. It also introduces heterogeneous photocatalysis using TiO_2 as a means of environmental remediation and presents a summary of this area of research over the years. The chapter concludes with the research objectives and a justification of the methodology used in achieving them.

Chapter two investigates the mechanism of controlled periodic illumination (CPI). This technique was previously proposed as a way of enhancing the low photonic efficiency of TiO_2 photocatalysis. This chapter investigates CPI using a novel controlled experimental approach and also compares it with continuous illumination for a full understanding of its mechanism and effect.

Chapter three is concerned with how to optimize photonic efficiency since the enhancements from CPI alone are not sufficient. Certain factors necessary for optimum photonic efficiency are studied in detail using laboratory experiments. The effect on photonic efficiency when CPI is applied with these factors in place is also investigated. Theoretical models related to photonic efficiency under CPI are also evaluated and experimental results from chapter two are reproduced and validated.

Chapter four is the conceptualization, design and evaluation of a novel photoreactor for gas phase photocatalysis. The photonic efficiency of VOC degradation is studied and correlated with other parameters unique to VOCs in the gas phase. The focus of the chapter is on the evaluation of the reactor's performance considering its novel immobilized configuration.

Chapter five is the concluding chapter which summarises the findings in the thesis, how the objectives were met, the contributions of the research and recommendations for future work.

CHAPTER II

2. MECHANISM OF CONTROLLED PERIODIC ILLUMINATION

2.1. Introduction

Generally, photo-driven processes such as photography, photochemical splitting of water, photocatalysis and photosynthesis are preceded by photo-induced charge separation. The incident photons that initiate this process in photocatalysis are however, not efficiently used and the competition between recombination of charge carriers and their reaction with adsorbed reactants is the major event limiting the photoefficiency of the process[79]. Large scale photocatalytic treatment systems have to be efficient in the utilization of photons and be more economical to be able to compete with other relatively cheap methods of purification such as adsorption on activated carbon which do not destroy the pollutants completely.

2.1.1. Efficiency of the Photocatalytic process

In photocatalytic degradation studies (homogeneous and heterogeneous), the efficiency of the photocatalytic process is referred to as the quantum yield, which can be defined as the number of molecules changed divided by the number of absorbed photons, assuming all photons are absorbed by the catalyst and losses due to light scattering are negligible[48, 51]. For a species *i*, the quantum yield φ is:

$$\varphi x_i \equiv \frac{\pm(d[X_i]/dt)_0}{d[hv]_{abs}/dt} \qquad (2.1)$$

Where

- φx_i is the quantum yield for x_i
- $d[x_i]/dt$ is the initial rate of formation or degradation of x_i
- $d[hv]/dt$ is the rate of photon absorption by the catalyst

When determining the quantum yield or efficiency, a combination of the total pathway probabilities for the hole and electron must be considered, for an ideal system, the quantum yield is directly proportional to the rate

of charge transfer processes (k_{CT}) and is inversely proportional to the sum of both bulk and surface electron-hole recombination rate (k_R) and the charge transfer rate (k_{CT}) and is given by the following equation (2.2):

$$\varphi \alpha \frac{k_{CT}}{k_{CT} + k_R} \quad (2.2)$$

Diffusion of the products into the solution is assumed to be rapid without the reverse reaction of reduction by electrons and oxidation by holes. In the absence of recombination, quantum yield will have an ideal value of 1 for photocatalytic processes. However, in real systems, recombination occurs and the concentration of holes and electrons at the surface is not equal.

2.1.2. Enhancement of photocatalytic efficiency

A lot of effort has been directed at understanding the fundamental and engineering aspects of TiO_2 photocatalysis with the primary aim of improving its efficiency. Previous studies have shown that quantum yields in dilute aqueous suspensions are usually below ~10% while quantum yields of oxidation of organic species in the gas phase exceed 50% under weak UV illumination[80, 81]. Various methods of improving efficiency have been studied; Disdier *et al*.[82] employed metal semiconductor modification which increases efficiency by trapping electrons in platinum modified TiO_2, thus suppressing electron-hole recombination. Jiang *et al*.[83] demonstrated the enhancement of photocatalytic efficiency by an extra electric field across the semiconductor photocatalyst, the electric field promotes the separation of electron-hole pairs and prevents their recombination. Sczechowski *et al*.[84] recorded a 500% increase in the photonic efficiency of formate decomposition through controlled periodic illumination (CPI).

2.1.3. Controlled periodic illumination (CPI)

Under continuous illumination, a steady supply of photons is provided for the photocatalytic oxidation reaction; this results in low quantum yields during the process[85]. Controlled periodic illumination (CPI) is based on a series of alternate light and dark periods (T_{on}/T_{off}) and has been previously reported as a means of increasing the photonic efficiency and improving the conversion rate of reactants or formation of products in TiO_2 photocatalysis[84-87]. It is based on a hypothesis by Sczechowski *et al*.[84] who hypothesized that continuous introduction of photons may result in the build-up of charges and photogenerated intermediates such as superoxide ion and hydroxyl radicals (fig. 2.1). These intermediate species are involved in the photocatalytic oxidation of the organic substrate but can also participate in reactions that favour electron-hole recombination resulting in a low efficiency of the oxidation process. It was suggested that periodically illuminating the TiO_2 particle at short intervals would inhibit the build-up of intermediates and reduce the rate of recombination reactions.

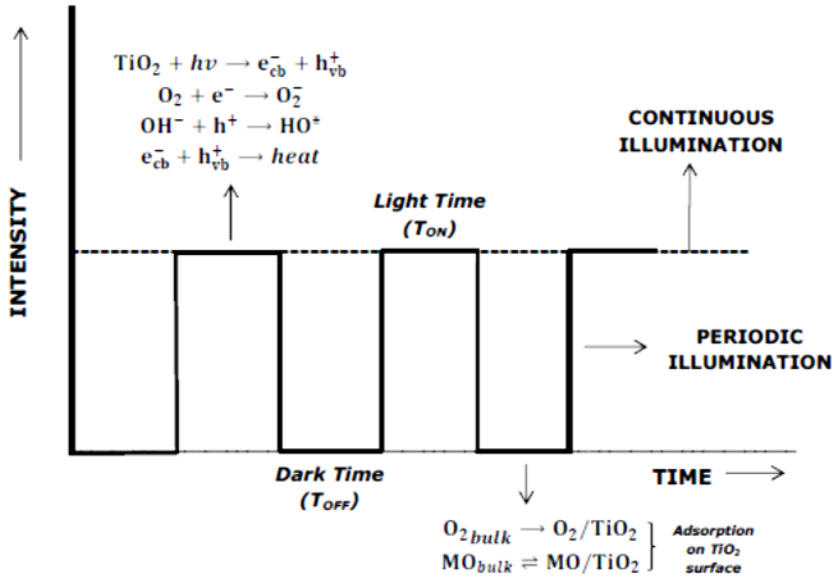

Figure 2.1: Schematic diagram of CPI of methyl orange showing T_{on} and T_{off}.

Sczechowski *et al*. suggested photons are not needed for the rate-limiting step to take place and after a critical dark recovery period,

photons should be introduced again. For their experiment, they used a channel photoreactor shown in figure 2.2, with a total system volume of 750 mL, 3 g of TiO_2 catalyst and 6 mL concentrated sodium formate solution so that the reactant mixture had an initial concentration of 50 ppm of total organic carbon (TOC). A 40 W black light was used to provide different light and dark times by wrapping sections of the bulb in aluminum foil. The length of the unwrapped sections was taken to be the illumination time as the reactant mixture flowed underneath the light source. They reported an increase in the photonic efficiency of the oxidation of formate ion in the aqueous phase by 500% with an illumination time of 72 ms and dark recovery time of 1.45 s.

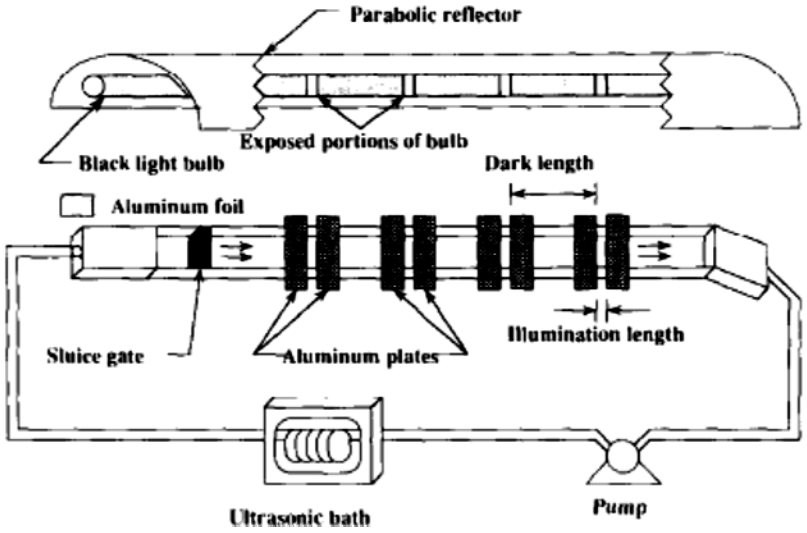

Figure 2.2: The channel photoreactor used by Sczechowski *et al*.[84].

The essence of the hypothesis is that under continuous illumination of TiO_2 suspension, there is a build-up of charges and this leads to recombination of electron-hole pairs which eventually diminish the efficiency of the photocatalytic process. Periodically illuminating the catalyst will generate a very limited amount of electron-hole pairs and help prevent the build-up of these species thereby increasing efficiency. This hypothesis was also investigated by Stewart and Fox[87], they studied the effect of varying the dark recovery time on the photonic efficiency of the photocatalytic oxidation of 1-octanol and photocatalytic reduction of *p*-nitroacetophenone in a non-aqueous media, using Degussa P25 TiO_2. They reported a 1.8 fold improvement in the net photonic efficiency of 1-

octanol oxidation to octanal but no improvement in the reduction of *p*-nitroacetophenone to *p*-aminoacetophenone and suggested that a dark recovery time between intermittent excitation lowers the steady state concentration of the adsorbed intermediates and helps prevent charge carrier recombination which is detrimental to efficiency.

2.1.4. Novel approach to the investigation of controlled periodic illumination

In recent years, there has been tremendous progress in LED lifetime, illumination efficiency and total lumen output[88]. This new generation high-bright UV-LEDs can be electronically controlled, allowing variable on and off times on a millisecond time-scale. Consequently these sources may be more effective for CPI than incandescent lamps which cannot be turned on and off alternately at a similar time-scale therefore requiring the use of complex mechanical shutters[89]. Furthermore, using an electronic controller, it is possible to independently control the T_{on} and T_{off}, hence varying the photon absorption time and the time for rate limiting steps in the photocatalytic process. These LEDs could potentially be utilised in large scale reactors allowing periodic illumination to be used in such processes. Such application of periodic illumination would be more challenging using traditional UV irradiation sources as incorporation of mechanical shutters in such reactors would require more complex engineering and hence cost.

This chapter investigates the effect of light and dark time periods on photonic efficiency of methyl orange and rose bengal degradation by employing a controlled experiment approach using a novel UV-LED illuminated photoreactor. The LEDs used in this study have a narrow emission spectrum with a peak at 360 nm (appendix A.8), unlike conventional UV lamps which have broad emission spectra over a range of wavelengths. Methyl orange and rose bengal were selected for the study because they show virtually no absorption of the UV light emitted from the LEDs. This ensured that a photocatalytic process was solely responsible for the dye degradation and not photolysis as exhibited by

dyes such as acid red 51 which easily degrade by photolysis under broad UV illumination[90].

2.2. Experimental methods and materials

Photocatalytic oxidation experiments were carried out in the aqueous phase using a prototype photoreactor. Two compounds were involved in the study and the experimental conditions remained the same for each experiment.

The two reagents used in the study were methyl orange (MO) and rose bengal (RB), they were supplied by Sigma-Aldrich and used as received. Calibration plots for these compounds were prepared with their absorption spectra measured at the highest peaks (Appendix A.1) using a Perkin Elmer Lambda 950 UV/VIS spectrometer (fig. 2.3). Degussa P25 which is a powdered catalyst having nanaoparticles of 30 nm and consisting of crystalline anatase and rutile in the ratio 80:20 was supplied by Evonik and used in all experiments as received. The UV-LEDs used in the study were supplied by AP Technologies and characterized in the lab to determine their optimum operation parameters with a Coherent fieldmaster GS and LM-2UV power sensor.

(a)

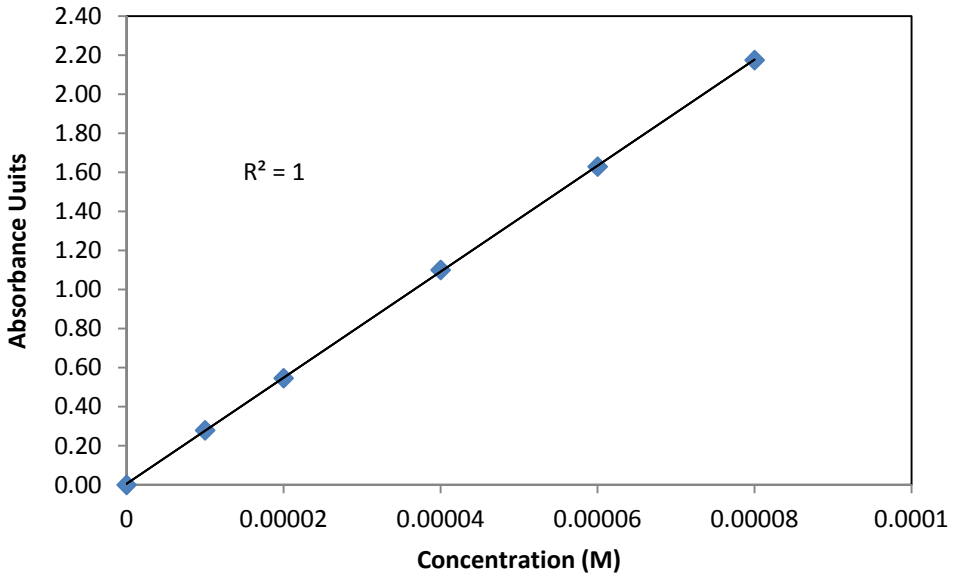

(b)

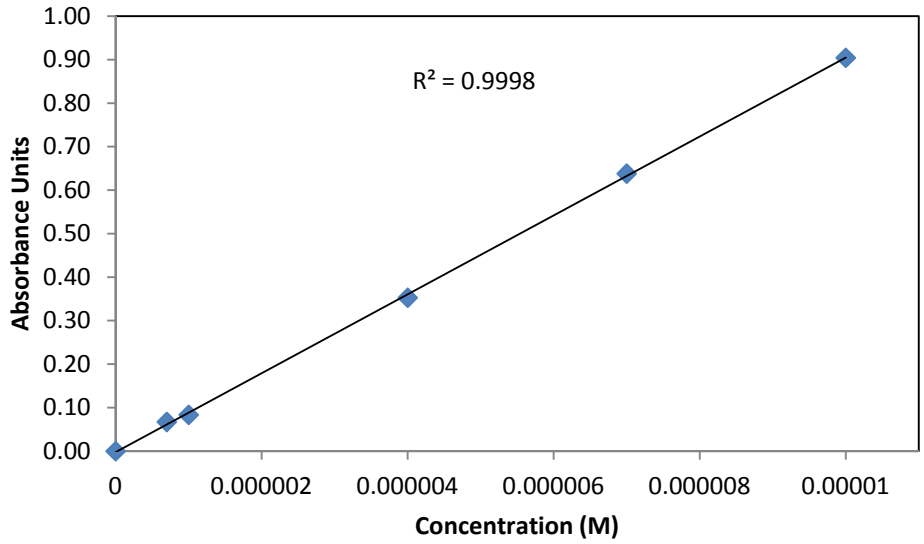

Figure 2.3: Calibration plots of (a) methyl orange dye and (b) rose bengal dye.

For all the experiments, samples of 1 mL were taken in triplicate with a syringe and filtered using a 0.45 µm syringe filter and then centrifuged with an Eppendorf centrifuge 5410 for approximately 10 minutes to separate the powdered catalyst from the sample.

2.2.1. Experimental setup

The experimental setup for the study involved a designed prototype photoreactor which allows for the high frequency pulsing of the UV-LED light source. The pulsing of the LEDs for periodic illumination was controlled by an astable multivibrator; this digital pulsing circuit was designed to operate at a range of duty cycles therefore generating different pulse widths (Appendix A.7). The photoreactor unit was designed using the LEDs connected on stripboards, with six LEDs on each strip and affixed around a PMMA tube; this unit (fig. 2.4) was connected to the astable multivibrator and powered by a Farnell TOPS/2 power supply unit.

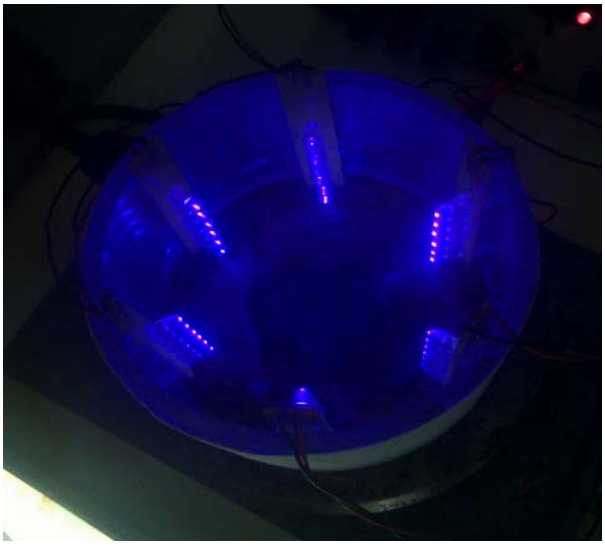

Figure 2.4: Lighting scheme of designed photoreactor.

The photoreactor was placed on a magnetic stirrer with a 250 mL beaker placed within the interior of the photoreactor, serving as the reaction vessel, the TiO_2 suspension along with the compound to be degraded were stirred continuously in the beaker during the experiments with an Ikamag RCT magnetic stirrer. The circular array of LEDs provided illumination from all directions with the magnetic stirrer ensuring the fluidization of the reaction mixture. Figure 2.5 shows a schematic diagram of the experimental setup.

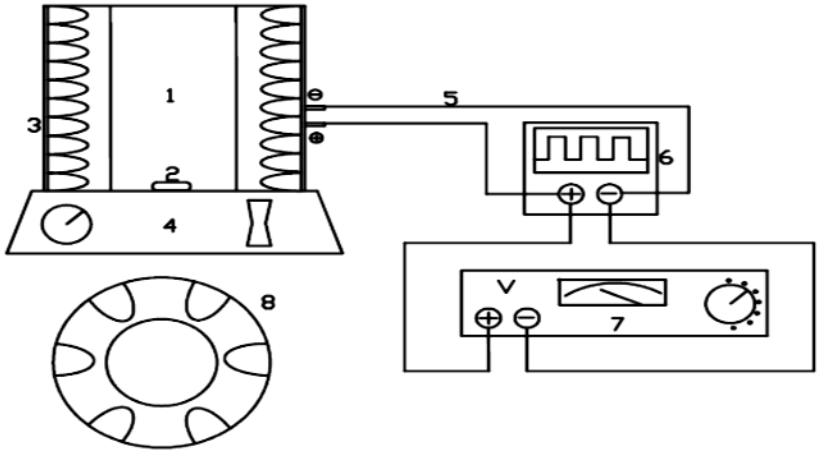

Figure 2.5: Schematic diagram of experimental setup; 1. reaction vessel, 2. stir bar, 3. UV-LEDs attached to outer tube, 4. magnetic stirrer, 5. electric wire connection, 6. pulsing circuit, 7. power supply, 8. aerial view of photoreactor.

2.2.2. Optimisation of photoreactor

The photoreactor unit was optimized with respect to the UV light intensity required for the methyl orange degradation, catalyst loading and operating hours. The optimum parameters of the photoreactor were chosen with their impact on photonic efficiency taken into consideration.

- UV-LED light output

First of all, it was important to ensure the LEDs' light output stability, this was tested in an experiment lasting over six hours to ensure their suitability for the experiments (fig. 2.6). An LED was connected to a power supply and the light beam was directed to a photodiode which generates a voltage based on the intensity of light incident on the sensor.

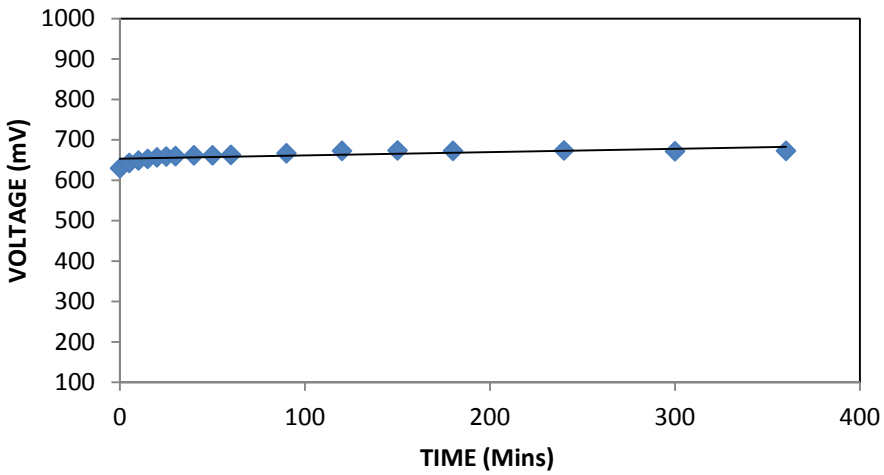

Figure 2.6: FoxUV LEDs stability test over six hours.

The results show this voltage was stable over an operation period of six hours indicating no drop in light intensity or loss of efficiency due to overheating of the LEDs. This is consistent with the manufacturer's life test data on the datasheet which showed stability over 1200 hours[91].

- Optimum light intensity

An experiment to determine the optimum light intensity for the operation of the reactor was carried out using the degradation reaction of methyl orange at different light intensities; methyl orange was chosen as the model pollutant because it is a common pollutant from the textile industry and it is very soluble in distilled water because of the presence of sulphonic groups in its structure[92]. It also undergoes either photo-oxidation or reduction on illuminated TiO_2[93] without the formation of intermediates which can interfere with the reaction. The intensity was varied by changing the number of strips of LEDs. Each strip had 6 LEDs with each LED having a radiant power of 435 μW. The result shown in figure 2.7 shows a linear increase in the percentage degradation up until six strips where the reaction becomes non-linear and approaches saturation.

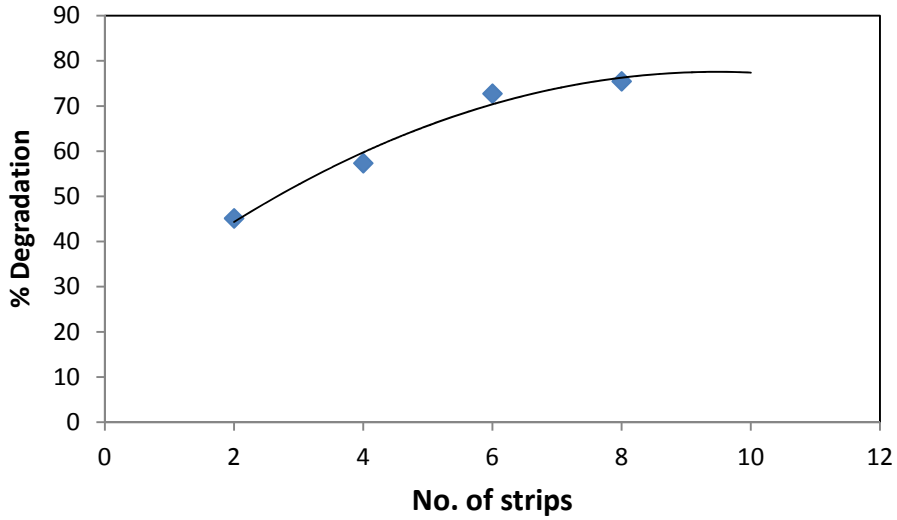

Figure 2.7: Effect of light intensity on the photocatalytic degradation of methyl orange under 140 min of continuous illumination.

At very weak light illumination, the reaction rate of methyl orange degradation is first-order i.e. increases linearly with increasing intensity but this is catalyst dependent, while at intermediate levels of illumination, the rate of reaction will increase with the square root of intensity (half order) and at high intensity, the rate is independent of the light intensity[94, 95] such that when number of strips used is between 2 and 6;

$$r \alpha I^{1},\ r = k[\mathrm{MO}] \qquad (2.3)$$

but when number of strips used is greater than 6, it approaches

$$r \alpha I^{0.5},\ r = k[\mathrm{MO}]^{2} \qquad (2.4)$$

Where r is the reaction rate, I is the light intensity, k is the reaction rate constant and [MO] is methyl orange concentration. This happens because at low light intensity, the predominant reaction is charge separation with a negligible amount of charge recombination but at intermediate levels of illumination, charge recombination competes with separation, this leads to low reaction rates. The light intensities at two, four and six strips were 590 mWm^{-2}, 1190 mWm^{-2} and 1780 mWm^{-2} respectively and these are low intensities relative to the reaction volume, concentration and loading. The intensity at eight strips on the other hand at 2370 Wm^{-2} is in the

medium intensity range, hence the non-linear relationship. For this reason, six strips were chosen as the optimum intensity for this photoreactor and were used in all experiments except where the lowering of the intensity was required.

- Optimum catalyst loading

Generally, kinetic studies on photocatalysis have shown that degradation reaction rates are directly proportional to the loading of the catalyst, but the reaction rate begins to decrease when the kinetic constant reaches a maximum value at a certain level of concentration and rate becomes no longer dependent on the dye concentration[96]. In order to determine the optimum loading of catalyst, experiments were carried out to determine the effect of TiO_2 loading on methyl orange degradation (fig. 2.8).

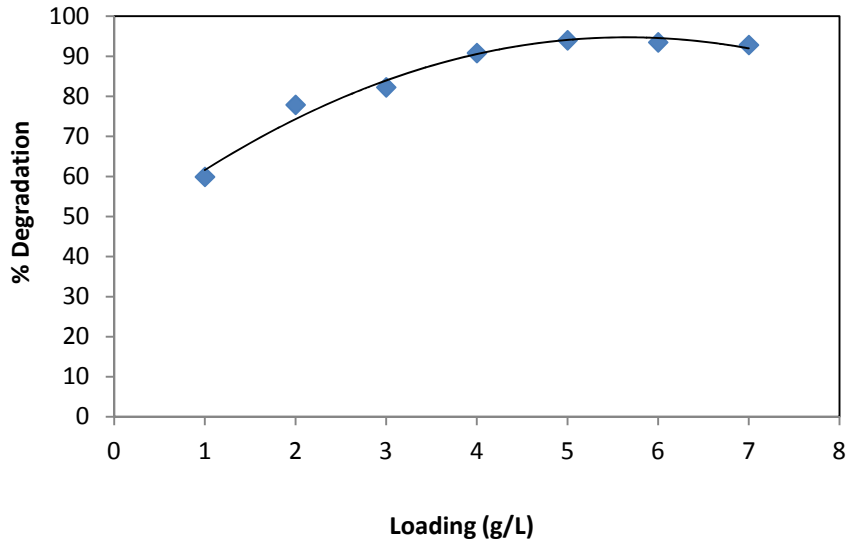

Figure 2.8: Effect of catalyst loading on methyl orange degradation.

The results show an increase in degradation rate when the catalyst loading was increased from 1 g/L to 5 g/L, this is because the degradation of the dye molecules takes place on the TiO_2 surface, therefore an increase in TiO_2 loading results in an increase in the surface area of TiO_2, leading to a higher degradation rate. The optimum loading was 5 g/L because of the monochromatic light emitted from the UV LEDs at 360 nm which is below the band gap energy of TiO_2 hence, a greater light absorption rate by the catalyst. At loadings beyond 5 g/L, increase

in reaction rate is greatly reduced and this has been reported to be as a result of oxygen supply to the catalyst surface at high catalyst loading being the rate-limiting step[97], also the turbidity of the solution increases with an increase in catalyst, leading to light scattering hence fewer particles undergo excitation. This decline in the rate of degradation at high loadings may also be as a result of the deactivation of already activated molecules when they collide with ground state molecules[98] as well as the quantum yield approaching a value of φ =1.

2.2.3. Photocatalytic degradation experiments

The degradation experiments were carried out with 100 mL solution of model pollutant, TiO_2 was suspended in the solution with a loading of 0.5 g and a magnetic stirrer was used to fluidize the solution. Each experiment had duration of 170 minutes including 30 minutes of dark adsorption and sample aliquots of 1 mL were taken at regular intervals. Control experiments (Appendix A.3) were carried out for both TiO_2 and UV light; the TiO_2 control involved carrying out the pollutant degradation experiment under the same conditions in the absence of UV light while the UV control involved carrying out the same experiment in the absence of TiO_2. This was necessary to ensure that degradation was photocatalytic and not just adsorption by the catalyst or photolysis by the UV light. The amount of degradation was determined using the equation[95]:

$$\% \text{ Degradation} = \left[1 - \frac{A_t}{A_0}\right] \text{x } 100 \qquad (2.5)$$

Where A_0 is the initial dye absorbance/peak area before degradation and A_t is the dye absorbance/peak area after time *t*.

2.2.4. Determination of photonic efficiency

The photonic efficiency, ζ of the photocatalytic degradation process was calculated as the rate of reaction of the photocatalytic degradation divided by the incident photon rate[99, 100].

$$\zeta = \frac{\text{Reaction rate (M } s^{-1})}{\text{Incident photon rate (M } s^{-1})} \qquad (2.6)$$

The reaction rate, *r* was calculated as change in concentration with time,

$$r = \frac{C_1 - C_0}{\text{Time}} \quad (2.7)$$

where C_0 is the concentration at the start of illumination and C_1 is the final concentration while the incident photon rate from the UV LEDs determined by the ratio of the total energy of the LEDs to the energy of a single photon was calculated to be 4.85×10^{-8} einsteins L^{-1} s^{-1}.

2.2.5. Photon controlled experimental approach

Controlled experiments help to eliminate the uncertainties that may be associated with results of experiments. The experiments for studying the mechanism of controlled periodic illumination were designed in a controlled experiment fashion (Table 2.1) in order to increase confidence in the outcome of the study.

Table 2.1: Photon controlled experimental approach used in the study.

EXPERIMENT	DEPENDENT VARIABLE	INDEPENDENT VARIABLE	CONTROLLED VARIABLE
1	Photonic Efficiency	T_{on}/T_{off}	Period
2	Photonic Efficiency	T_{off} / Period	T_{on}
3	Photonic Efficiency	T_{on} / Period	T_{off}

The photonic efficiency remained as the dependent variable throughout the different sets of experiments, while the period, T_{on} and T_{off} each served as controlled variables in one set, and independent variable in other sets of experiments, hence providing a critical evaluation of their effects on photonic efficiency.

2.3. Results and discussion

2.3.1. Photocatalytic degradation of methyl orange

The degradation of methyl orange (fig. 2.9) was studied under continuous illumination and CPI at different duty cycles and neutral pH, starting with an initial concentration of 2.5×10^{-5} M, a reaction pathway for MO degradation is proposed based on previous studies[101-103].

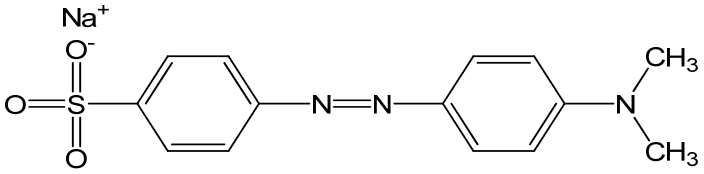

Figure 2.9: Molecular structure of methyl orange.

The TiO_2 particles absorb UV light, leading to the generation of charge carriers. These photogenerated species have to be separated and trapped immediately otherwise recombination occurs, evolving energy as heat.

$$\mathrm{TiO_2} \xrightarrow{hv} \mathrm{e_{cb}^- + h_{vb}^+} \quad (2.8)$$

$$\mathrm{e_{cb}^- + h_{vb}^+} \longrightarrow heat \quad (2.9)$$

The generated holes trapped by the lattice oxygen are transferred to preadsorbed H_2O or directly react with H_2O/OH^- to generate $HO^\bullet$ free radical, the main oxidizing species which gets adsorbed on the TiO_2 particle.

$$\mathrm{OH_{ads}^- + h_{vb}^+} \longrightarrow \mathrm{HO_{ads}^\bullet} \quad (2.10)$$

$$\mathrm{H_2O_{ads} + h_{vb}^+} \longrightarrow \mathrm{HO_{ads}^\bullet + H^+} \quad (2.3)$$

Simultaneously, methyl orange molecules diffuse from the bulk solution to the surface of the TiO_2 particle where it is adsorbed or attached to the preadsorbed H_2O/OH^-.

$$\mathrm{MO_{bulk}} \rightleftharpoons \mathrm{MO/TiO_2} \quad (2.4)$$

$$\mathrm{MO_{bulk}} \rightleftharpoons \mathrm{MO/OH^-(H_2O)/TiO_2} \quad (2.5)$$

The adsorbed hydroxyl radical, $\mathrm{HO_{ads}^\bullet}$ reacts directly with the adsorbed methyl orange or oxygen yielding a peroxy free radical which further reacts with methyl orange[104].

$$\mathrm{HO_{ads}^\bullet + MO_{ads}} \longrightarrow \text{peroxy free radical} \quad (2.6)$$

$$\mathrm{HO_{2_{ads}}^\bullet or\ HO_{3_{ads}}^\bullet + MO_{ads}} \longrightarrow \text{colourless product} \quad (2.7)$$

Figure 2.10 shows the percentage degradation of methyl orange increased as the duty cycle also increased. This increase is as a result of more photons being released into the reactor at higher duty cycles than at low duty cycles. This results in more charge-carriers generated

thereby producing more oxidizing species and consequently, a higher amount of degradation.

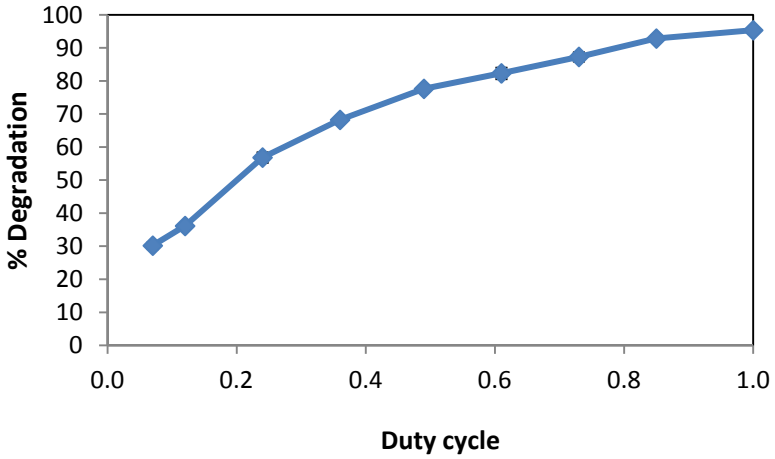

Figure 2.10: Photocatalytic degradation of methyl orange under CPI at different duty cycles.

2.3.2. Effect of catalyst loading on methyl orange degradation under CPI

The photonic efficiency of the photocatalytic degradation of methyl orange under continuous illumination and CPI was investigated at different loadings of TiO_2. The maximum light intensity (I_{max}) from the LEDs was 1780 mWm^{-2}. The light time (T_{on}) was set at 3.36 s while the dark time (T_{off}) was also set at 3.36 s, resulting in a duty cycle, γ of 0.5.

$$\gamma = \frac{T_{on}}{T_{on} + T_{off}} \qquad (2.8)$$

Where γ is the duty cycle, T_{on} is the light time and T_{off} is the dark time.

It was observed that methyl orange degradation was higher for continuous illumination than CPI for all loadings while the photonic efficiency recorded under continuous illumination was found to be lower than that under CPI (fig. 2.11).

(a)

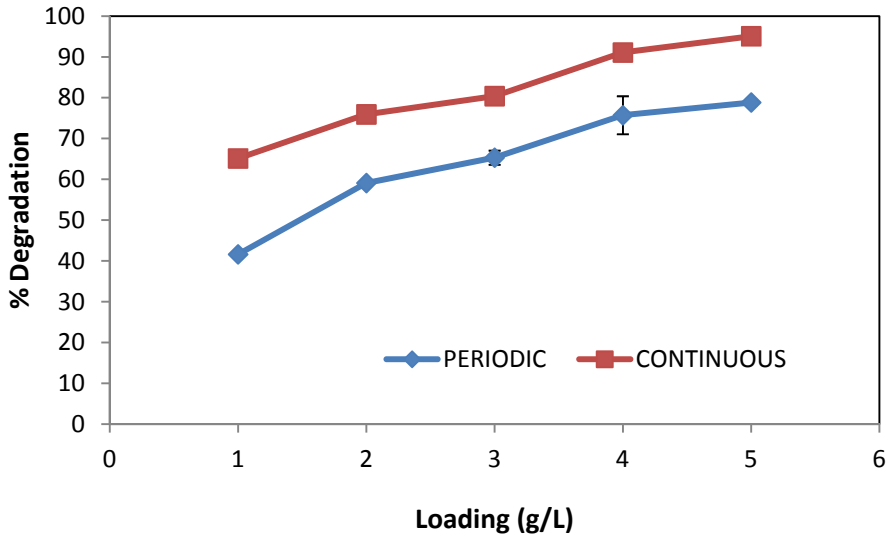

(b)

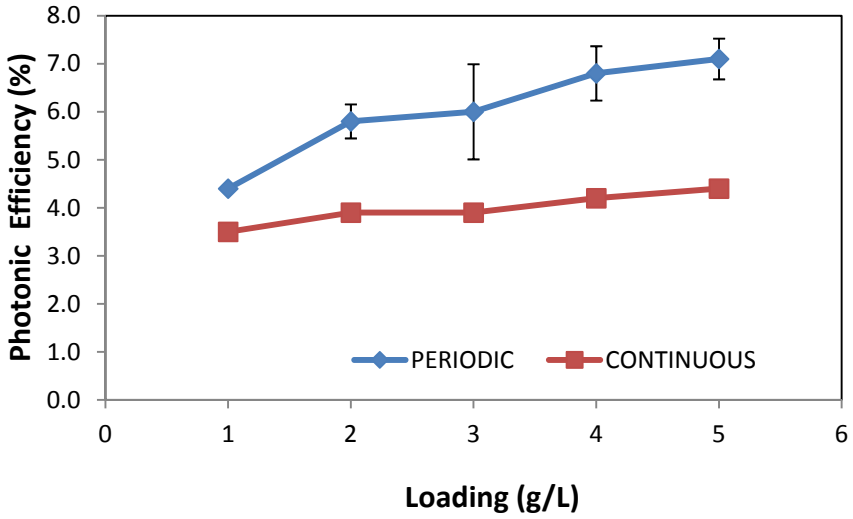

Figure 2.11: (a) Percentage degradation of methyl orange under CPI and continuous illumination; (b) Photonic efficiency of methyl orange degradation under CPI and continuous illumination.

The higher degradation rate of continuous illumination was as a result of the average UV intensity being higher than the average intensity under CPI, as a result more photons were available for degradation of the pollutant over the same reaction period. The higher photonic efficiency recorded under CPI has been attributed to the inefficient use of light

under continuous illumination by Upadhya and Ollis[85], but more recent studies by Buechler *et al*. have suggested that mass transport limitations of oxygen or the substrate to the catalyst surface is responsible for the CPI effect observed here[105]. It was also observed that a higher photonic efficiency was recorded at higher catalyst loading; this can be explained by the higher reaction rates that result from the higher surface area provided since the reaction rate is directly related to the photonic efficiency.

2.3.3. Effect of the duty cycle (γ) on Photonic efficiency

The duty cycle, γ of a controlled periodic illumination is defined as the ratio of the total illumination period to the total operating period and is given in (2.16). What this means is a duty cycle of 0.5 or 50% means the lights are on 50% of the time. An experiment to determine its effect on the photonic efficiency of the photocatalytic degradation of methyl orange was set up with T_{on} and T_{off} varying to give different values of γ at the same periods i.e. given the primary steps occurring during the light time as;

$$Charge - carrier\ generation \qquad TiO_2 \xrightarrow{hv} e^-_{cb} + h^+_{vb}$$

$$Charge - carrier\ recombination \qquad e^-_{cb} + h^+_{vb} \longrightarrow heat$$

$$Charge - carrier\ trapping \qquad h^+_{vb} \longrightarrow h^+_{tr} \qquad (2.9)$$

$$e^-_{cb} \longrightarrow e^-_{tr} \qquad (2.10)$$

and the slower steps of radical formation and interfacial charge transfer, which occur during the dark time (or light time) depending on the pulse duration and lifetimes of generated charges, the various steps for this experiment were constrained within a period of ~1 s, while γ varied accordingly with T_{on} and T_{off} variations. The light time was varied from as little as 72 ms which had a duty cycle of γ = 0.07 to γ = 1 (continuous illumination). Figure 2.12 shows an increase in photonic efficiency as the duty cycle decreases, the highest photonic efficiency was recorded at the lowest value of γ and vice versa indicating an inversely proportional

relationship between photonic efficiency and γ, this is because generally for photocatalytic reactions, a low light intensity results in a high photonic efficiency and periodically illuminating the catalyst is similar to lowering the light intensity when the catalyst is continuously illuminated[106].

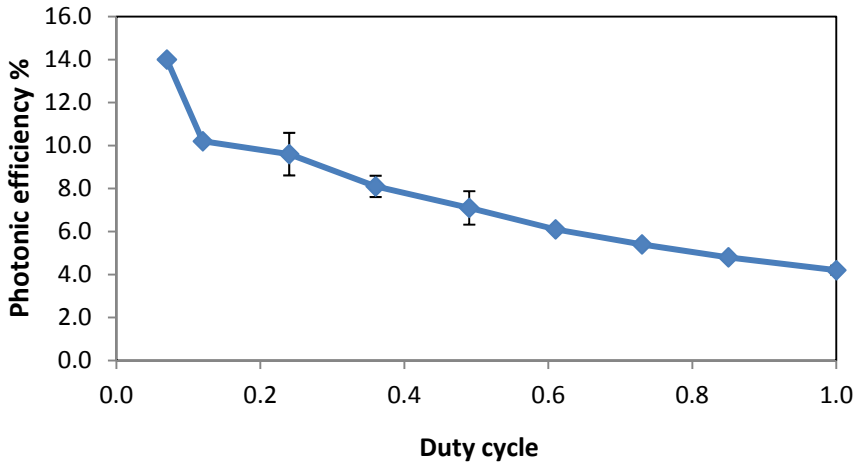

Figure 2.12: Effect of duty cycle on photonic efficiency of methyl orange degradation (See table 3.1 for details of light and dark times).

Photonic efficiency increases with T_{on} reduction because of a corresponding increase in T_{off}. This implies a brief period of charge-carrier generation and less time for charge-carrier recombination (the primary reason for low efficiency[107]) as a result of a decreasing T_{on}. The corresponding increase in T_{off} gives rise to the adsorption of MO to the catalyst surface while also giving ample time for the interfacial charge transfer of electrons to adsorbed oxygen, a step previously identified as rate-limiting in the photocatalytic process[86, 108].

$$O_2 + e^- \longrightarrow O_2^- \qquad (2.19)$$

2.3.4. Significance of the light and dark times

The photonic efficiency of photocatalytic oxidation by illuminated TiO_2 in a non-aqueous media is influenced by the length of the dark time, this was demonstrated by Stewart and Fox[87] who reported an increase in the photonic efficiency of the oxidation of 1-octanol in non-aqueous media by almost 100% when the T_{off} was increased from 0.1 s to 1.0 s. In order to

fully understand the mechanism of controlled periodic illumination in the photocatalytic oxidation of MO, the effect of light and dark times was investigated. Two sets of experiments were carried out in this investigation; the first set involved keeping T_{on} constant at 1.0 s while T_{off} varied from 0.1 s to 1.0 s, corresponding to an incident photon rate of 4.85×10^{-8} einsteins L^{-1} s^{-1} for all values of γ, hence charge-carrier generation and recombination rates, (2.8) and (2.9) and any other reactions occurring during T_{on} were controlled and identical for varying values of γ while the main events of T_{off} (adsorption/desorption) were monitored at $T_{off,\ min}$ = 0.1 s to $T_{off,\ max}$ = 1.0 s. The result in figure 2.13 shows a 38% improvement in the photonic efficiency as T_{off} increases, this dark recovery time has been suggested by Upadhya and Ollis to be devoted to the re-adsorption of oxygen/MO onto the surface of the TiO_2 catalysts.

$$\left.\begin{array}{l} O_{2_{bulk}} \longrightarrow O_2/TiO_2 \\ MO_{bulk} \rightleftharpoons MO/TiO_2 \end{array}\right\} \text{Adsorption on } TiO_2 \qquad (2.11)$$

The oxygen subsequently reacts with the excess electrons hence inhibiting recombination with holes. This improvement is, however, sensitive to the oxygen re-adsorption/reduction rate which is the slowest step in the photocatalytic reaction.

In the second set of experiments, T_{off} was kept constant at 1.1 s, thereby constraining dark time events within that time frame and T_{on} varied from 0.1 s to 1.1 s, thus, incident photon rates had a minimum value of 4.85 x 10^{-9} einstein L^{-1} s^{-1} and maximum value of 5.34 x 10^{-8} einstein L^{-1} s^{-1}, there was also an improvement in photonic efficiency. This improved photonic efficiency reached a minimum value of 6.5%, at the maximum incident photon rate because of the prolonged occurrence of reactions (2.8) and (2.9) without a corresponding increase in time for reactions (2.13) and (2.20). This demonstrates the importance of both the light and dark times when TiO_2 is periodically illuminated, but while increasing T_{off} from 0.1 s to 1.1 s resulted in a 38% increase in photonic efficiency, decreasing T_{on} from 1.1 s to 0.1 s increased the photonic efficiency by 89%.

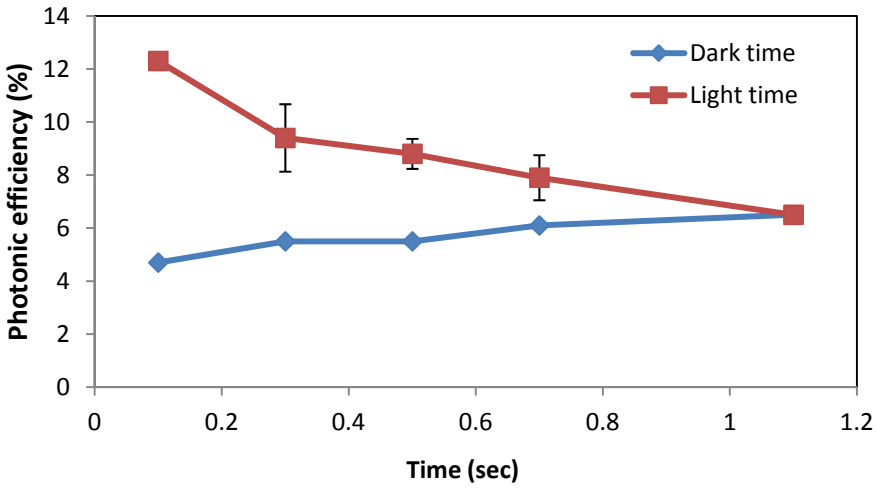

Figure 2.13: Individual effects of light and dark times on photonic efficiency.

An attempt to further understand the results of the three sets of experiments carried out and how they relate to the photonic efficiency was made by taking the results of the three experiments and representing them all on one graph (fig. 2.14).

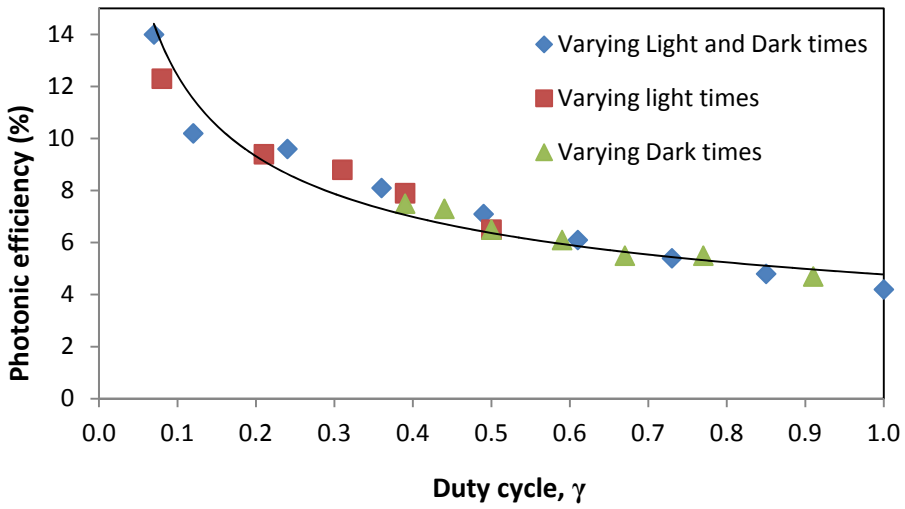

Figure 2.14: General photonic efficiency trend of methyl orange degradation at different T_{on} and T_{off} cycles.

The photonic efficiency of methyl orange degradation shows a downward trend in its value as the duty cycle increases, irrespective of a decrease in the light time (T_{on}) or increase in the dark time (T_{off}). This means the main reason for the increase in photonic efficiency of methyl orange

photocatalytic oxidation observed in the three sets of experiments is the duty cycle rather than the duration of light and dark times. These results agree with the findings of a previous study by Cornu *et al*.[80] which concluded that photonic efficiency of formate ion oxidation by TiO_2 suspensions under periodic illumination is not limited by adsorption/desorption or mass diffusion.

2.3.5. Photonic Efficiency as a function of light intensity

Under periodic illumination, the pulsing effect of the LEDs over the operating period results in reduction of the average light intensity, I_{avg}. As the duty cycle is also reduced, this I_{avg} is further reduced. Photonic efficiency however has been previously reported to increase when the intensity, I_{max} entering the reactor is lowered[106] and it continues to increase until the reaction becomes photon-limited[81]. Furthermore, quantum yields of simple photocatalytic oxidation reactions such as 2-propanol oxidation on TiO_2 in ambient air reach maximum values when the intensity of UV light is low and this is because of minimal losses from charge-carrier recombination and a high coverage of the adsorbed organic substrate[53]. To further understand the actual effect of CPI and how it increases photonic efficiency as opposed to reducing the light intensity under the same conditions, the light intensity was reduced to I_{max} = 1190 mWm^{-2} and experiments were carried out under the same conditions as the first set of experiments previously outlined (fig. 2.15). By varying the power densities, the photons per light pulse of both experiments were different while T_{on} was the same i.e. reactions in (2.8) and (2.9) had the same duration, but occurred at different absorption rates, while T_{off} duration was also the same with reactions in (2.13) and (2.20) times being identical.

(a)

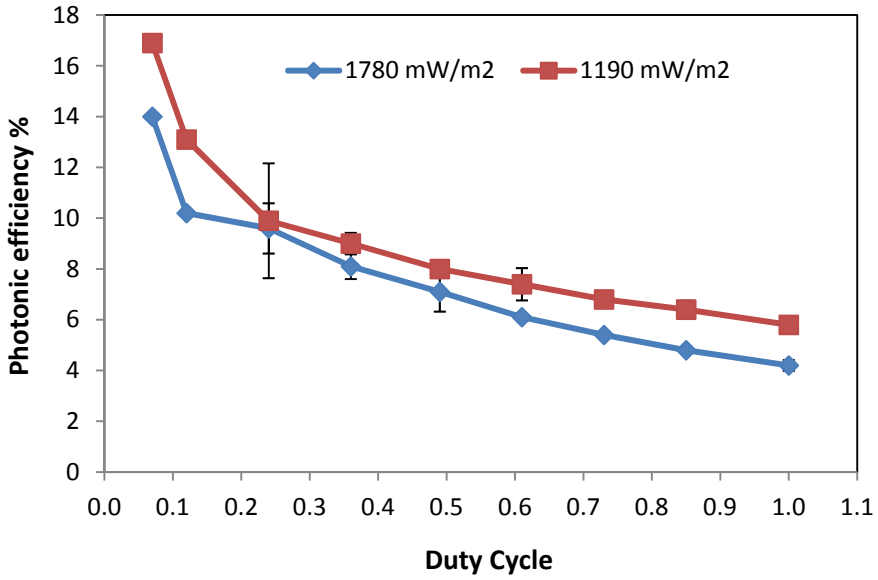

(b)

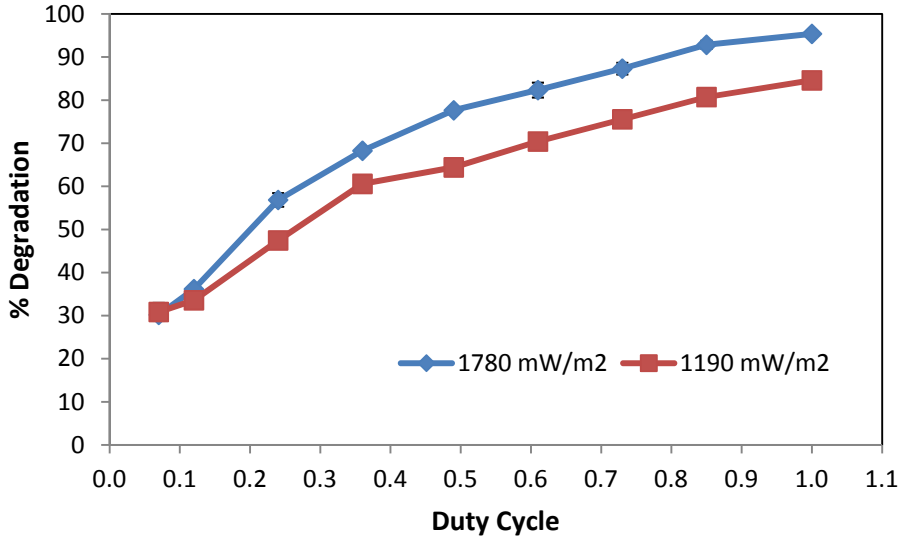

Figure 2.15: (a) Photonic efficiency of methyl orange degradation at different light intensities; (b) Percentage degradation of methyl orange after 170 minutes.

The results show that the photonic efficiency of the photocatalytic oxidation of methyl orange at the lower intensity of I_{max} =1190 mWm^{-2} is greater by an average of 1.5 percentage points than that at the higher intensity (I_{max}=1780 mWm^{-2}) but the degradation follows the opposite trend, at the lower intensity, the percentage degradation is lower than at

the higher intensity, this is because the total number of photons available for photocatalysis is lower than that at a higher intensity, therefore at higher intensities photons are abundant for the conversion of reactants leading to high conversion rates.

Since the high photonic efficiencies that are reported from CPI are as a result of reduction of the average intensity, it is important to compare photonic efficiencies of CPI with continuous illumination at equivalent average intensities. Continuous illumination experiments were carried out at given average powers (mW), the resulting photonic efficiency of the oxidation of methyl orange under these conditions were compared with the equivalent photonic efficiencies at the same average powers under CPI (fig. 2.16).

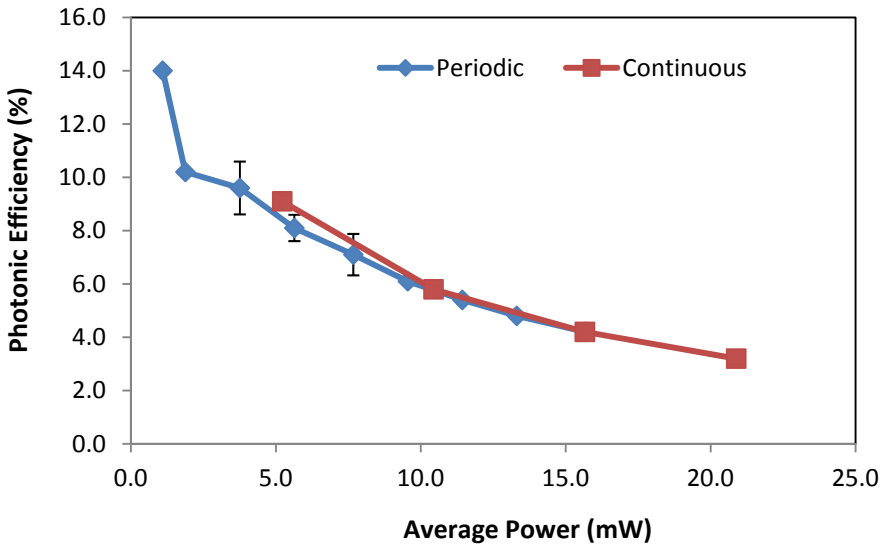

Figure 2.16: Comparison of photonic efficiency under CPI and continuous illumination at equivalent light intensities.

The results show that at equivalent average power, the photonic efficiency under CPI is the same as or almost equal to that under continuous illumination, hence no advantage is gained by using CPI when the average light intensity or the average radiant power is equal to that under continuous illumination.

2.3.6. Photocatalytic degradation of rose bengal

The photocatalytic degradation of rose bengal at different duty cycles was studied using the designed photoreactor, the aim was to validate the trends observed under methyl orange degradation with an entirely different dye compound. Rose bengal (fig. 2.17) was chosen because it belongs to an entirely different class of dye from MO which is an azo dye, RB is a tetraiodo-substituted dye with the chemical formula $C_{20}H_2Cl_4I_4Na_2O_5$ and belongs to the xanthenes class. It shows unusual photochemical and spectroscopic properties such as large absorption coefficient in the visible light region and it has a high tendency for intersystem crossing, producing a photochemically active triplet excited state in the process[109].

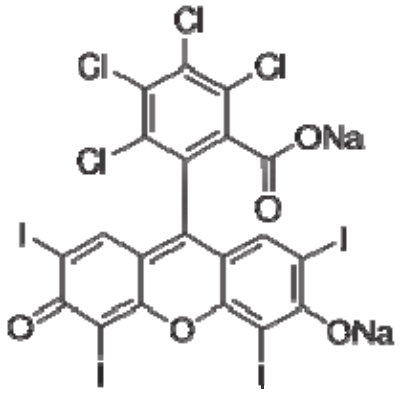

Figure 2.17: Molecular structure of rose bengal.

Rose bengal is an anionic molecule which has a molecular weight that is three times that of methyl orange and a high adsorption on TiO_2 at neutral pH, this high adsorption was controlled by increasing the pH of the reaction solution to 9.6 therefore pH studies could not be carried out with this dye. A mechanism for RB degradation as proposed by Sharma *et al*.[110] indicates $OH^{\bullet}$ as the oxidizing species, oxidizing the dye to its Leuco form.

$$^1RB_o + h\nu \longrightarrow {}^1RB_1 \qquad (2.12)$$

$$^1RB_1 + ISC \longrightarrow {}^3RB_1 \qquad (2.13)$$

$$ZnO + h\nu \longrightarrow e_{cb}^- + h_{vb}^+ \qquad (2.14)$$

$$h^+ + OH^- \rightarrow OH^\bullet \quad (2.15)$$

$$^3RB_1 + OH^\bullet \rightarrow \text{Leuco RB} \quad (2.16)$$

$$\text{Leuco RB} \rightarrow \text{colourless product} \quad (2.17)$$

The initial concentration of rose bengal was 1x 10^{-5} M, figure 2.18 shows an increase in percentage degradation as the duty cycle increased, a similar trend was observed in methyl orange degradation.

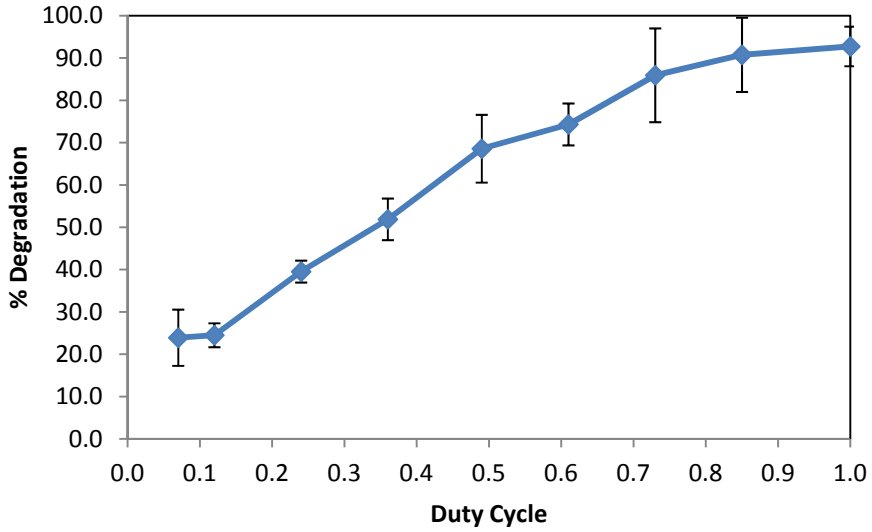

Figure 2.18: Photocatalytic degradation of rose bengal under CPI.

The photocatalytic degradation of rose bengal showed a similar trend to that of methyl orange, as duty cycle increased, the per cent degradation also increased. This is because an increase in duty cycle is an increase in I_{max} and generally for photocatalytic reactions, rate of reaction and amount of substrate degraded increases with increasing UV intensity.

2.3.7. Photonic efficiency of rose bengal degradation

The photonic efficiency of the photocatalytic degradation of rose bengal at various duty cycles was determined using equation (2.6), there was a general increase in photonic efficiency with reducing duty cycle in a similar fashion to methyl orange dye (fig 2.19).

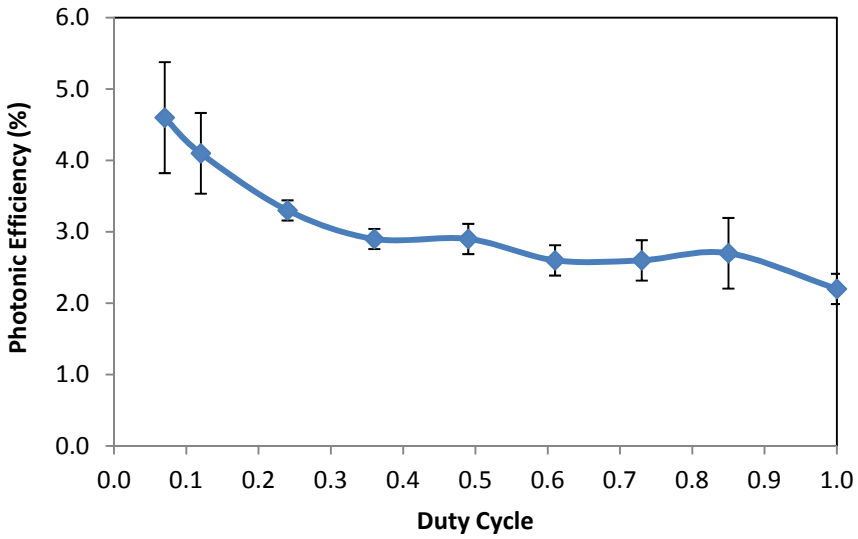

Figure 2.19: Effect of duty cycle on photonic efficiency of rose bengal degradation.

In a similar way to the methyl orange experiment, the reactions of (2.8), (2.9), (2.13) and (2.20) were restricted to a period of ~1 s while T_{on} and T_{off} varied alternately to keep the period constant at different duty cycles, therefore making the period the controlled variable, T_{on} and T_{off} the independent variable while the photonic efficiency was the dependent variable. This indicates an inverse dependence of photonic efficiency on duty cycle.

2.3.8. Impact of light and dark times on rose bengal photonic efficiency

In order to ascertain the trends of impact of T_{on} and T_{off} on photonic efficiency which were observed in the methyl orange experiments, the light and dark time were further controlled in separate experiments with rose bengal dye in order to study their effects on the photonic efficiency. The light and dark time were varied and controlled by the same amount as the methyl orange experiments with the same sequence of light time and dark time reactions taking place (fig. 2.20).

(a)

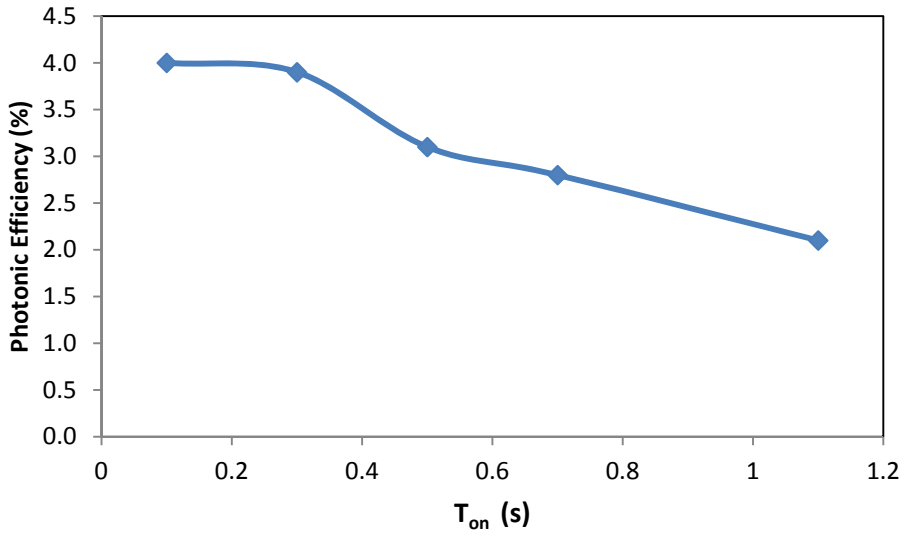

(b)

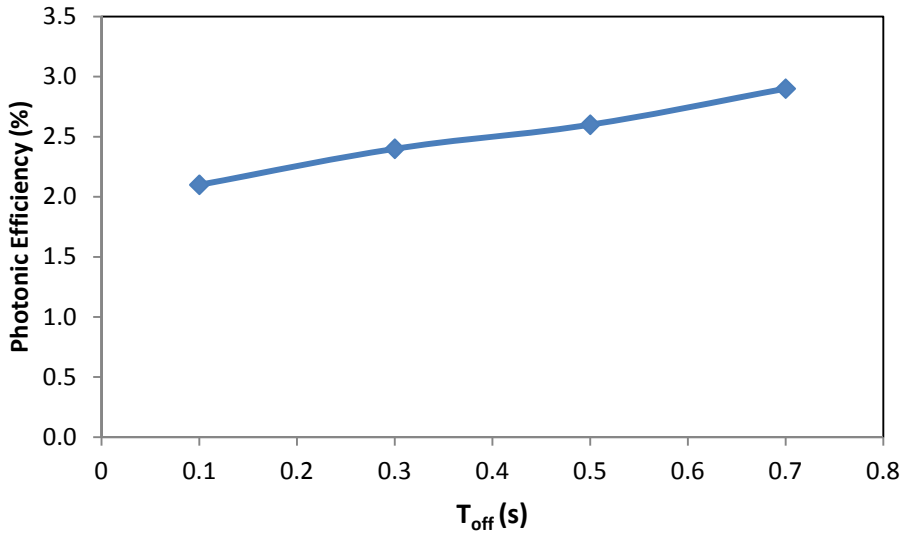

Figure 2.20: Impact of light and dark times on photonic efficiency of rose bengal photodegradation.

The photonic efficiency trends with regards to the individual impact of T_{on} and T_{off} in the photodegradation of rose bengal correspond to that observed in methyl orange. This shows experimentally that both T_{on} and T_{off} contribute to the increase in photonic efficiency irrespective of the reagents involved in the photocatalytic reaction when under CPI. However, the efficiency enhancement from a decreased light time may be more significant than those from an increased dark time.

2.3.9. Overall impact of γ on photonic efficiency

When the overall photonic efficiency trend is plotted using the three sets of experiments, the inverse relationship and dependence of photonic efficiency on the duty cycle is confirmed, indicating a lesser effect of T_{on} and T_{off} compared to γ (fig 2.21).

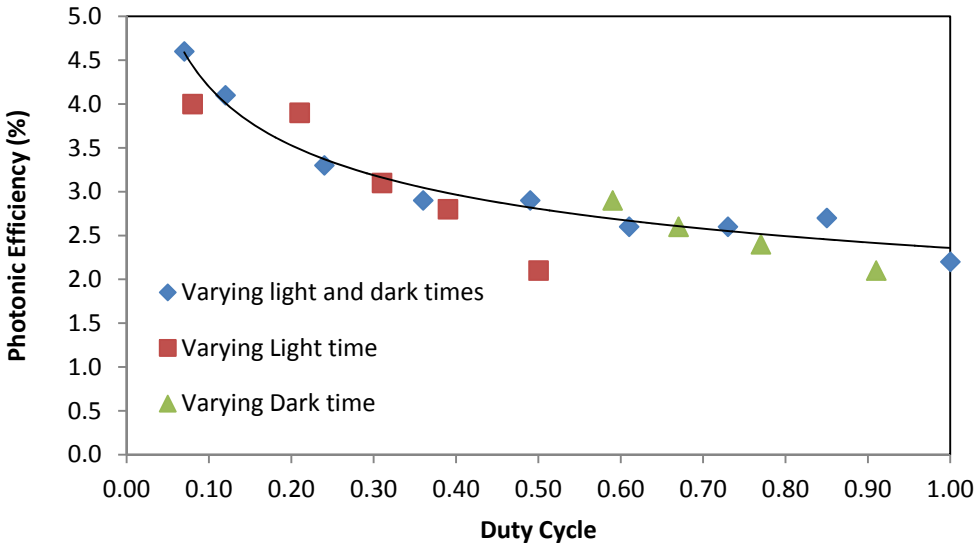

Figure 2.21: Photonic efficiency trend of rose bengal degradation at different T_{on} and T_{off} cycles.

This trend establishes the fact that while T_{on} and T_{off} are responsible for photonic efficiency increases, it is their combined effect as γ that ultimately determines the photonic efficiency improvement of photocatalytic reactions under CPI.

2.4. Conclusion

The use of controlled periodic illumination with UV-LEDs for enhancing photonic efficiency of photocatalytic decomposition processes in water has been investigated using methyl orange and rose bengal as model compounds. The impact of the length of light and dark time periods (T_{on}/T_{off} times) on photo-degradation and photonic efficiency using a UV LED illuminated photoreactor has been studied. The results have shown an inverse dependency of the photonic efficiency on duty cycle and a very little effect of T_{on} or T_{off} time periods, indicating no effect of rate

limiting steps through mass diffusion or adsorption/desorption in the reaction. For this reactor, the photonic efficiency under controlled periodic illumination (CPI) matches to that of continuous illumination, for the same average UV light intensities. Under CPI conditions, the photonic efficiency is inversely related to the average UV light intensity in the reactor, in the millisecond time regime.

CHAPTER III

3. THEORETICAL MODELLING AND OPTIMISATION OF PHOTONIC EFFICIENCY UNDER CONTROLLED PERIODIC ILLUMINATION

3.1. Introduction

In heterogeneous photocatalysis using TiO_2, the Langmuir-Hinshelwood (L-H) rate equation is the simplest model consistent with Langmuir's equilibrium isotherm and is widely applied to photocatalytic reactions[38, 96]. The model (3.1) interprets the photocatalytic rate of reaction, r as a product of the reaction rate constant, k_r of surface species (photogenerated and substrate) and the extent of substrate adsorption, K_{ads}. Competition for adsorption by other species is represented by adding the terms $K_{ads}C$ to the denominator.

$$-\frac{\partial C}{\partial t} = r = k_r \frac{K_{ads}\, C}{1 + K_{ads}\, C} \qquad (3.1)$$

Where the rate r is taken as an initial rate r_0, C is taken as the equilibrium concentration C_e, k_r is the reaction rate constant under experimental conditions and K_{ads} is the Langmuir adsorption coefficient. The model is best applied to reactions that follow the pathway of; (i) adsorption of reacting species on the catalyst surface, (ii) reaction involving adsorbed species, (iii) desorption of reaction products. This rate equation can be significantly influenced by γ of CPI and electrostatic attraction between reactants and catalyst surface which is controlled by the pH; these two parameters are important in optimizing the photonic efficiency of photocatalytic reactions which is proportional to the rate of reaction.

3.1.1. Effect of pH on photocatalytic rate and photonic efficiency

The pH of the TiO_2 nanoparticle suspension plays an important role in photocatalytic reactions taking place on the TiO_2 surface. It can have significant influence on particle stability and/or aggregation, Fermi-level

shifts which determine reduction potentials of electrons, zeta potential of TiO_2 colloids[111], band edge positions and electrostatic interactions of electron donors and acceptors[44, 112] (fig. 3.1).

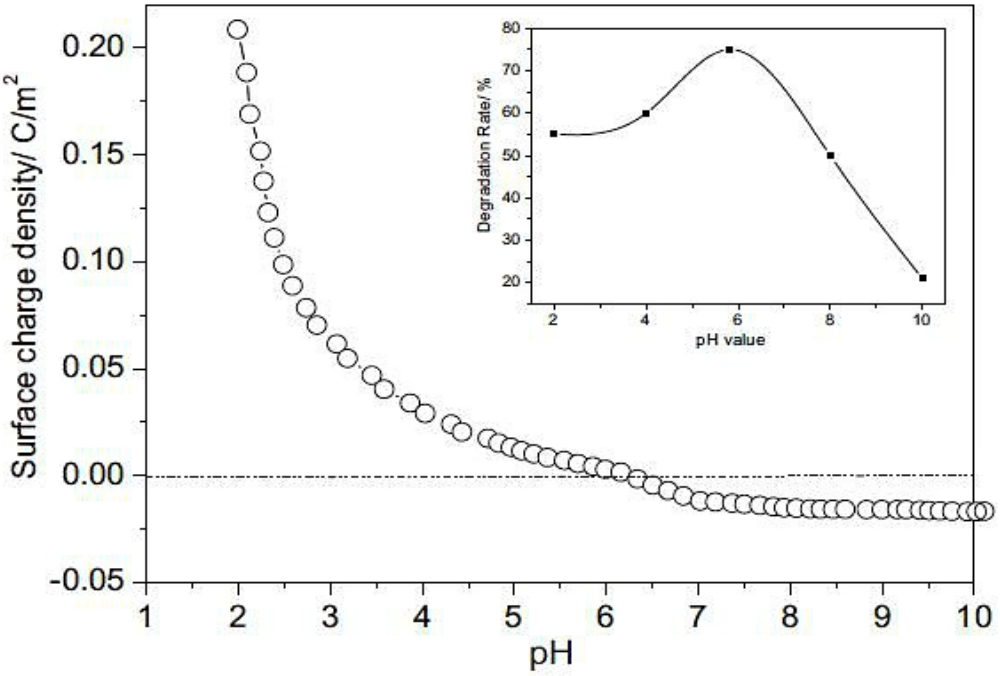

Figure 3.1: Effects of pH on surface charge density of modified P25 catalyst in the degradation of congo red dye from study by Guo *et al*.[113]

The effects of pH have been reported in the literature to have various outcomes which include; a weak dependence of the reaction rate on pH[51], higher photocatalytic conversions at both acidic and alkaline pH, varying effects of pH in the presence of different cations, anions and neutral molecules[114], pH independent photo-oxidation rates[115] and the formation of intermediates[116]. The pH also has an influence on the efficiency of the photocatalytic process, Kormann *et al*.[114] first investigated the influence of pH on photocatalytic efficiency and reported that the photonic efficiency of TiO_2 catalysts at low pH can be decreased by simple anions such as HCO_3^- and Cl^- which have a negligible effect at high pH. Cornu *et al*.[93] found higher photocatalytic quantum yields at extreme pH as a result of a shift in the electrical potential of TiO_2 particles. As a result of these multiple roles, the interpretation of the effects of pH can sometimes be a difficult task.

3.1.2. pH studies under controlled periodic illumination

Studying the effects of pH under controlled periodic illumination (CPI)[84, 100]; a technique based on a series of alternate light and dark periods (T_{on}/T_{off}) which was previously reported as a means of increasing the photonic efficiency and conversion rates in TiO_2 photocatalysis can provide information on the pH-influenced dynamics of the redox reactions taking place during photocatalytic oxidation. Using this technique, Cornu *et al*.[93] observed two distinct transitions in the differential reactivity of oxidizing and reducing species in methyl orange photo-oxidation, the characteristic times of these transitions was determined to be an exponential function of the solution pH.

3.1.3. A modified Langmuir-Hinshelwood rate model for controlled periodic illumination

Chen *et al*.[89] in the decomposition of *o*-cresol under controlled periodic illumination modified the Langmuir-Hinshelwood rate model by incorporating the parameters which account for the pulsing effect of reactions under CPI. Using this model (3.2), they obtained a good agreement between the model and experimental data of *o*-cresol decomposition rates at various initial concentrations (fig.3.2).

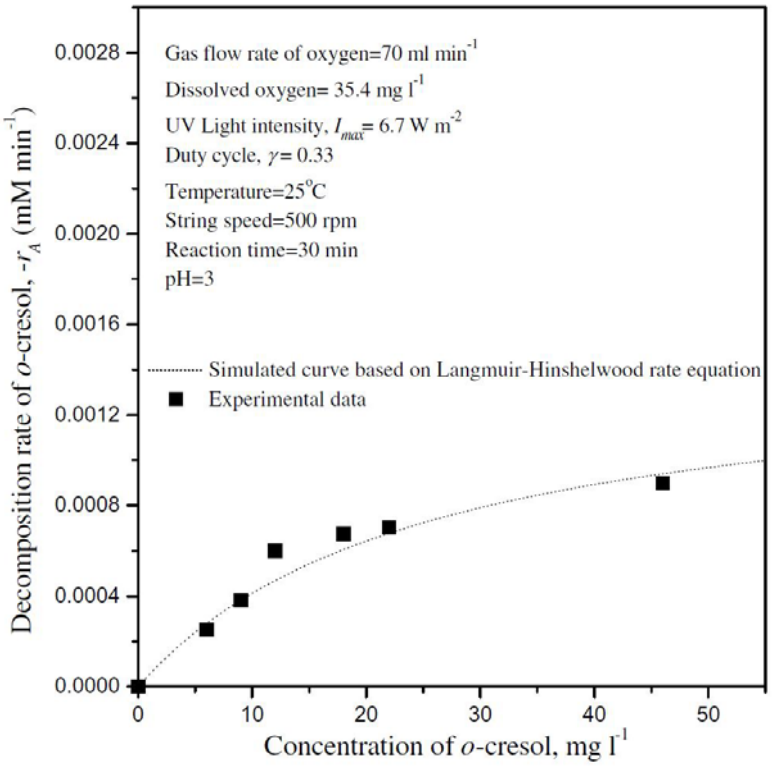

Figure 3.2: Correlation between model and experimental data for o-cresol decomposition using the modified L-H model[89].

The reaction was assumed to take place on the outer surface of the TiO_2 particle and for a photoreactor under periodic illumination, the average light intensity and order of light intensity were incorporated into the rate equation as follows:

$$-\frac{\partial C}{\partial t} = r_0 = k_r(\gamma I_{max})^m \frac{K_{ads}\, C_e}{1 + K_{ads}\, C_e} \qquad (3.2)$$

Where γ is the duty cycle of UV illumination, I_{max} is the light intensity (I_{avg}= γI_{max}) and m is the order of light intensity.

3.1.4. Mathematical model for photonic efficiency under controlled periodic illumination

Upadhya and Ollis[85] proposed a transient kinetic model to show rapid photo-oxidation of surface reactants by the oxidizing species (h_{vb}^+) accounts for high efficiencies in CPI experiments. The model formulation assumed the entire photocatalytic process to occur on a single TiO_2

particle, the factors affecting quantum yield are summarised in the following reactions:

$$TiO_2 + hv \rightarrow e^-_{cb} + h^+_{vb} \quad (\textit{light absorption}) \quad (3.3)$$

$$e^-_{cb} + h^+_{vb} \rightarrow \text{heat (energy)} \quad (\textit{recombination}) \quad (3.4)$$

$$h^+_{vb} + A \rightarrow A^+ \quad (\textit{hole-organic reaction}) \quad (3.5)$$

$$e^-_{cb} + B \rightarrow B^- \quad (\textit{electron transfer to } O_2) \quad (3.6)$$

Quantum yield of the organic substrate was defined as an integral part of the instantaneous quantum yield over time;

$$\varphi = \int k_1\big(h^+(t)\big)\Omega_a(t)dt / \int k_g l dt \quad (3.7)$$

Where k_1 is the oxidation reaction rate constant, h^+ is the hole concentration, Ω_a is the surface fractional coverage of organic substrate, k_g is the light absorption rate constant and l is the incident light intensity. A high quantum yield will be characterized by a high h^+ and total surface coverage of the TiO_2 particle with reactants. Light and dark periods are incorporated for a TiO_2 particle under periodic illumination and the resultant quantum yield is given as:

$$\varphi_{periodic} = \int^{T_{on}+T_{off}} k_1 n_A\big(h^+(t)\big)\Omega_A(t)dt / \int^{T_{on}} k_g l dt \quad (3.8)$$

$$\varphi_{continuous} = \int^{T_{on}} k_1 n_A (h^+)_{ss}\Omega_{A_{ss}} dt / \int^{T_{on}} k_g l dt \quad (3.9)$$

Where n_A is the number of surface sites for organic substrate, T_{on} is the light time, T_{off} is the dark time. The period for the periodic illumination was kept constant at 1 s for different γ from $0 < \gamma \leq 1$. Hole concentration is a function of time and is described by equation (3.10).

$$\frac{d(h^+)}{dt} = k_g l - k_r(h^+)(e^-) - k_1(h^+)\, n_A\Omega_A \quad (3.10)$$

3.1.5. Optimising photonic efficiency through pH effects and controlled periodic illumination

The pH has a strong influence on the standard driving force, -ΔG°' for interfacial charge transfer[117], -ΔG°' determines the rate constant for interfacial electron-transfer (fig. 3.3).

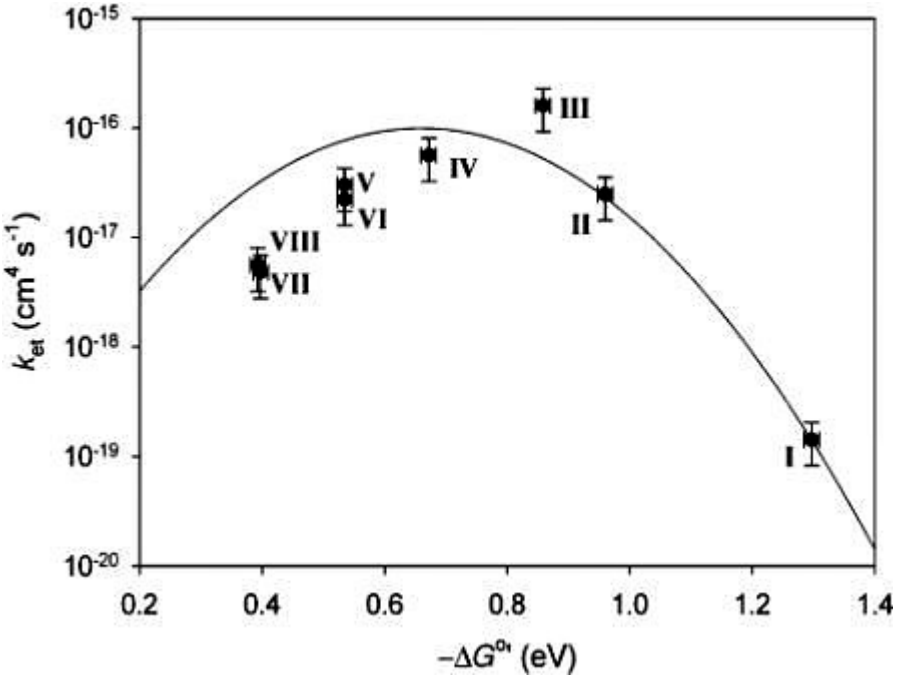

Figure 3.3: Dependence of electron-transfer rate constant on -ΔG°'[117].

In alkaline medium, the standard redox potential of e_{cb}^- is more negative while an acidic medium results in that of h_{vb}^+ being more positive[93], CPI can be used to ensure T_{on} approaches charge-carrier lifetimes thus reducing carrier recombination or design T_{on} to match the characteristic time for interfacial electron-transfer to O_2 which is the slowest step in the photocatalytic reaction[48]. Likewise T_{off} which is devoted to the replenishment of O_2 can also be adjusted to an optimum duration to facilitate further removal of excess e_{cb}^- generated in the next T_{on}[87].

In this chapter, the effect of pH on the photonic efficiency of TiO_2 photocatalysis has been investigated by studying the photodegradation of methyl orange within a range of γ under continuous and controlled periodic illumination. Methyl orange dye was selected for the study because of its anionic nature which corresponds to the electrostatic

interactions required for the study. Ultraviolet light emitting diodes (UV-LEDs) have recently become an alternative UV source to conventional lamps in photocatalysis research[118-121] have the advantage of high efficiency, minimum heat generation, suitability for periodic illumination, narrow band emission and long life[122, 123]. This study pioneers the use of UV-LEDs to study the effect of pH on photonic efficiency of TiO_2 photocatalysis under controlled periodic illumination. The triple effect of pH, γ and characteristic times of primary redox processes as well as the role of oxidizing species on the photonic efficiency trends in the photocatalytic reaction are also investigated.

3.2. Theoretical methods and solution

The two models used in the study were of varying degrees of complexity and both required the use of software applications. The methods employed were also in agreement with the published literature.

3.2.1. Model solution

For the mathematical modelling of methyl orange photo-oxidation rates using the modified L-H model, Microsoft office 2007 excel spreadsheets were used. The inbuilt formulas were sufficient for the calculations required in the model solution. The model solution for photonic efficiency under CPI required a more advanced mathematical software application because of the stiff set of differential equations, Mathematica 9 computational software program was adopted.

3.2.2. Base case parameter values

The same values adopted from the literature by Upadhya and Ollis[85] were used for the constants and parameters in the study. In order to solve (3.10), a steady state approximation was adopted for electron concentration, it was calculated from typical values of h_{vb}^+ quantum yields[124] with the assumption that equal number of holes and electrons are generated. Surface fractional coverage was taken to be constant, it was assumed to be $7 \times 10^{12}\ \mathrm{cm}^{-2}$. An assumption of 50 photons absorbed in T_{on} of 1 s was also made.

3.3. Experimental methods and materials

The experimental materials employed in this investigation are the same as those in the preceding chapter (section 2.2); the TiO_2 catalyst (Degussa P25) was supplied by Evonik and used as received. Methyl orange dye supplied by Sigma-Aldrich was used as the model pollutant. The methods are similar but vary in the adjustment of pH, concentration and the use of the constant period experimental design of CPI to study the interaction between several factors affecting photonic efficiency.

3.3.1. Design of photocatalytic experiments

Three sets of experiments were performed by irradiating TiO_2 suspensions in a stirred photoreactor (fig. 2.4). A high loading of the TiO_2 photocatalyst at 5 g/L which was the optimum for the low UV intensity employed in the experimental setup. It was suspended in 100 mL methyl orange solution in distilled water with concentration of $1x10^{-5}$ M. The photocatalytic degradation of methyl orange solution was carried out over a period of 170 min including 30 min of dark adsorption which was experimentally determined as the time taken for adsorption equilibrium at room temperature, pH adjustments only resulted in more dye molecules adsorbed with no impact on time taken.

3.3.2. Experimental pH and duty cycle

The three experiments were carried out at pH 4, 7 and 9.6, the pH values of the resulting suspension were adjusted using carbonate-bicarbonate buffer capsules for alkaline pH and nitric acid for acidic pH; both supplied by Sigma-Aldrich. The TiO_2 suspension was illuminated under steady and intermittent UV light regimes resulting in five duty cycles, each with varying light and dark times (T_{on}/T_{off}) as shown in Table 3.1.

Table 3.1: Light regimes for continuous and periodic illumination showing duty cycle and frequency of pulsing.

DUTY CYCLE (γ)	Average UV Intensity ($\mu W/cm^2$)	T_{ON} (ms)	T_{OFF} (ms)	PERIOD (ms)
0.01	1.8	10	966	976
0.05	8.9	50	924	974
0.07	12.5	72	904	976
0.24	42.7	234	740	974
0.49	87.2	474	500	974
0.73	129.9	708	266	974
1.00	178.0	CONTINUOUS ILLUMINATION		

The array of LEDs, stirring of slurry and small diameter of the reaction vessel ensured maximum interaction between photons and catalyst and the elimination of dead zones within the reactor. Light pulses for intermittent illumination were generated by an electronic astable multivibrator.

3.4. Experimental results and discussion

The photo-oxidation process is initiated by the illumination of the TiO_2 suspension to generate charge-carriers; e_{cb}^- and h_{vb}^+ (3.11). The photogenerated holes oxidize preadsorbed H_2O and OH^- to produce $OH^\bullet$ radical (3.12). The results of this study propose methyl orange photo-oxidation by free $OH^\bullet$ radicals and surface-trapped $\{Ti^{IV}OH^\bullet\}_{ads}^+$ acting as the oxidizing agents with respect to γ and the pH of the solution. However, most organic compounds can also be oxidized directly by h_{vb}^+ depending on the experimental conditions[125, 126].

$$TiO_2 + h\nu \rightarrow h_{vb}^+ + e_{cb}^- \quad (3.11)$$

$$OH^- + h_{vb}^+ \longrightarrow OH^\bullet \quad (3.12)$$

3.4.1. Photo-oxidation of methyl orange at pH 4, 7 and 9.6

Experiments were carried out to investigate the influence of pH on the photonic efficiency of methyl orange photo-oxidation in acidic, neutral and alkaline media at various γ. An initial concentration of $1x10^{-5}$ M was used and the experiments were carried out at pH 4, 7 and 9.6 with γ within the range γ = 0.01 - 1.00. Methyl orange showed a steady rate of degradation at all experimental conditions because the reaction pathway involves unstable intermediates that are less reactive than methyl orange and present in low concentrations[127, 128].

However, for pH 7 and 9.6 at γ = 0.01 and 0.05, T_{on} was very brief resulting in extremely weak average UV intensity of 1.8 μW/cm^2 and 8.9 μW/cm^2 respectively. The electrostatic attraction between methyl orange molecules and the TiO_2 catalyst required for the Langmuir-Hinshelwood type surface reaction was also weak at pH 7 and 9.6 compared to pH 4 which recorded substantial degradation. Consequently, no change in methyl orange concentration was recorded for pH 7 and 9.6 at γ = 0.01 while change in concentration was negligible after the introduction of photons at γ = 0.05. In addition, for these pH, the weak average UV-LED intensity and weak electrostatic attraction were significant and influential in the determination of photonic efficiency (fig. 3.4) which showed a downward trend at γ < 0.07.

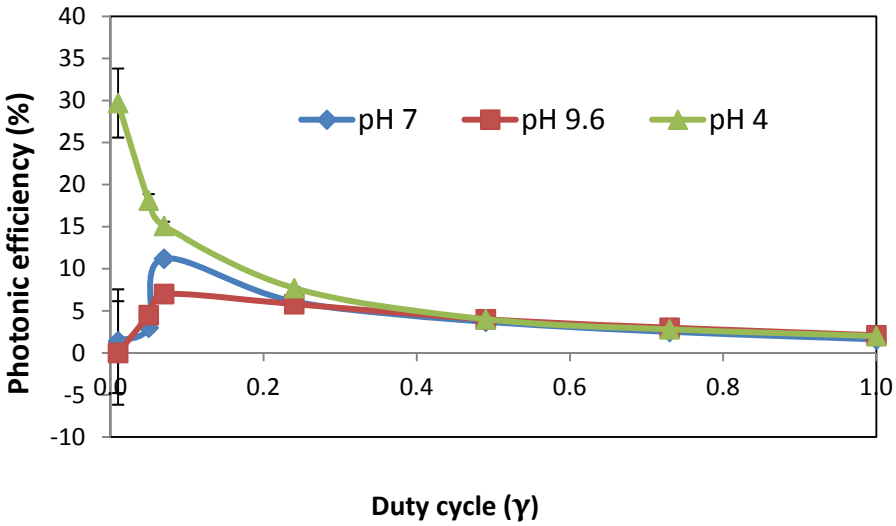

Figure 3.4: Continued increase of photonic efficiency at γ < 0.07 for pH 4.

This however does not suggest trends opposing results of previous studies[93] which also showed under acidic conditions, an oxidative pathway (UV absorbance at 468 nm) was followed for the MO destruction while at higher pH a reductive pathway (UV absorbance at 247 nm) was observed. Hence, experimental results from γ = 0.07 to γ = 1.0 were employed in the analysis. A 100 percent degradation of the dye was observed before the total reaction time elapsed for pH 4 and 7 at γ = 0.73 and γ = 1 respectively (fig.3.5) while degradation at pH 9.6 was slower and lower with the highest percentage degradation of 88 percent recorded at γ = 1.

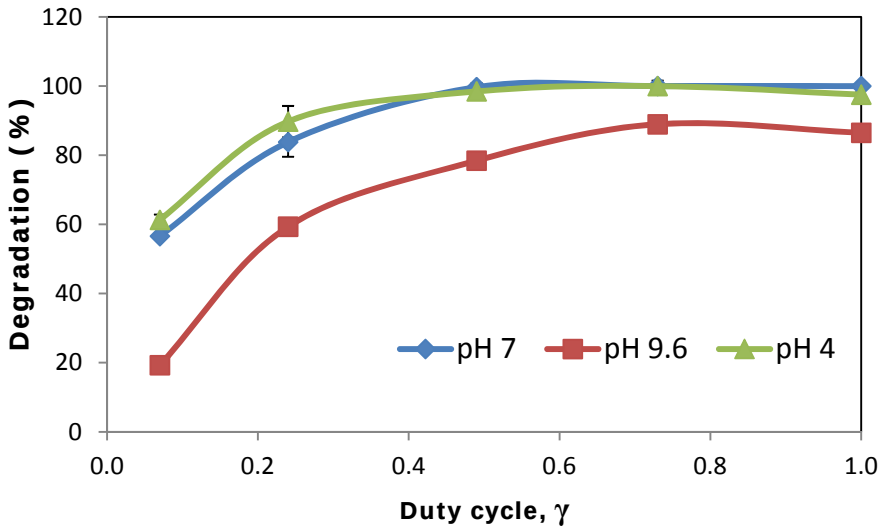

Figure 3.5: Amount of methyl orange photodegradation after total reaction time (170 min) at acidic, neutral and alkaline pH

The photonic efficiency of the photo-oxidation reaction was observed to increase with decreasing γ (fig. 3.6), obtained photonic efficiencies were comparable for the three pH values at γ = 1, 0.73 and 0.49.

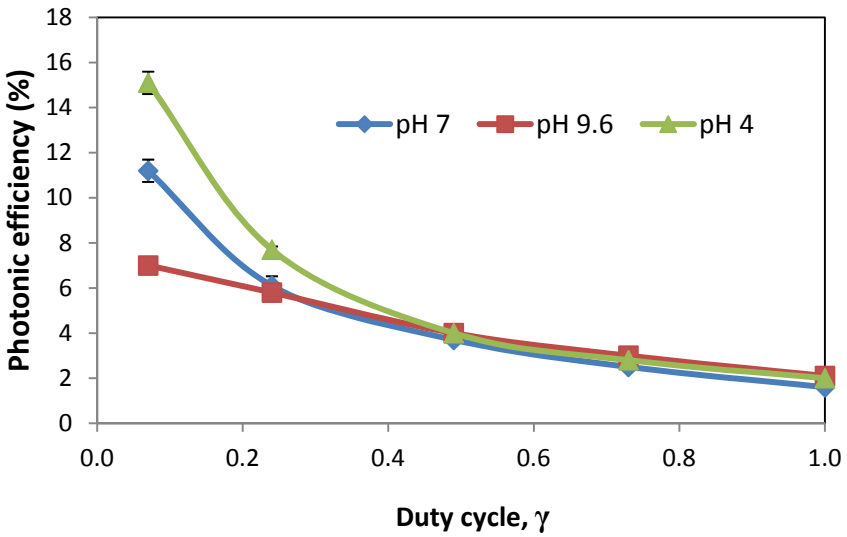

Figure 3.6: Photonic efficiency of methyl orange degradation at γ = 0.07–1.00

In order to ensure accuracy in the calculation for percentage degradation and photonic efficiency profiles of the reaction at the various pH, the reaction time was taken to be the time from the start of the reaction to a time just before complete degradation in pH 4 and 7 where the experiment goes on for about 40 min after complete degradation (fig 3.7). This was necessary to avoid inaccuracies in the calculation of the photonic efficiency which is expressed as the rate of reaction per incident photons therefore a reaction time of 100 min was used for analysis of the results.

(a)

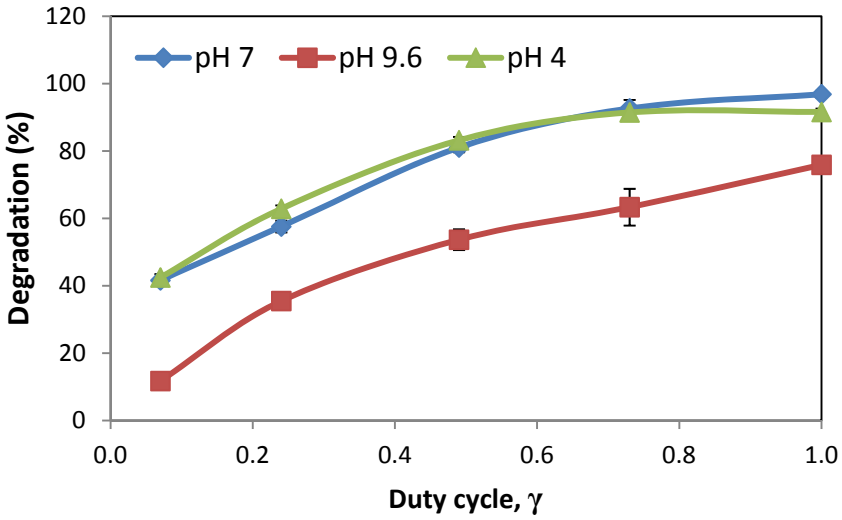

(b)

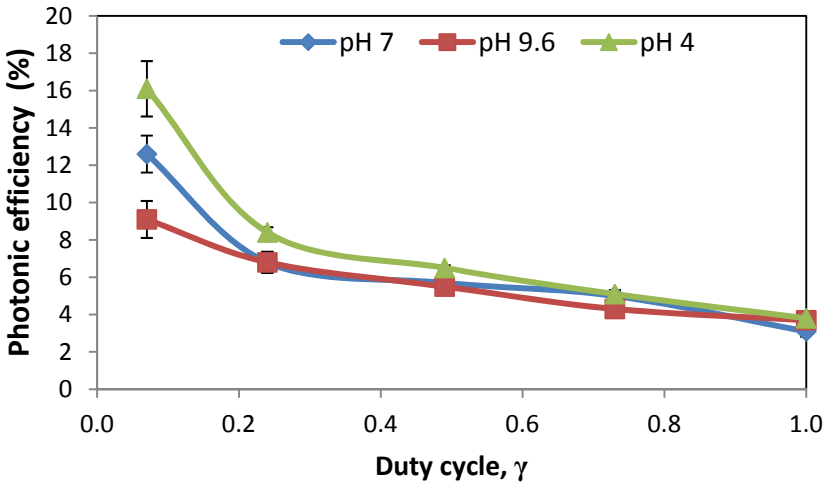

Figure 3.7: Adjusted profiles at various duty cycles of (a) photodegradation of methyl orange; (b) photonic efficiency of methyl orange photodegradation

The trend of methyl orange degradation and photonic efficiency remained the same after adjustment of data points indicating a fundamental trend in the reaction mechanism.

3.4.2. Effects of pH on methyl orange photo-oxidation under controlled periodic illumination

The experimental results show a higher percentage of degradation as γ increases irrespective of pH and particularly at pH 4 and 7 which had almost twice the amount of degradation for pH 9.6 at each γ. This is due to the higher adsorption of methyl orange dye molecules unto the TiO_2 surface at acidic and neutral pH (fig. 3.8).

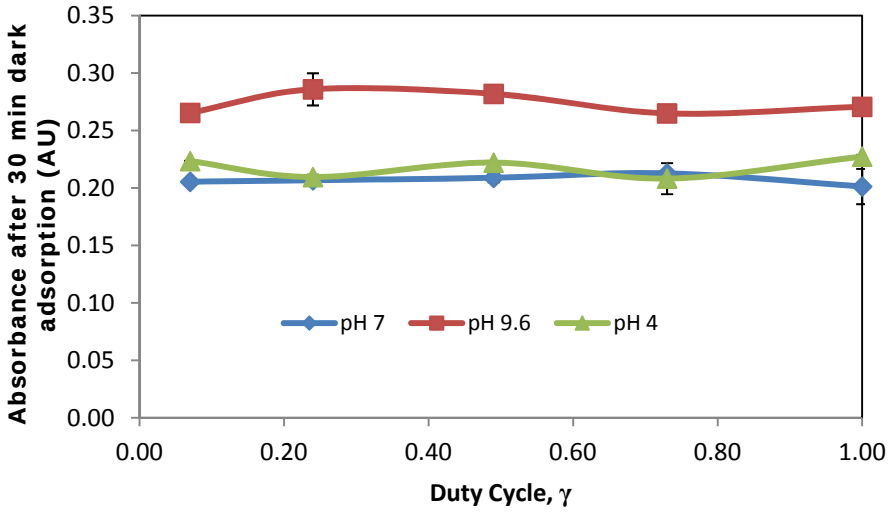

Figure 3.8: Effect of pH on adsorption of methyl orange on TiO_2 surface

Methyl orange is an anion with a negatively charged sulphonic group while TiO_2 (Degussa P25) has a point of zero charge of ~6.25[129] and is positively charged in acidic media. This leads to a strong electrostatic attraction between the dye molecules and TiO_2 surface at these pH with the attraction at pH 4 stronger than that at pH 7. This pH influenced adsorption has been reported to be a critically important step for photocatalytic oxidation to take place and enhances photodegradation efficiency[130, 131]. On the other hand in alkaline pH, TiO_2 is negatively charged giving rise to a coulombic repulsion between the negatively charged methyl orange substrate and TiO_2 surface[132] therefore, preventing or inhibiting the adsorption of substrate molecules on the catalyst hence resulting in a lower degradation of dye molecules.

The degradation rates at pH 4 and pH 7 are observed to approach similar values, this could be as a result of pre-adsorption of the substrate on the catalyst surface prior to the commencement of the photocatalytic reaction. At pH 4, the electrostatic forces of attraction between surface-trapped hole/catalyst surface and dye molecules is strongest resulting in a high density of methyl orange ions on the surface without any catalyzed photoreaction (which is characteristic of dyes) taking place (3.13 -3.14). This is due to the wavelength of UV illumination at 360 nm being lower than methyl orange UV absorption wavelength hence, limiting photon absorption by the catalyst.

$$\mathrm{Dye_{ads}} + \mathrm{hv} \rightarrow \mathrm{Dye^{\bullet}_{ads}} \qquad (3.13)$$

$$\mathrm{Dye^{\bullet}_{ads}} + \mathrm{TiO_2} \rightarrow \mathrm{Dye^{+\bullet}_{ads}} + \mathrm{TiO_2(e^-)} \qquad (3.14)$$

At pH 7 the solution is neutral and electrostatic forces of attraction are weak however, the effects of pH on photocatalytic rates favour a faster degradation of methyl orange at this high pH because of a strong influence on the standard driving force for interfacial charge transfer[117]. It has been shown pH may affect the rates of TiO_2 photocatalysis by causing a shift in the electrochemical potential of the TiO_2 surface[133, 134] thus, the standard redox potential of e_{cb}^- is more negative at high pH therefore forcing O_2 reduction (3.15) which is the rate limiting step in photocatalytic reactions and consequently, a high amount of methyl orange degradation at this pH.

$$\mathrm{O_2} + \mathrm{e^-_{cb}} \rightarrow \mathrm{O_2^-} \qquad (3.15)$$

This effect is not characteristic of pH 9.6 because of the very strong coulombic repulsion that exists between the TiO_2 surface and methyl orange molecules.

3.4.3. Role of active oxidative species

Photogenerated holes have a high quantum yield of 5.7×10^{-2} for ordinary photocatalytic reactions[124] and are readily trapped at the hydrated TiO_2 surface during the oxidation of surface-bound OH^- ion groups to $OH^{\bullet}$

radicals because of their small effective mass[135] (3.16). Furthermore, $OH^{\bullet}$ radicals adsorbed on the surface of the hydroxylated TiO_2 particle are easily assimilated and are indistinguishable from surface-trapped holes[136]. The resulting $\{Ti^{IV}OH^{\bullet}\}^{+}_{ads}$ is readily available for oxidative reactions with the surface adsorbed methyl orange (3.17).

$$h^{+}_{vb} + > Ti^{IV}OH \rightarrow \{Ti^{IV}OH^{\bullet}\}^{+} \qquad (3.16)$$

$$\{Ti^{IV}OH^{\bullet}\}^{+}_{ads} + MO_{ads} \rightarrow \text{colourless product} \qquad (3.17)$$

The results suggest that the two oxidizing species responsible for methyl orange photo-oxidation; surface-trapped holes $\{Ti^{IV}OH^{\bullet}\}^{+}_{ads}$ and free $OH^{\bullet}$ radical are dominant at different pH when impacted on by a T_{on}/T_{off} cycle (fig.3.9). Studies by Ishibashi *et al.*[124] have shown that quantum yields of $OH^{\bullet}$ radical production during TiO_2 photocatalysis are generally lower than those of h_{vb}^{+}. However, at high γ such that $\gamma \geq 0.49$, charge-carrier recombination occurs by second-order kinetics[137], this means rapid depletion of charge-carriers especially the highly oxidative h_{vb}^{+} before and after trapping. This leads to photo-oxidation in the bulk solution by free $OH^{\bullet}$ radical, the oxidative species with a lower redox potential being the predominant.

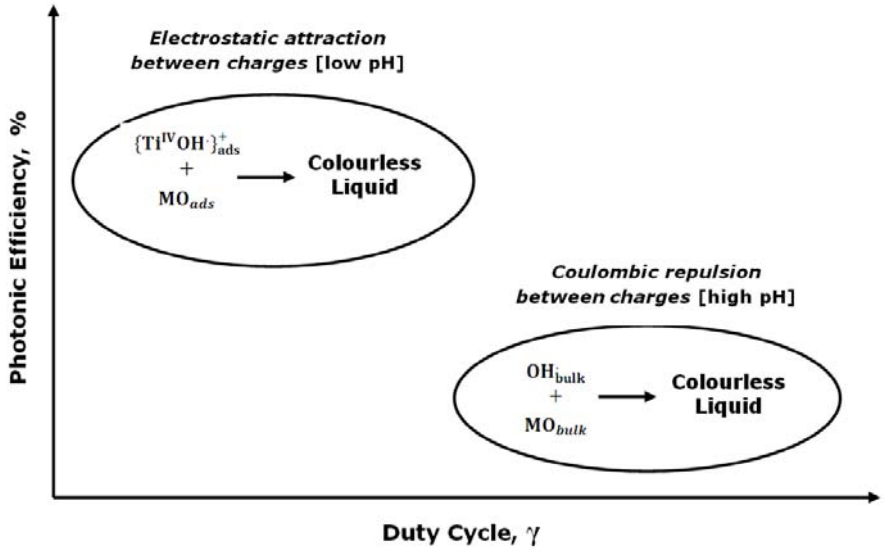

Figure 3.9: Effect of pH and γ on the role of oxidizing species

At pH < 7 with $\gamma \leq 0.49$, the reaction is characterised by low charge-carrier recombination because of the brief illumination periods and methyl orange molecule which acts as a hole scavenger strongly bound to the photocatalyst surface due to the strong electrostatic attraction between the opposite charges. This leads to surface-mediated reactions being the prominent stoichiometry observed[138, 139].

At pH > 7 with $\gamma \geq 0.49$, the reaction is characterized by weak adsorption as a result of the coulombic repulsion between TiO_2 which has a negative charge in alkaline pH and the similarly charged dye anion. High charge-carrier recombination may also limit $\{Ti^{IV}OH^{\bullet}\}^{+}_{ads}$ at the surface thus, the predominant oxidizing species is the free electrically neutral $OH^{\bullet}$ radical having an unpaired electron. The $OH^{\bullet}$ radical primarily attacks places on the methyl orange molecule having the greatest value of double-bond characters giving rise to photo-oxidation of methyl orange by $OH^{\bullet}$ radical in the bulk solution[140] (3.18).

$$OH^{\bullet}_{bulk} + MO_{bulk} \longrightarrow \text{colourless product} \qquad (3.18)$$

3.4.4. Overall effect of pH and γ on photonic efficiency

The pH and γ both affect the dynamics of the photocatalytic reaction in separate ways however, there is a combined effect of these two on the photonic efficiency of the photocatalytic reaction. In figure 3.6, the photonic efficiency of methyl orange photodegradation follows a similar trend across the three pH values investigated when γ falls within the range $\gamma > 0.24$. In this region, the pH has a lesser influence on the photonic efficiency than γ and the increasing efficiency observed is as a result of a decrease in the illumination time and a corresponding decrease in γ. Charge-carrier generation which occurs in $\sim 10^{-15}$s [48] is typically high because of the prolonged T_{on} which far exceeds 10^{-15}s and this leads to high recombination rates leading to low photonic efficiency. At $\gamma \leq 0.24$, the photonic efficiency of the reaction shows a peculiar trend as the effects of pH become significant and the divergence of the trend with respect to pH is accentuated with the further decreasing γ. At $\gamma = 0.07$, charge-carrier recombination is low and photonic efficiency reaches

the highest value for all three pHs because of the decreasing γ and brief T_{on}. The photonic efficiency at this γ is found to be a function of pH and the recorded increase is not symmetrical across the pH investigated.

The photonic efficiency at γ = 0.07 is greatest at pH 4 and lowest at pH 9.6 because of the resultant effect the pH, γ and oxidizing species all have on the photocatalytic reaction. The pH has a direct effect on the rate of interfacial-electron transfer which reduces with reducing pH[141] while γ is a function of T_{on} which inhibits charge-carrier recombination as T_{on} decreases[85, 89]. Both parameters have an influence on the role of the oxidative species in the reaction and also on optimizing the process of interfacial charge-transfer and charge-carrier lifetime for maximum photonic efficiency. The trend indicates that photonic efficiency is greatest when electrostatic attraction is highest at pH 4 with surface $\{Ti^{IV}OH^{\bullet}\}^{+}_{ads}$ mediated oxidation and T_{on} approaches the characteristic time for interfacial-electron transfer which is in the millisecond domain, this trend can also be extrapolated to charge-carrier lifetimes which have characteristic times below the shortest T_{on} in this study.

3.5. Theoretical results and discussion

The theoretical results are the results of mathematical modelling of reaction rates and quantum yields of methyl orange degradation at pH 7 alone. Where appropriate, data from the experimental study was used to validate the employed models.

3.5.1. Photocatalytic rate modelling

The experimental data showed the effect of duty cycle (2.16) on photocatalytic degradation rates of methyl orange. An initial concentration of 2.5 X 10^{-2} mM was used for all values of γ, the period (T_{on} + T_{off}) was kept constant while T_{on} and T_{off} were varied. The reaction order, *n* which represents the exponent of the concentration of MO in the rate equation varied with γ (Table 3.2.), I_{max} was < 200 Wm^{-2} therefore *m* was taken to be first-order[98], K_{ads} and k_r were obtained from the plot of $1/r_0$ against 1/γ, the intercept was equal to $1/k_r$ while the slope

provided the solution for $1/k_rK_{ads}$[142] hence, the values of K_{ads} and k_r were 0.645 dm^3mol^{-1} and 4.85×10^{-4} $mMmin^{-1}$ or min^{-1} with respect to the reaction order.

Table 3.2: Experimental conditions for methyl orange photodegradation under controlled periodic illumination

γ	I_{avg} (Wm^{-2})	r_{40} ($mMmin^{-1}$)	n
0.07	0.13	2.38E-05	0
0.12	0.21	2.50E-05	0
0.24	0.43	7.50E-05	0
0.36	0.64	1.00E-04	0
0.49	0.87	1.25E-04	0
0.61	1.09	1.50E-04	1
0.73	1.30	1.75E-04	1
0.85	1.51	1.85E-04	1
1.00	1.78	2.11E-04	1

An increase in photocatalytic rates was observed with increasing γ for the experimental and model data (fig. 3.10), this is as a result of an increase in the average intensity of illumination. Generally for photocatalytic reactions, a linear relationship exists between photo-oxidation rates and light intensity at low light intensities, the relationship tends towards a square root relationship as intensity increases and eventually rate becomes independent of intensity at very high intensities[94]. The results however show a significantly dissimilar trend with the experimental data having a non-linear trend while the model follows a linear trend. Also, there is a significant difference in the order of magnitude of the determined rates of reaction and this results in a poor fit of the experimental data by the model.

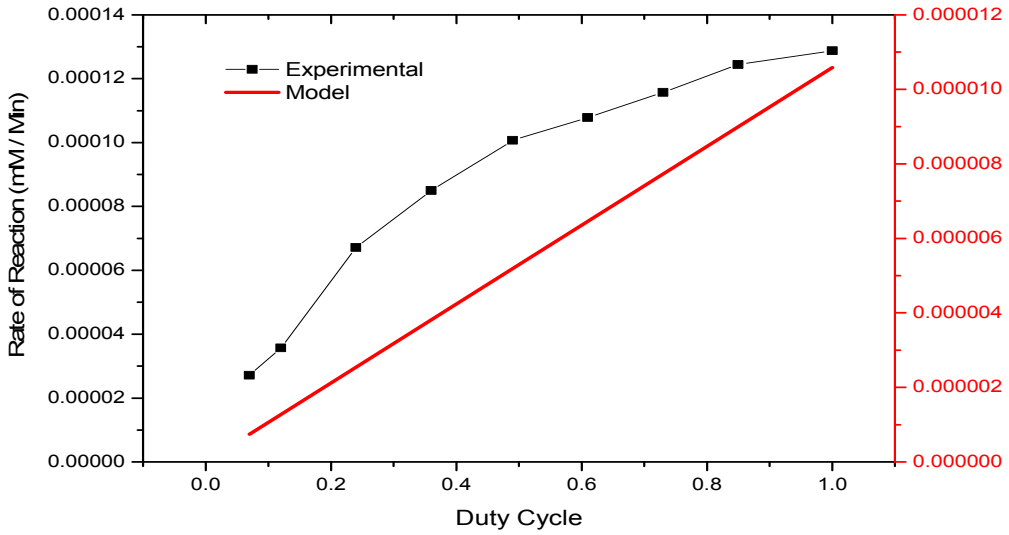

Figure 3.10: Correlation of modified L-H model data with experimental for methyl orange degradation rates at different γ

Chen *et al*. who first reported the use of this model reported a good fit to the experimental rates[89], their plot involved reaction rates at several concentrations and a single γ. The experiments monitor reaction rates at a single concentration but several γ, the varying I_{avg} as a result of changing γ has a significant influence on the model rates and this accounts for the significant disagreement between the model and experimental rates in trend and magnitude. Photocatalytic reactions under periodic illumination involve complex transient mechanisms therefore developing a model for the dependence of the reaction rate on the experimental parameters over the reaction time can be difficult. The dependence of the constants K_{ads} and k_r on the intensity of UV illumination is well established [143-146](3.19, 3.20), this is not accounted for in the modified L-H model.

$$K_{ads} \alpha\ 1/\gamma\ I_{max} \qquad (3.19)$$

$$k_r \alpha\ \gamma\ I_{max} \qquad (3.20)$$

The variation of the constants K_{ads} and k_r with UV intensity implies their values when obtained from a plot of $1/r_0$ against $1/\gamma$ will not give a truly representative value for each γ in the modified L-H model. Furthermore,

orders of reaction rate dependence on photon flux and reagent concentration are independent of each other[147], this presents a problem for the model as reaction order with respect to concentration changes with an effect on k_r while order of photon flux remains the same.

3.5.2. Quantum yield modelling

The quantum yield modelling of the photocatalytic degradation of methyl orange confirmed the same trends from experimental data which were previously reported in the literature[100], the effect of a constant period and varying T_{on} and T_{off} on the quantum yield was modelled (fig. 3.11), all events required for photocatalytic oxidation (3.3-3.6) were constrained in 1 s such that $T_{on} + T_{off} = 1$ s for all duty cycles.

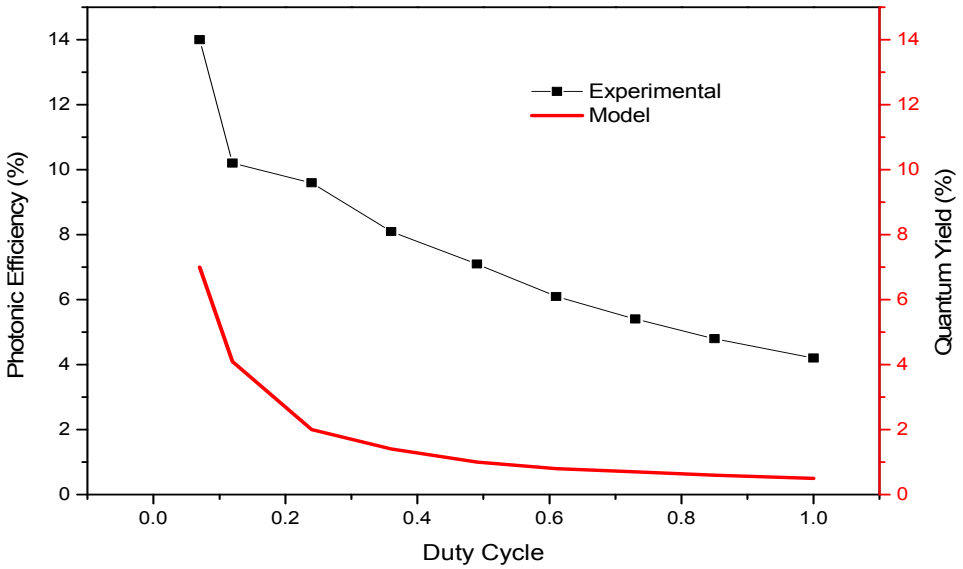

Figure 3.11: Decreasing duty cycle resulting in a corresponding rise in quantum yield and photonic efficiency

A general increase in quantum yield as duty cycle decreased was observed indicating an inverse relationship between φ and γ. Quantum yield and photonic efficiency differ because of the difference in accounting for photons, φ takes into account the amount of photons absorbed by the catalyst and this is affected by, reflection, transmission and scattering which is significant and can vary as much as 13% - 76% depending on conditions[148]. Photonic efficiency on the other hand takes

into consideration only the incident photons on the photocatalyst, assuming all photons are absorbed and light-losses are negligible.

The model agreement with the experimental data in the modelling of the effect of T_{on} and T_{off} on φ followed a similar trend. When T_{on} was kept constant while T_{off} varied, the contributing effect of T_{off} to quantum yield was observed. The approach taken involved the light time events mainly (3.3) taking place within 1 s therefore having a controlled impact on φ while the dark time events were varied by increasing T_{off} from 0.1 s to 1 s, the resulting range for the duty cycle was $\gamma = 0.39 - 0.91$ (fig. 3.12).

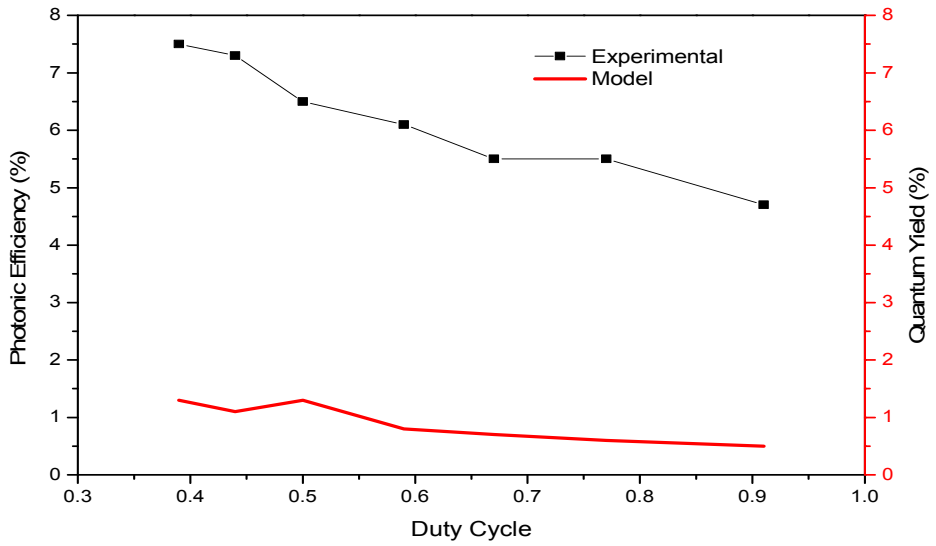

Figure 3.12: Contributing effect of T_{off} to quantum yield enhancement

The dark period is devoted to the replenishment of surface adsorbed species by the transfer of electrons to adsorbed oxygen (3.6) and/or the adsorption of oxygen onto the surface. Consequently, a higher rate constant for these steps will result in higher quantum yields. Figure 3.12 shows the relatively small improvements in quantum yield as T_{off} increases in agreement with previous experimental results. The resulting increase in quantum yield was inferior to the same effect produced by an increasing T_{on}, this is as a result of the sensitivity of the dark period to the rate-limiting nature of (3.6) [85, 108].

In the third modelling result, the experimental light time was varied while the dark time was kept constant. This produced the effect of an increase in I_{avg} and higher photon absorption by the photocatalyst as T_{on} increased, without a corresponding increase in T_{off}. The modelled results (fig. 3.13) show the quantum yield improvement with decreasing duty cycle.

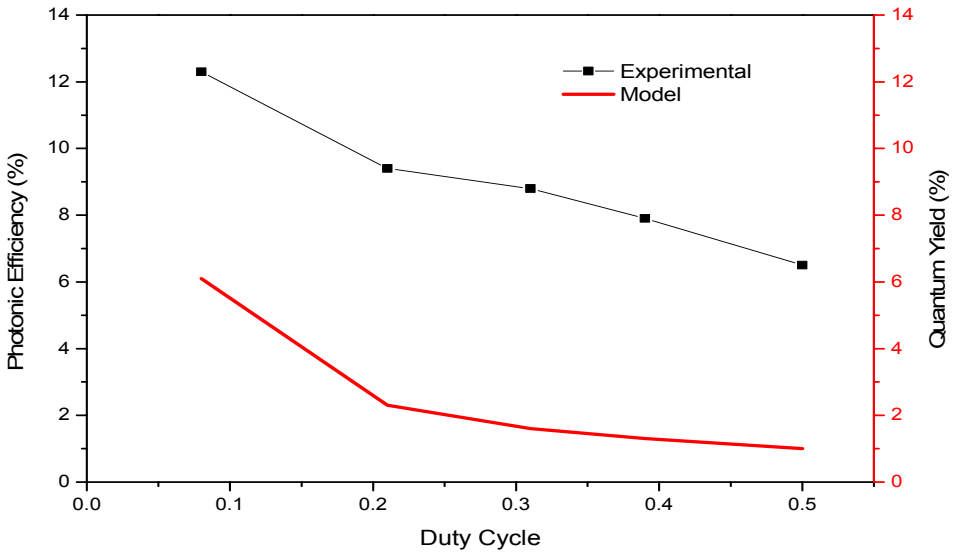

Figure 3.13: Contributing effect of T_{on} to quantum yield enhancement.

As T_{on} increased, more time was available for (3.3), which is the first step in the photocatalytic process, giving rise to (3.4) resulting in a decrease in quantum yield. The modelling further reiterates the experimental findings which show that decreasing T_{on} at constant T_{off} has a greater effect on quantum yield than increasing T_{off} at constant T_{on} or varying both alternatively by varying the period. Table 3.3 shows the values of γ, T_{on} and T_{off} used in the modelling of φ as carried out in the study.

Table 3.3: Values of γ, T_{on} and T_{off} used for theoretical modelling of φ.

Varying Period			**Varying T_{on}**			**Varying T_{off}**		
γ	T_{on} (S)	T_{off} (S)	γ	T_{on} (S)	T_{off} (S)	γ	T_{on} (S)	T_{off} (S)
0.07	0.07	0.90	0.08	0.1	1.0	0.39	1.0	1.7
0.12	0.12	0.86	0.21	0.3	1.0	0.44	1.0	1.4
0.24	0.23	0.74	0.31	0.5	1.0	0.50	1.0	1.1
0.36	0.35	0.62	0.39	0.7	1.0	0.59	1.0	0.7
0.49	0.47	0.50	0.50	1.1	1.0	0.67	1.0	0.5
0.61	0.59	0.38				0.77	1.0	0.3
0.73	0.71	0.27				0.91	1.0	0.1
0.85	0.83	0.15						
1.0	-	-						

The enhancement observed in the mathematical modelling of φ when controlled periodic illumination is employed is produced by the duty cycle, γ which is a function of T_{on} and T_{off} therefore their alternating effect contribute to the overall quantum yield enhancement. An overall trend of quantum yield enhancement as a result of reducing duty cycle using modelled data is plotted (fig. 3.14). This is in agreement with the result using experimental data[100] depicting a trend of increasing quantum yield as duty cycle decreases irrespective of T_{on} and T_{off}.

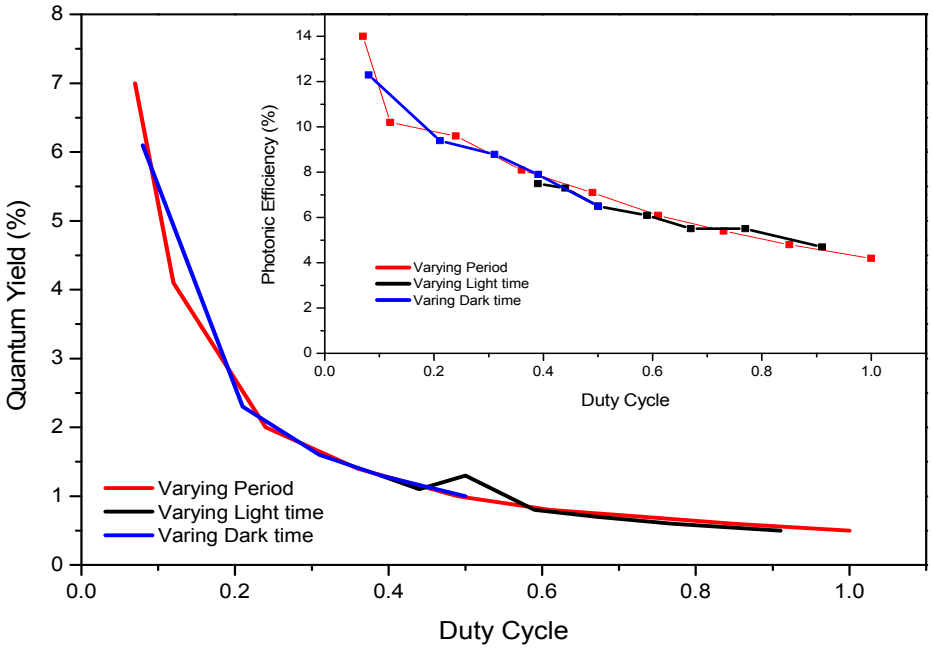

Figure 3.14: Overall quantum yield trend as a function of duty cycle with experimental result graph as an inset

3.6. Conclusion

Under controlled periodic illumination of TiO_2, photonic efficiency of photocatalytic oxidation in the aqueous phase is not only dependent on γ of illumination but the pH of the media. This chapter has investigated the resultant effect of pH and γ on methyl orange photodegradation and the results show little influence of pH at high γ. At low γ, the pH has a significant effect on photonic efficiency with the oxidative species and a match between T_{on} and interfacial electron-transfer also contributing to photonic efficiency enhancements. The chapter also includes theoretical studies of TiO_2 photocatalysis, several mathematical models exist for photocatalytic reactions using TiO_2 with light intensity distribution and reactor modelling receiving the most attention. The modified L-H rate equation used in the study is the most suitable for modelling photocatalytic reaction rates under controlled periodic illumination however, the influence of γ on the reaction order and the variation of the constants K_{ads} and k_r with UV intensity makes the model suitable only for reactions with a single γ. The quantum yield model although speculative,

gives a good agreement between the trends for the experimental data and model data. This suggests a potential for the formulation of more detailed models which provide a thorough understanding of the CPI effect and photocatalytic rates in the aqueous phase.

CHAPTER IV

4. DESIGN AND EVALUATION OF A NOVEL PHOTOREACTOR FOR GAS-SOLID PHOTOCATALYSIS

4.1. Introduction

In recent years, there has been a concentration of effort on the design of reactors for heterogeneous photocatalysis and this has led to different reactor configurations being reported in the research literature[52, 73, 149]. Photocatalytic reactors in heterogeneous photocatalysis bring together all elements such as photons, pollutant and catalyst that are required for the transformations of reactants, into a single unit that enables the monitoring and/or regulation of parameters such as mass transfer, temperature and concentration. This ensures that photons are adequately utilized, intermediate products can be identified and kinetics of the photocatalytic process can be studied therefore, the aim of reactor design is to optimize these elements and parameters to neutralize the pollutant completely and achieve the greatest possible yield.

In order to achieve this, a large catalyst surface area is essential. Catalysts in the powdered form provide a larger surface area than immobilized catalysts which have significantly reduced surface area. The use of immobilized catalysts has however, now been widely reported in the literature[150] because of its reduction of the cost of separating powdered catalysts from liquid in solid-liquid treatment processes and the reactor design possibilities it provides in gas-solid treatment. Different reactor configurations exists for gas-solid heterogeneous photocatalysis, Cassano and Alfano[75] identified the four most widely reported configurations in the photocatalytic literature to be monoliths[151], packed bed[152], catalytic walls[153] and fluidised bed[154] photoreactors with the immobilized catalysts reactors being the most commonly used.

The supports on which catalysts are immobilized vary greatly. Supports reported in the literature include but are not limited to glass, silica and optical fibre[155]. An ideal support should exhibit strong affinity for the

pollutants, strong binding with the catalyst, high specific surface area and not reduce catalyst reactivity as a result of the binding with the catalyst. In immobilized photoreactor development, the major challenges encountered are complications of reactor scale-up such as mixing, mass transport, reactant-catalyst contact and installation of catalysts and achieving a high ratio of activated catalyst to illuminated surface through efficient light intensity distribution inside the reactor[156].

In this chapter, the development of a photocatalytic impeller reactor (PIR) for gas phase photocatalysis with a potential to overcome the aforementioned challenges is reported. The performance of this new reactor will be evaluated through mass transfer analysis in the photo-oxidation of a VOC. Toluene vapour was used as a model pollutant and its degradation was used to evaluate the reactor performance.

4.2. Photocatalytic Impeller Reactor (PIR)

The photocatalytic impeller reactor (PIR) is a gas phase reactor which operates in principle as a stirred tank reactor. The reactor system consists of an ultra-band, 360 nm UV-LED (FoxUV^{TM}) array wrapped around the reaction chamber as the illumination source. The reaction chamber was made of transparent PMMA tubing permitting UV transmission hence, virtually all UV irradiation from the light source is incident in the reaction chamber. A vertically aligned stainless steel shaft running through the centre of the chamber supports the impellers in the reactor. The impellers consist of glass slides (Fisherbrand FB58620) coated with TiO_2 and the coated slides are inclined at 30° and arranged perpendicularly to each other on circular discs, the immobilized TiO_2 film makes the impellers photoactive. A model of the impeller is shown in figure 4.1.

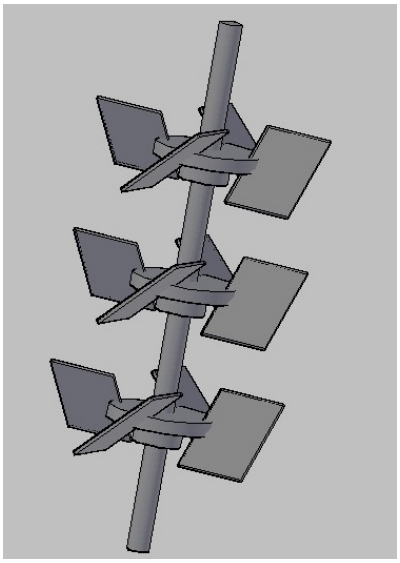

Figure 4.1: Model of the photocatalytic impeller supported on a central shaft.

The shaft is supported at the top and bottom by ball bearings which make its rotation possible and sealed at the bottom with a double lip Viton rubber shaft seal where it exits the chamber and connects to a reversible synchronous motor. The reactor is sealed at the bottom with Viton gaskets as well as the top where three ports are located, the ports are an outlet sealed with propylene 2-way ball valves having Viton seals, an inert septum sealed inlet and a sampling port fitted with a filter and valve. Figure 4.2 shows a schematic diagram of the designed reactor.

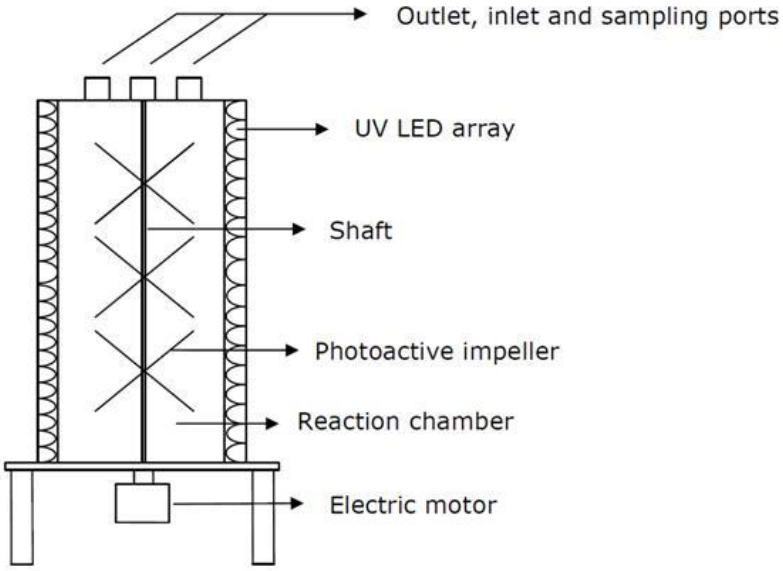

Figure 4.2: Schematic of photocatalytic impeller reactor.

4.3. Design and construction of photoreactor

The design and construction of the photoreactor was carried out in three distinct stages with each stage involving a separate design process and outcome. The design processes included a computational fluid dynamics (CFD) modelling of the flow field within the photoreactor, synthesis and immobilisation of TiO_2 on glass slides and the preparation of computer aided design (CAD) engineering drawings and material selection for the manufacture and construction of the photoreactor unit.

4.4. CFD modelling of immobilized gas phase photoreactor

The computational model for the photoreactor simulated hydrodynamics within the reaction chamber and provided an understanding of the flow field of the novel photoreactor configuration. Commercial CFD software ANSYS Fluent 13.0 was used to perform the simulations.

4.4.1. Governing equations

For the modelling of the photoreactor, it is assumed that the fluid (VOC) is under turbulent steady state flow, Newtonian, having constant physical properties, incompressible, isothermal and non-reactive. With these assumptions and using the Reynolds-averaged Navier-Stokes (RANS), the CFD model involved solving the continuity equation (4.1), time-averaged conservation of species equation (4.2) and Reynolds-averaged Navier-Stokes equation (4.3) as follows[157]:

Mass conservation equation

$$\nabla \cdot \left(\overline{U}\right) = 0 \tag{4.1}$$

Momentum conservation equation

$$\nabla \cdot \left(\rho\overline{UU} + \rho\overline{uu}\right) = -\nabla\overline{P} - \nabla \cdot \overline{\tau} \tag{4.2}$$

Species conservation equation

$$\nabla \cdot \left(\rho\overline{U}\overline{m_i} + \rho\overline{um_i'}\right) = -\nabla \cdot \overline{J}_i \quad i = 1, 2, \ldots, N-1 \tag{4.3}$$

Where the time-averaged value is indicated by the overbar, ρ is density, P is pressure, τ is the viscous stress tenor, J_i is the diffusive flux of species, m_i is the mass fraction of species, and u is the fluctuating flow velocity. Specification of the mass fluxes and turbulent stresses in terms of time-averaged variables is the major challenge in the modelling of turbulent flow. There are several proposed turbulence models[158, 159], but none of them is universally suitable for all conditions, therefore turbulence models need to be selected specifically for the problem being considered.

4.4.2. Hydrodynamic model

The hydrodynamic turbulence model employed in the simulation of this photoreactor is the RNG $\kappa-\varepsilon$ model, this model was used because it is more reliable and accurate for a wider class of flows than the other models[160]. The transport equations for the model are given as equations (4.4) and (4.5):

$$\frac{\partial}{\partial t}(\rho k)+\frac{\partial}{\partial x_i}(\rho k u_i)=\frac{\partial}{\partial x_j}\left(\alpha_k \mu_{\text{eff}}\frac{\partial k}{\partial x_j}\right)+G_k+G_b-\rho\epsilon-Y_M+S_k \tag{4.4}$$

and

$$\frac{\partial}{\partial t}(\rho\epsilon)+\frac{\partial}{\partial x_i}(\rho\epsilon u_i)=\frac{\partial}{\partial x_j}\left(\alpha_\epsilon \mu_{\text{eff}}\frac{\partial \epsilon}{\partial x_j}\right)+C_{1\epsilon}\frac{\epsilon}{k}(G_k+C_{3\epsilon}G_b)-C_{2\epsilon}\rho\frac{\epsilon^2}{k}-R_\epsilon+S_\epsilon \tag{4.5}$$

In the equations, G_k is the generation of turbulent kinetic energy as a result of mean velocity gradients, G_b is the generation of turbulent kinetic energy as a result of buoyancy, Y_m is the effect of fluctuating dilalation in compressible turbulence to the overall rate of dissipation, $_\varepsilon$ and $_k$ are inverse effective Prandtl numbers for ε and κ respectively, S_ε and S_k are user-defined source terms. $C_{1\varepsilon}$ and $C_{2\varepsilon}$ are constants whose values are derived analytically by the RNG theory. The default values used by ANSYS Fluent are 1.42 and 1.68 respectively.

4.4.3. Boundary conditions

Boundary conditions are required for the hydrodynamic model; they specify fluxes such as momentum, energy, mass in the computational domain. The boundary conditions for this modelling being a batch reactor were simply defined as follows; an impeller wall, a fluid zone and the reactor wall. The standard wall function was selected for the near-wall treatment.

4.4.4. Moving reference frame modelling

The equations of fluid flow in ANSYS Fluent are solved in a stationary (inertial) reference frame by default. When modelling moving parts such as impellers, the flow around the impellers is of interest hence solving the fluid flow equations in a moving (non-inertial) reference frame (MRF) is advantageous (fig.4.3). Activating an MRF modifies the equations of motion, therefore incorporating other terms which are a result of the transformation from stationary to moving reference frame.

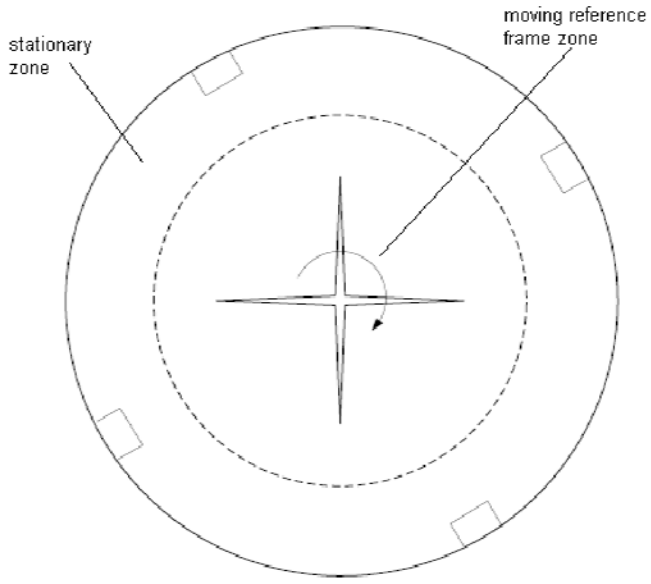

Figure 4.3: Moving reference frame modelling with a single impeller[144].

The computational domain for this photoreactor because of its simple geometry is taken as a single reference frame (SRF)[161]. The impeller wall was defined to rotate with the fluid zone which was taken as the reference frame while the reactor wall which forms a surface of

revolution about the axis of rotation was defined as non-moving with respect to the stationary coordinate system with an absolute velocity of zero.

4.4.5. Numerical solution method

ANSYS 13.0 Fluid Flow Fluent was used to perform the simulations, the SIMPLE algorithm was used for the pressure-velocity coupling scheme. First order upwind spatial discretization scheme was employed. The simulation was initialized with the default values using the standard initialization method and the relative to cell zone reference frame. The number of iterations was set to 1175 and convergence of the numerical solution was monitored on the scaled residuals for the three different simulations.

4.4.6. Mass transfer in the PIR reactor

Generally for immobilized reactors, the surface area of the catalyst is greatly reduced therefore, reactants travel longer distances before reaching photocatalytically active sites. This results in mass transfer limitations in immobilized reactors[162]. Mass transfer which is driven by a gradient in chemical potential or convection forces within reactors, in the photocatalytic impeller reactor is aided by the rotating motion of the photocatalytic modified rushton impellers which provide a radial flow of the gas/vapour within the reactor. Ansys Fluent 13 was used to perform a flow field simulation within the reactor during operation using the RNG k-ε turbulence model (fig.4.4).

(a)

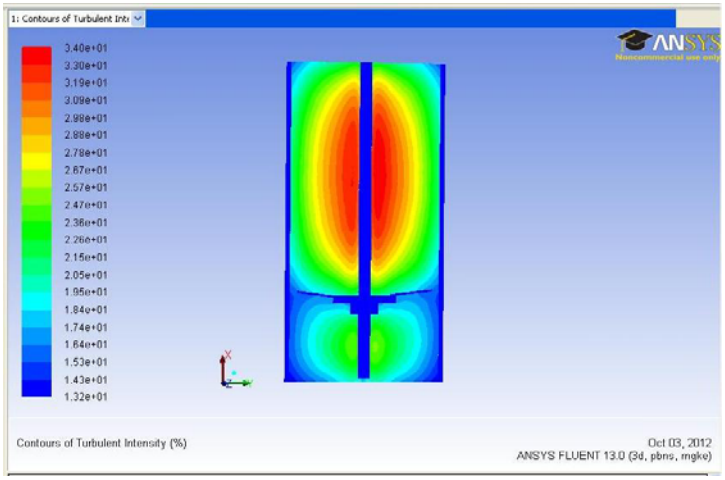

(b)

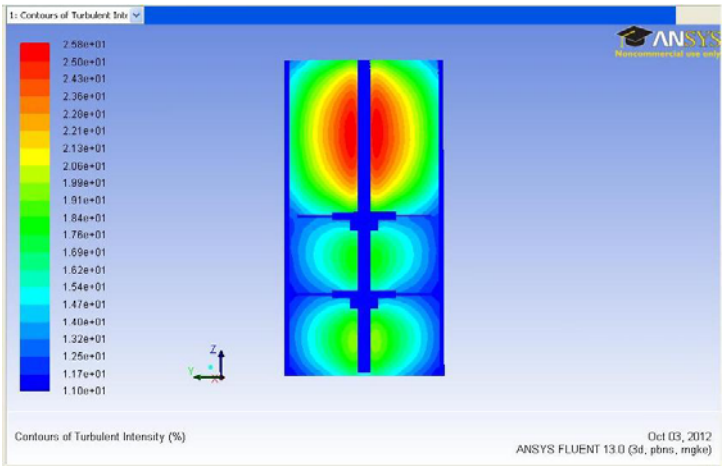

(c)

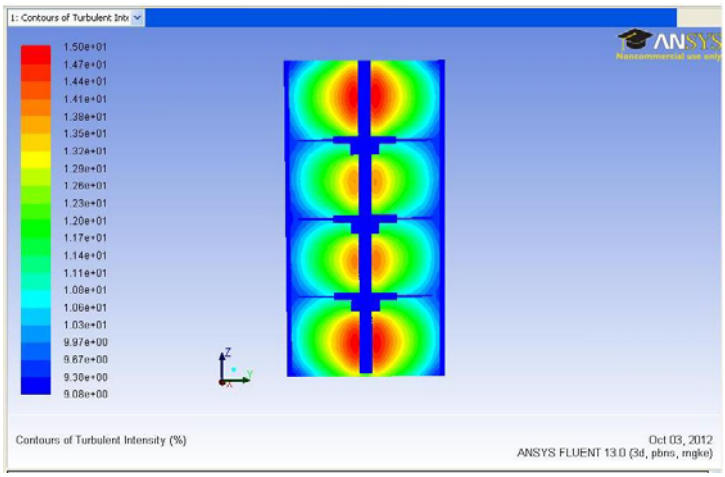

Figure 4.4: Flow field simulation in the photocatalytic impeller reactor comparing different numbers of impellers (a) 1 impeller (b) 2 impellers (c) 3 impellers.

The simulation was run with the impeller blades at 30℃, rotational speed of 478 rpm with toluene vapour as the fluid. However, in a photocatalytic impeller reactor with single pollutant molecule, rapid mixing is not the objective but the elimination of concentration gradients. For this reactor design, this is achieved with three 4-bladed impellers of equal clearance which distribute the turbulence uniformly, creating separate zones while reducing areas with little or no kinetic energy as a result of the flow.

The reactor has an illuminated catalyst surface area per unit reactor volume of 17.57 m^{-1} which is a lower limit of the real value due to the porous morphology of the immobilized TiO_2. The diffusion flux of the toluene vapour through the thin-film simultaneously with photocatalytic degradation of gaseous molecules is described by equation (4.6)[163]:

$$\delta q/\delta t = D_s (\delta^2 q/\delta z^2) - k\, I^m\, q^n \qquad (4.6)$$

where q is the concentration of sorbed gaseous molecules in the thin-film catalyst, D_s is the effective diffusivity, in the catalyst, k is the photocatalytic reaction rate constant, I is the illumination intensity, z is the distance from the catalyst support surface, t is the reaction time while m and n are constants of reaction order. The first term on the right hand side accounts for internal mass transfer and is a product of toluene diffusivity in air (D_s = 8.49E-6 m^2/s) and Fick's second law of diffusion while the second term accounts for the photocatalytic reaction taking place.

4.5. Immobilized TiO_2 catalyst preparation

The photocatalyst used in the photoreactor was titanium dioxide, titania sol was synthesized in situ through the sol-gel process. The synthesized titania sol was immobilized on glass slides of dimension 38 mm × 26 mm through the dip coating process and annealed to produce crystalline thin film coatings. An overview of the process is shown in figure 4.5.

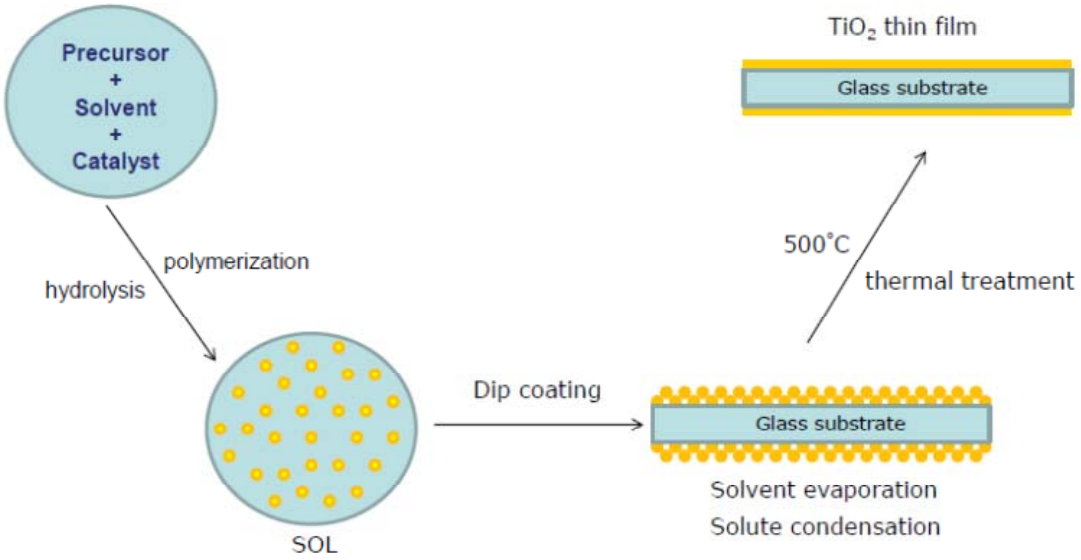

Figure 4.5: An overview of the catalyst preparation process.

The synthesized thin films were characterized to determine the thickness, elemental composition, surface structure, crystalline form, UV absorbance and photoactivity.

4.5.1. Sol-gel synthesis

The sol-gel process involves a precursor in a solvent undergoing polycondensation reactions leading to the formation of an oxide network. Its aim is to dissolve the desired compound in a liquid so it can be brought back as a solid in a controlled manner. The process has several advantages such as homogeneity, it enables mixing at atomic levels, preparation of multi component compounds, purity, ease of processing, ambient temperature, and low cost. Hydrolysis of a titanium alkoxide precursor is the primary process of TiO_2 synthesis by the sol-gel process and there are two different routes depending on the processing parameters[164, 165];

i. The polymeric route – the solvent used is usually an alcohol and the hydrolysis reaction is carefully controlled by the introduction of a small amount of water. An acid catalyst (HNO_3 or HCl) is added to complex the alkoxide prior to the hydrolysis reaction hence decreasing the reaction rate. The outcome is an amorphous film

which needs to be annealed in a furnace at a specific temperature depending on the required form, to produce crystalline films.

ii. Excess water hydrolysis route – water in large quantity with respect to the alkoxide precursor is employed as the solvent in this route, hydrolysis occurs rapidly resulting in the formation of ultrafine nanoparticles[166] which agglomerate quickly, resulting in large aggregates having macroscopic dimensions[167]. The aggregates are broken down by peptization using an inorganic acid (HNO_3 or HCl) to form a colloidal suspension containing crystalline nanoparticles which are predominantly anatase[168].

The polymeric route was employed in the synthesis of titania sols for the TiO_2 photocatalysts. The sol was prepared using titanium(IV)isopropoxide (TTIP) as the precursor, propan-2-ol as the solvent and nitric acid (HNO_3) as the catalyst with a limited amount of water for the hydrolysis reaction. Propan-2-ol (65 mL) was added to 5 mL of TTIP and stirred vigorously for 2 hours. A mixture of 51 µL HNO_3, 349 µL distilled water and 5 mL propan-2-ol was added dropwise and stirring continued for a further 15 minutes.

The process begins with the vigorous hydrolysis reaction which takes place between TTIP and water can be represented by equation (4.7)[169].

$$\mathrm{Ti(OC_3H_7)_4 + xH_2O \rightarrow Ti(OC_3H_7)_{4-X}(OH)_X + xHOC_3H_7} \qquad (4.7)$$

Then a propagation step which is the condensation of hydrolyzed species and bridging of oxygen takes place, resulting in the formation of an inorganic network through a chain of polymerization and hydrolysis reactions (4.8)[165, 169].

$$\mathrm{2[Ti(OC_3H_7)_{4-x}(0H)_x] \rightarrow Ti(OC_3H_7)_{4-x}(OH)_{x-1} - O - Ti(OC_3H_7)_{4-x-1}(OH)_X + HOC_3H_7} \qquad (4.8)$$

The resulting sol was sonicated for 2 minutes and stored in plastic vessels.

4.5.2. Sol-gel deposition

The photocatalyst thin films were deposited on the glass substrate (Fisherbrand FB58620) through the dip coating process. The process has 5 steps; immersion, start-up, deposition, drainage and evaporation. The substrate was immersed into the sol at a constant speed and remained there for a 60 seconds after which it was withdrawn (start-up). Deposition takes place during withdrawal at a constant speed; the deposited layer is thicker when quickly withdrawn and thinner when withdrawn at a slow speed. The deposited film undergoes gravitational draining and evaporation which keeps the thin film thickness uniform[170]. These 5 steps are illustrated in figure 4.6.

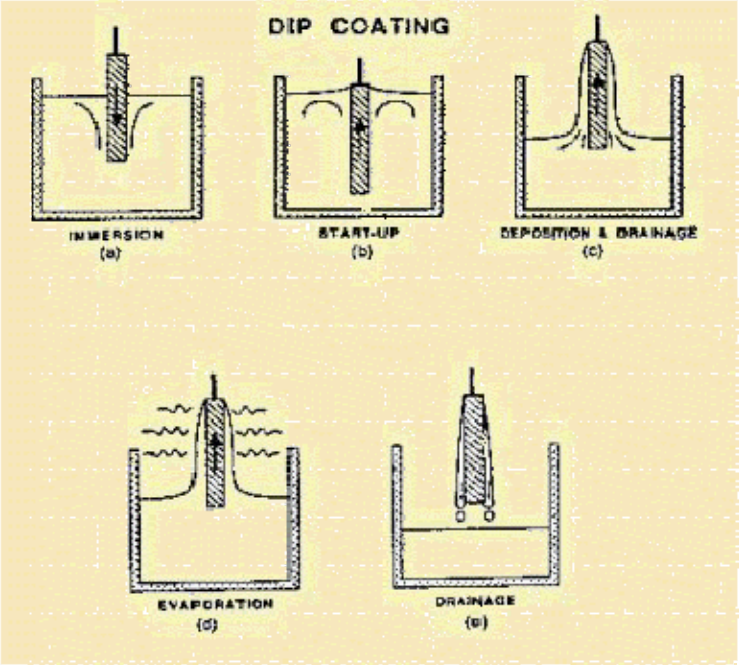

Figure 4.6: The stages in the dip coating process[170].

After sol deposition, the deposited film was air dried for 1 hour, undergoing solvent evaporation and solute condensation to form a composite layer having a chemical composition in which all titanium atoms form part of the network (4.9)

$$\mathrm{Ti(OC_3H_7 \text{ or } OH)_{2-y}\,(O)_y} \qquad (4.9)$$

The TiO_2 thin film as-deposited is amorphous, amorphous TiO_2 films are generally inactive but gain high photoactivity when coupled with metal

oxides[171, 172]. The amorphous thin film was annealed in a furnace for 1 hour where it underwent thermal treatment at 500℃ resulting in the formation of crystalline TiO_2 films. The molecular structure of the film after thermal treatment is such that all oxygen atoms bond with titanium atoms leading to a very homogeneous and pure oxide network and can be described by equation (4.10) proposed by Valtiera *et al*.[169].

$$2[\mathrm{Ti(OC_3H_7\ or\ OH)(O)}] + \mathrm{air} +> 400℃ \rightarrow 2\mathrm{TiO_2} + 3\mathrm{CO_2} \uparrow + 4\mathrm{H_2O} \uparrow \quad (4.10)$$

The thermal treatment fuses the TiO_2 particles together, decomposes any organic molecule and binds the titania film to the glass substrate. The final crystalline TiO_2 thin film was transparent and its adhesion to the glass substrate survives the adhesion test using an adhesive tape.

4.5.3. Characterization of TiO_2 thin films

The TiO_2 thin film was characterized in order to determine its physical and chemical properties such as chemical composition, crystalline structure, UV absorbance, film thickness and photoactivity.

i) Physical characteristics

An EVO LS10, Zeiss scanning electron microscope (SEM) was used to investigate the surface topography and thickness of the thin film coating. The coating had a smooth plain surface and had to be cracked in order to make the film visible and to expose a cross section from which the thickness could be determined (fig. 4.7).

(a)

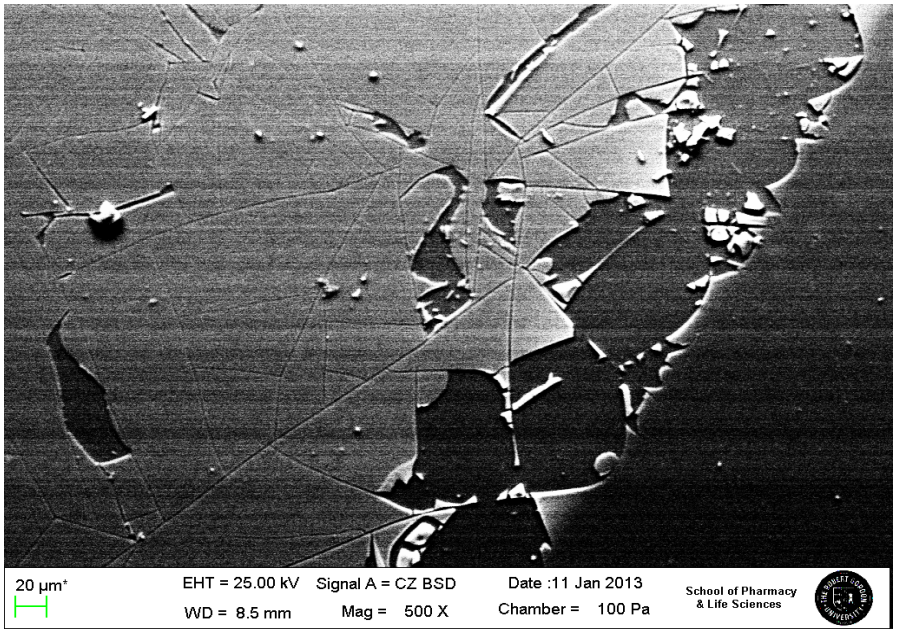

(b)

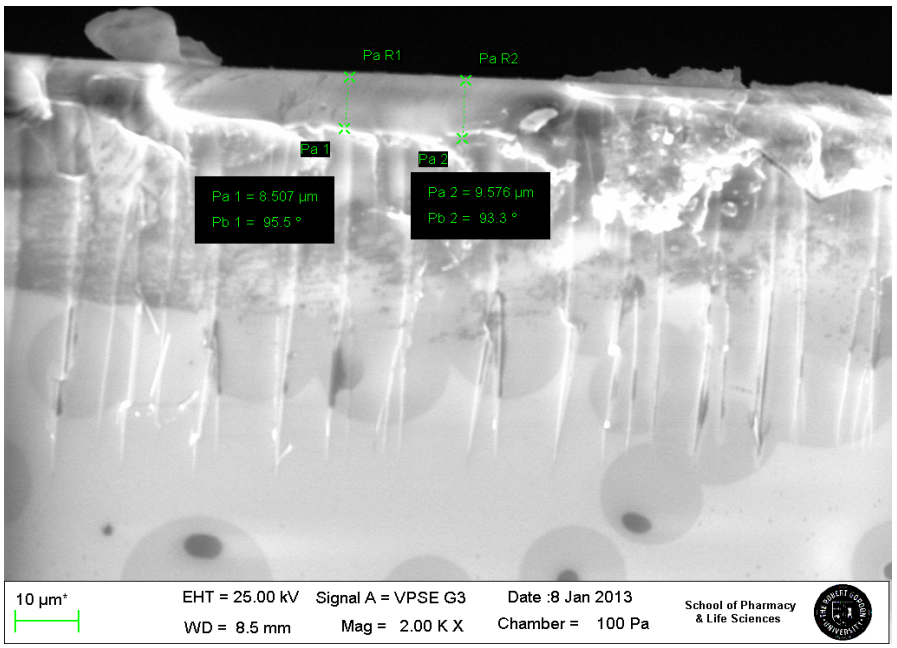

Figure 4.7: SEM image showing (a) Surface topography of cracked coating; (b) Cross section of coated substrate showing film thickness.

The thin film was continuous without cracks and has an average uniform thickness of 8 µm. The weight of the thin film coating was determined to be <0.001 g because the weight of the glass substrate, glass substrate after coating and after annealing were the same.

ii) Optical characteristics

The UV/Vis absorbance of the TiO_2 coating was measured using a Perkin Elmer Lambda 950 UV/Vis spectrometer (fig. 4.8).

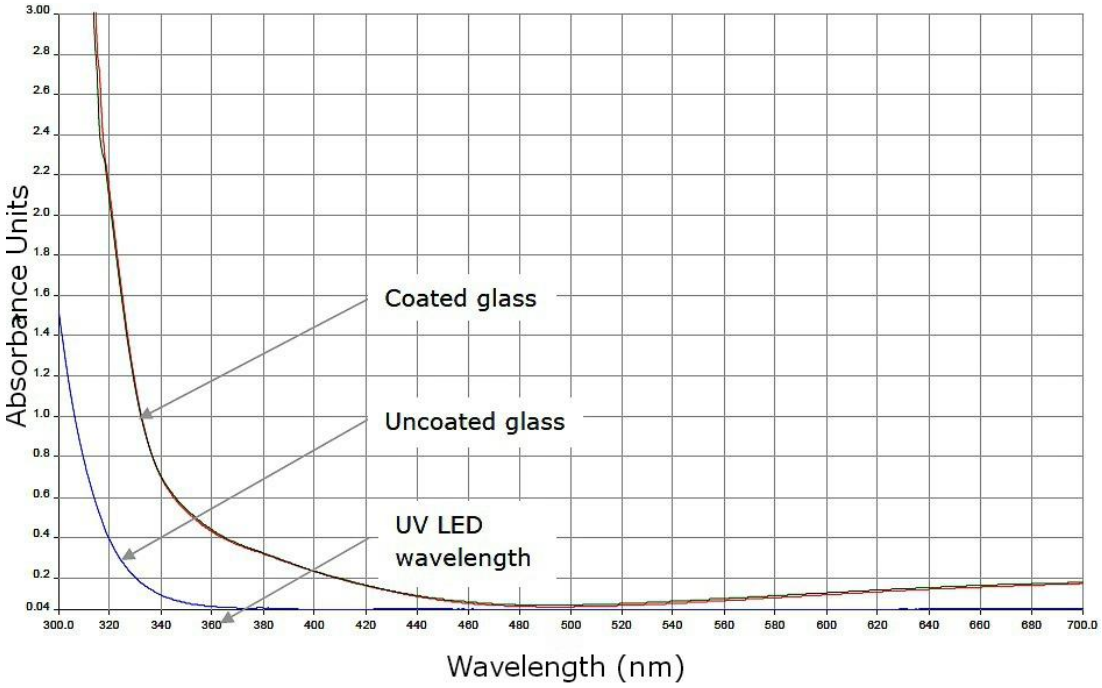

Figure 4.8: UV/Vis absorbance of uncoated substrate (blue) and coated substrate (red and green).

Air was used as the blank and then the absorbance of an uncoated and a coated glass substrate were measured. The results show an increase in UV absorbance from ~0.05 in the uncoated substrate to ~0.42 in the coated substrate at 360 nm, indicating UV absorbance by the TiO_2 coating at the wavelength of the illumination source.

iii) Elemental analysis and characterization

The elemental analysis and characterization of the TiO_2 coating was carried out using an Inca system, Oxford Instruments Energy dispersive X-ray spectroscopy (EDAX). This technique provides information on the composition of the thin film coating on the substrate (fig. 4.9).

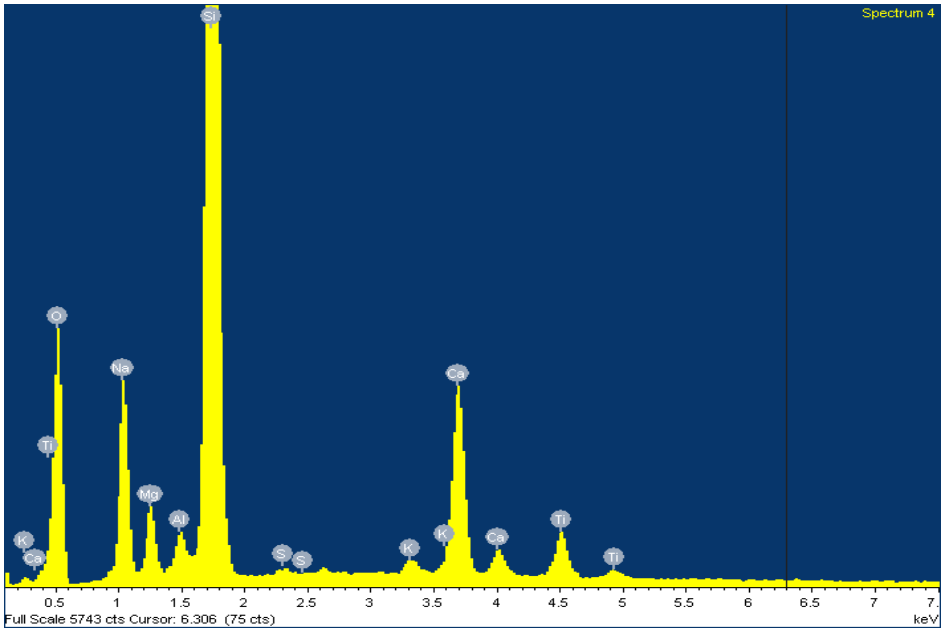

Figure 4.9: EDAX analysis results showing presence of titanium and oxygen in the thin film.

The analysis results showed the presence of the various elements the substrate is composed of, confirming it to be glass. Titanium and oxygen were also present in the thin film coating indicating the presence of TiO_2.

iv) Photoactivity

The photoactivity of the TiO_2 thin film coating was first tested using an RZ PhotoCat pen[173] which has an ink that changes from blue to orange upon UV irradiation on a photocatalytic surface. The blue ink readily turned to orange on the coated glass slides indicating the presence of a photoactive coating. Photocatalytic oxidation of a dye, using the degradation of methyl orange in the aqueous phase was used to test its reaction properties. Using the TiO_2 coated glass slides of dimension 25×15×1 mm and total surface area of 2490 mm^2, the photocatalytic degradation of 14 mL methyl orange solution of 1 µM concentration was carried out under continuous illumination (fig. 4.10).

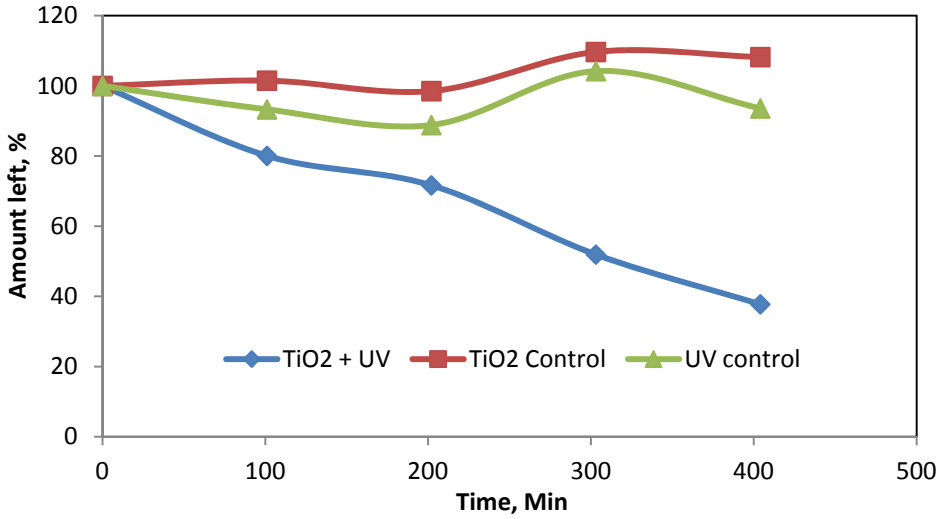

Figure 4.10: Photocatalytic degradation of methyl orange by TiO_2 thin film coated glass slide.

The results show a ~60% degradation of the methyl orange solution after six hours of irradiation by UV-LEDs, the reaction mixture was not stirred and was therefore mass transport limited. Control experiments were also carried out to investigate the effects of TiO_2 and UV light alone on the reaction.

4.6. Construction and manufacture of photoreactor unit

The two major steps in the construction of a photocatalytic reactor are the preparation of the engineering drawings and material selection for the reactor parts. These two steps follow conceptualization and design and precede the actual fabrication of the complete assembly.

4.6.1. Engineering drawings

The novel design and configuration of the gas phase photoreactor required that detailed engineering drawings were prepared for its construction. Figure 4.11 shows the engineering drawing of the photoreactor cover.

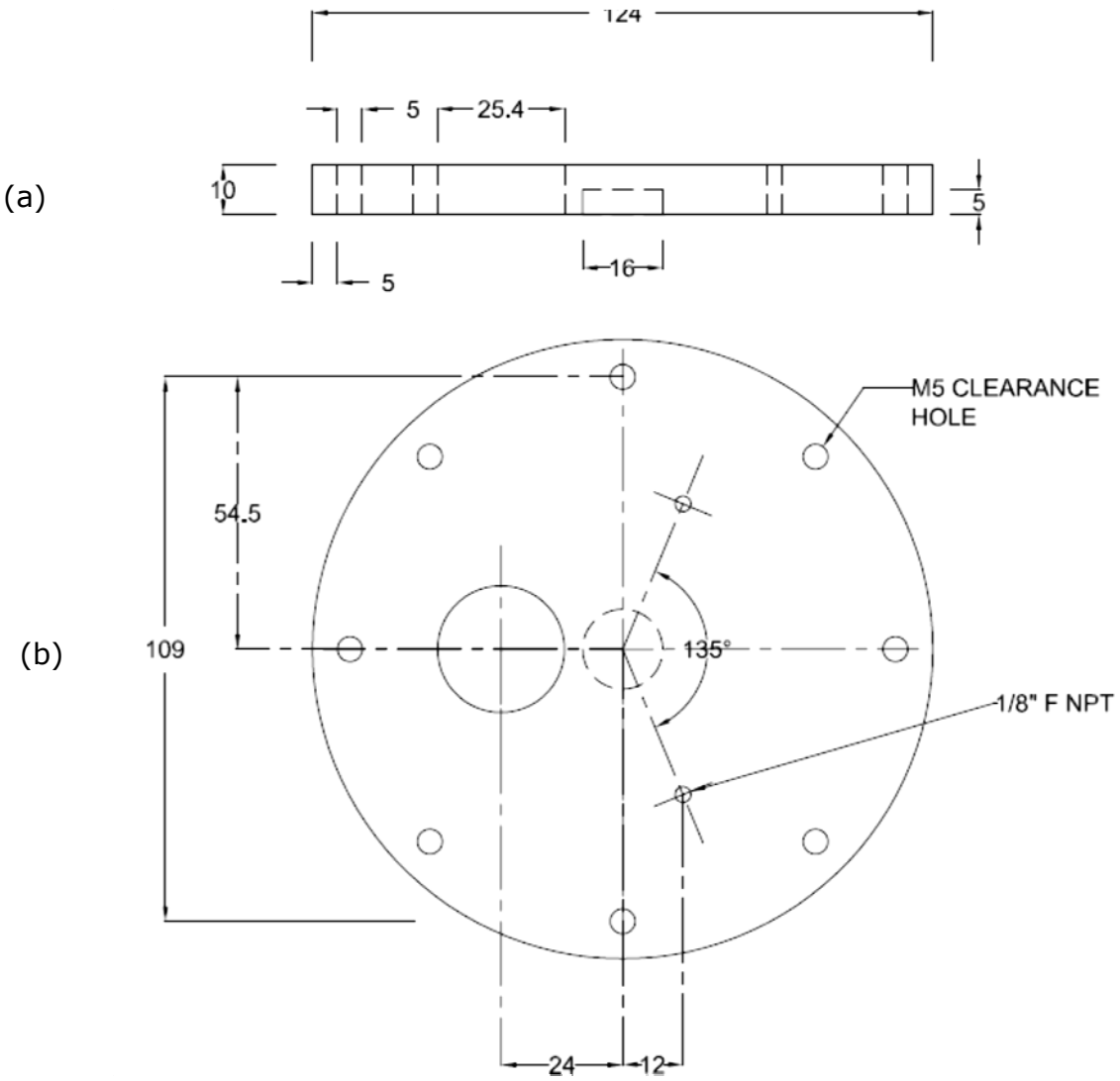

Figure 4.11: Engineering drawings showing (a) side elevation and (b) plan of photoreactor cover.

All engineering drawings (Appendix B) used were drawn using AutoCAD 2010 commercial software and were the basis for the fabrication of all the parts of the photoreactor.

4.6.2. Material selection

When designing and building a photoreactor, care has to be taken in selecting materials that are appropriate for the experimental work to be carried out, selected materials must be able to meet the performance goals of the photoreactor. A systematic selection approach was used and this involved scrutiny of the optical, chemical, thermal and mechanical properties of the materials used.

i) Sub-assembly

The sub-assembly which consisted of the reaction chamber, top and bottom covers and plates for the photoreactor were made of Poly(methyl methacrylate) (PMMA). The PMMA was manufactured by Evonik industries (PLEXIGLAS® XT) and had a 92% transmission of UV light and transparent. The reaction chamber was 200 mm in height, 3 mm thick and 94 mm ID.

ii) Seals

Silicone was used to seal the reaction chamber to the top and bottom plates to form the subassembly. The RTV silicone sealant was manufactured by Delta adhesives and was of engineering grade, this provided a robust but temporary seal which made maintenance relatively easy. Viton seals in the form of a shaft seal were used for the sealing of the photoreactor shaft while the sub-assembly top and bottom covers were sealed using Viton gaskets. Viton has a good resistance to chemical attack by toluene vapour and hydrocarbons in general. Its resistance to chemical attack increases with fluorine content [174] however, it is attacked by organic acids, ketones and acetone.

iii) Stainless steel shaft

A stainless steel shaft (316 grade) was used to support the discs on which the immobilized catalyst was fixed. Stainless steel was chosen to prevent oxidation of the metal shaft by toluene vapour and also because of its strength to support the weight of the immobilized catalyst structure and distribute the torque to the ball bearings. It was connected through a shaft seal to and coupled to an electric motor which provides the rotary motion of the immobilized photocatalyst.

iv) Polypropylene valves

The inlet and outlet valves (Cole-Parmer) on top of the photoreactor were made of polypropylene. Polypropylene has a fair resistance to chemical attack by toluene vapour which only has a moderate effect on

it. Internally, the valves had Viton seals which are also resistant to toluene vapour attack.

v) Sampling port

A custom designed sampling port made of the same grade PMMA as the sub-assembly was designed, this port was designed to fit with a water trap filter which connects to the VOC monitor for concentration monitoring of toluene vapour within the photoreactor (fig. 4.12).

(a) (b)

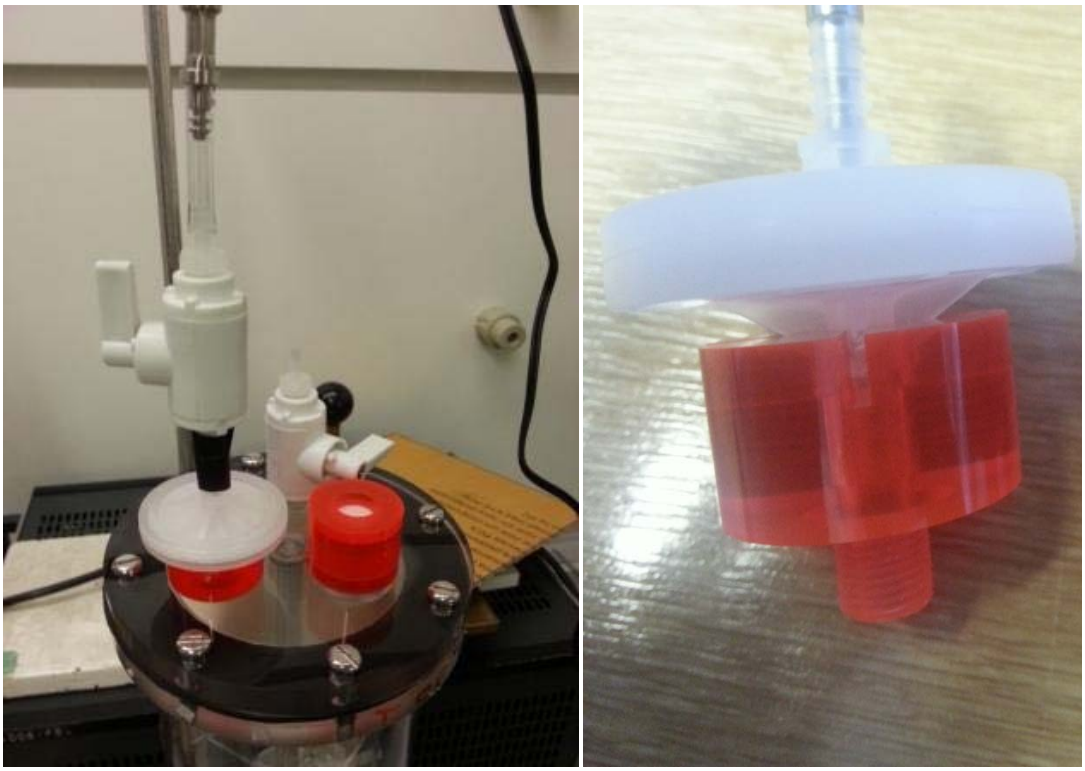

Figure 4.12: Reactor showing (b) custom designed sampling port with water trap filter attached and (a) arrangement of ports on the top of the photoreactor.

vi) Electric motor

The rotation of the Rushton impeller was made possible by a reversible synchronous geared AC motor manufactured by Crouzet. The motor was located beneath the sub-assembly and was connected to the Rushton impeller by the stainless steel shaft. Figure 4.13 shows the full assembly

of the photoreactor with the electric motor installed at the base and other stages of assembly.

(a) (b)

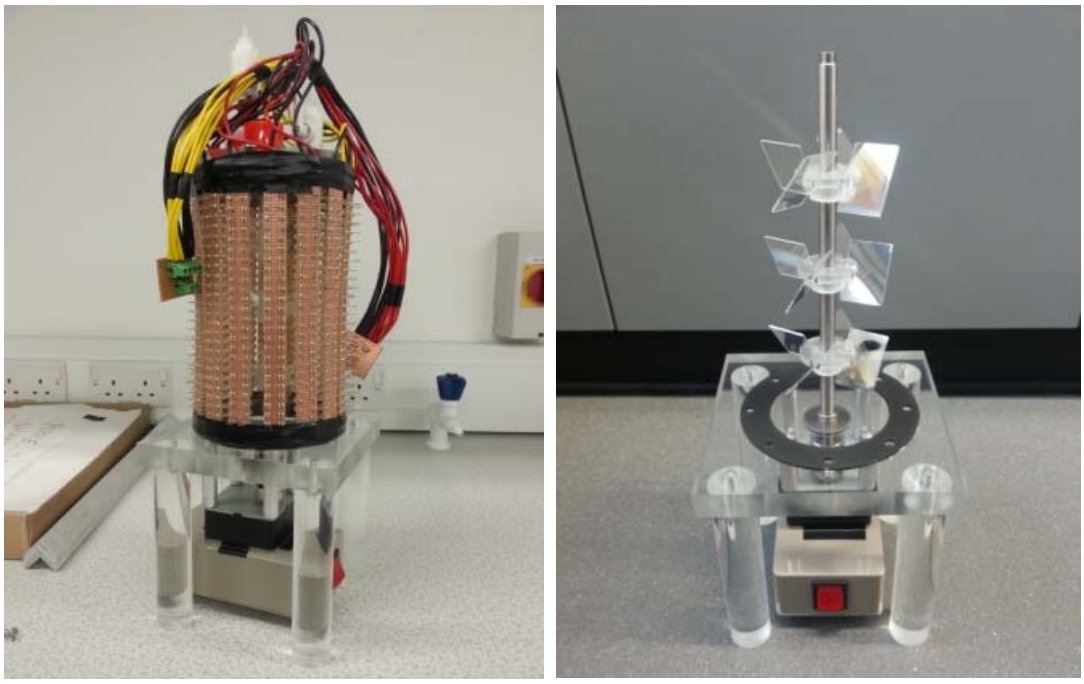

(C)

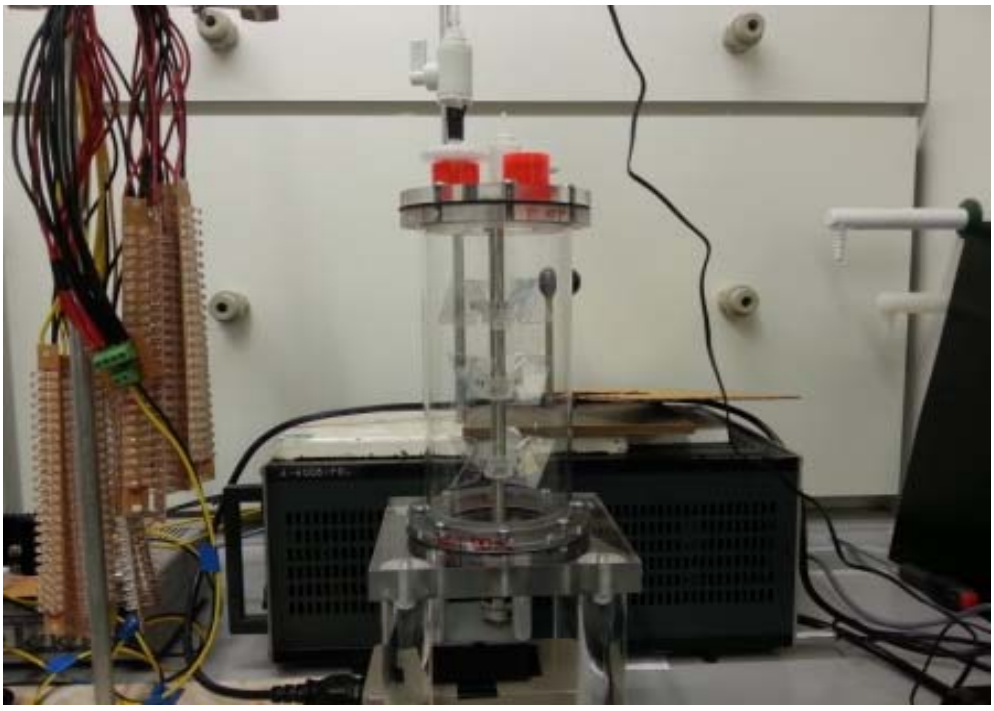

Figure 4.13: Designed photoreactor showing (a) full assembly (b) shaft and photocatalytic impellers (c) reactor without UV-LED array.

4.6.3. Leak test

The PIR photoreactor was designed for gas phase photocatalysis and so had to be gas-tight. A Thermo Scientific GLD PRO Leak Detector (fig. 4.14) which is able to detect minute leaks of all gasses was used for the test.

Figure 4.14: Leak test detector used to ensure the photoreactor was gas-tight.

The device is designed specifically for use with gas chromatography (GC) systems and it detects leaks using a thermal conductivity comparison between the probe gas and air as a reference.

4.7. Mode of operation

The designed photoreactor was operated in the batch mode for gas phase photocatalysis and because of the objective of the experimental work to be carried out, its mode of operation was put into consideration at every step of the design stage.

4.7.1. Light source

The geometry and shape of the reaction chamber and the full assembly was designed for the operation of UV-LEDs as the light source; because of the rotating immobilised photocatalyst, it was essential for illumination of the interior of the reaction chamber to come from a multi-directional source. UV-LEDs were designed in an array on stripboards and attached

to the top and bottom plates around the circumference of the reaction chamber (fig. 4.5).

(a) (b)

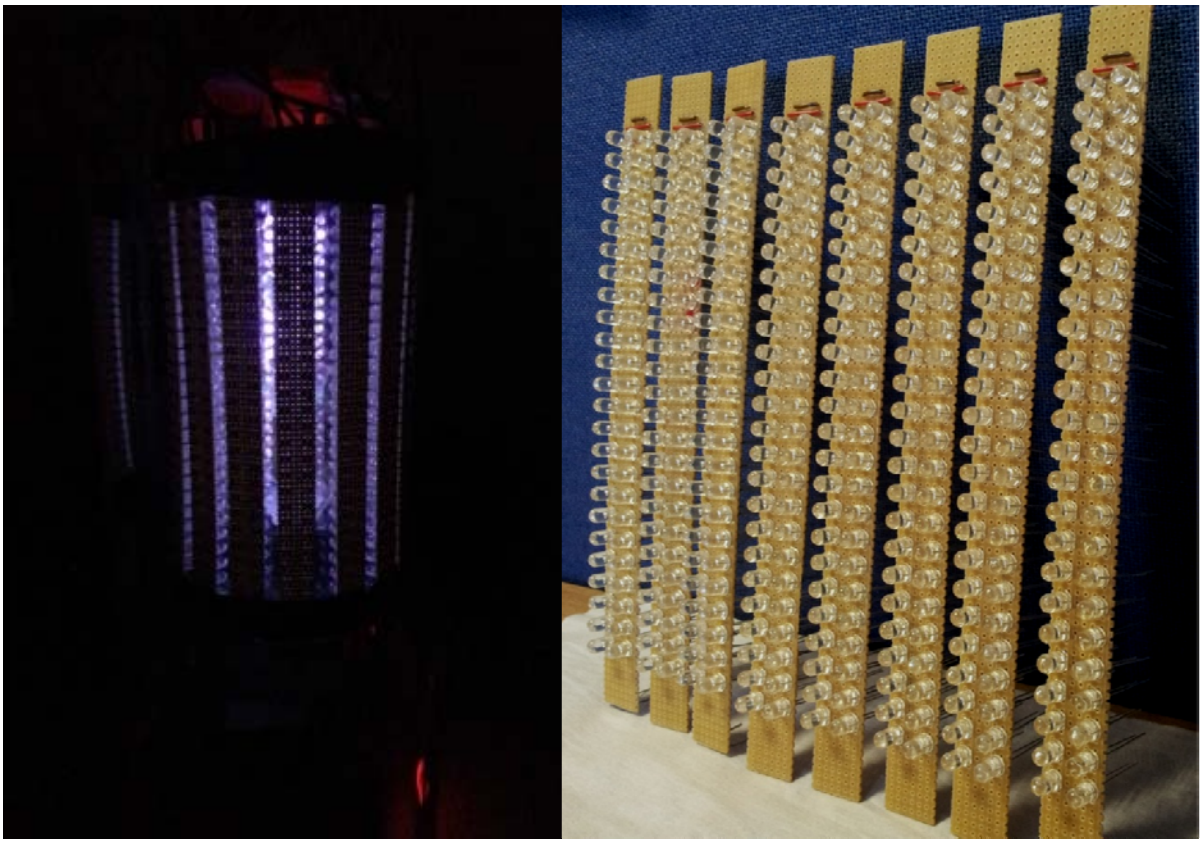

Figure 4.15: Designed photoreactor showing (a) UV-LED array for multi-directional illumination (b) UV-LED on strips.

4.7.2. Sample collection

The concentration of the sample VOC within the photoreactor was monitored using a MiniRae 2000 portable VOC monitor (fig. 4.16). The VOC monitor has a Photoionization Detector (PID) with an extended range of 0-10,000 ppm and a quick 3 second response time.

Figure 4.16: MiniRae 2000 VOC monitor used for monitoring sample concentration.

It is ideal for headspace sampling and can be operated in a discrete sampling mode or continuous sampling mode. The PID was connected by Tygon tubes to the sampling ports and used to monitor VOC concentration during the experiments.

4.8. Operation and evaluation of the PIR reactor

The performance of the designed photoreactor was evaluated with regard to photo-oxidation reaction rates, photonic efficiency of the photo-oxidation reaction and mass transfer limitation of the process. Mass transfer is particularly important because it has been reported to significantly reduce photocatalytic reaction rates in reactions that are diffusion controlled[175].

The fingerprint compound for the evaluation of the photoreactor was toluene. Toluene is one of the BTEX group of VOCs which is made up of benzene, toluene, Ethylbenzene and Xylene. The BTEX compounds are a major component of VOC emissions by the oil and gas industry because they are emitted during several oil and gas operations and toluene in particular is of interest in heterogeneous photocatalysis due to the eventual loss of activity by the catalyst that occurs during its photo-oxidation.

4.9. Experimental methods and materials

Known volume of toluene vapour (Fisher scientific) was withdrawn from toluene reagent headspace at room temperature using a gas tight syringe (SGE), and introduced into the air saturated reactor. Control measurements of toluene vapour concentration in the vacant reactor (fig. 4.17) were taken over a period of 1 h in the absence of both UV illumination and immobilized catalyst, with immobilized catalysts alone and with UV illumination alone.

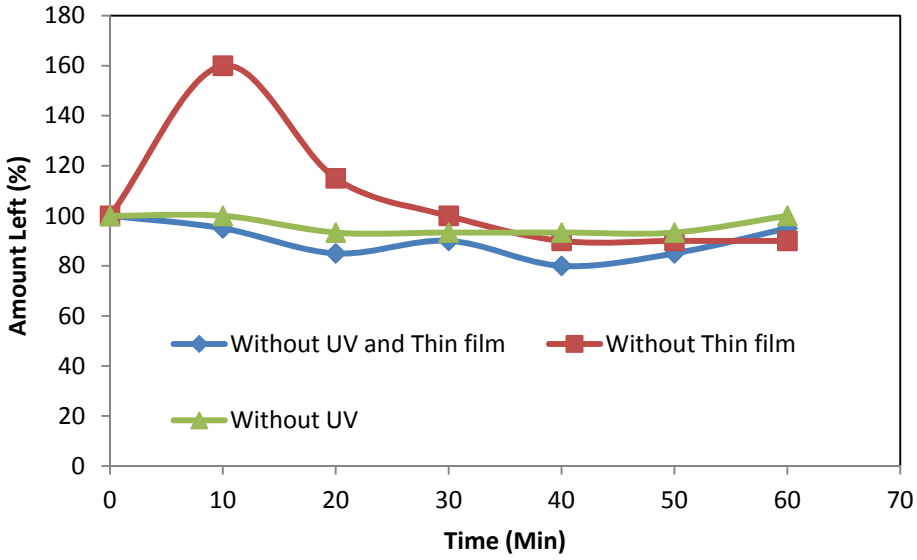

Figure 4.17: Control experiments of toluene vapour in the PIR reactor.

Photocatalytic degradation of toluene involved illumination of the immobilized catalysts by a UV-LED array of 5.58 Wm^{-2} intensity immediately after 10 mins of dark adsorption, followed by the rotation of the photocatalytic modified Rushton impellers at 10 RPM and real-time monitoring of toluene concentration with a VOC monitor (MiniRAE 2000). Reaction conditions were at room temperature and atmospheric pressure.

4.10. Toluene photo-oxidation in the PIR reactor

The stoichiometry and reaction pathway of complete mineralization of toluene by TiO_2 photocatalysis has been widely studied and reported[176, 177](fig.4.18), its photo-oxidation in gas-solid photocatalysis is characterized by the formation of solid intermediates which bond strongly to the immobilized TiO_2 thin film[178].

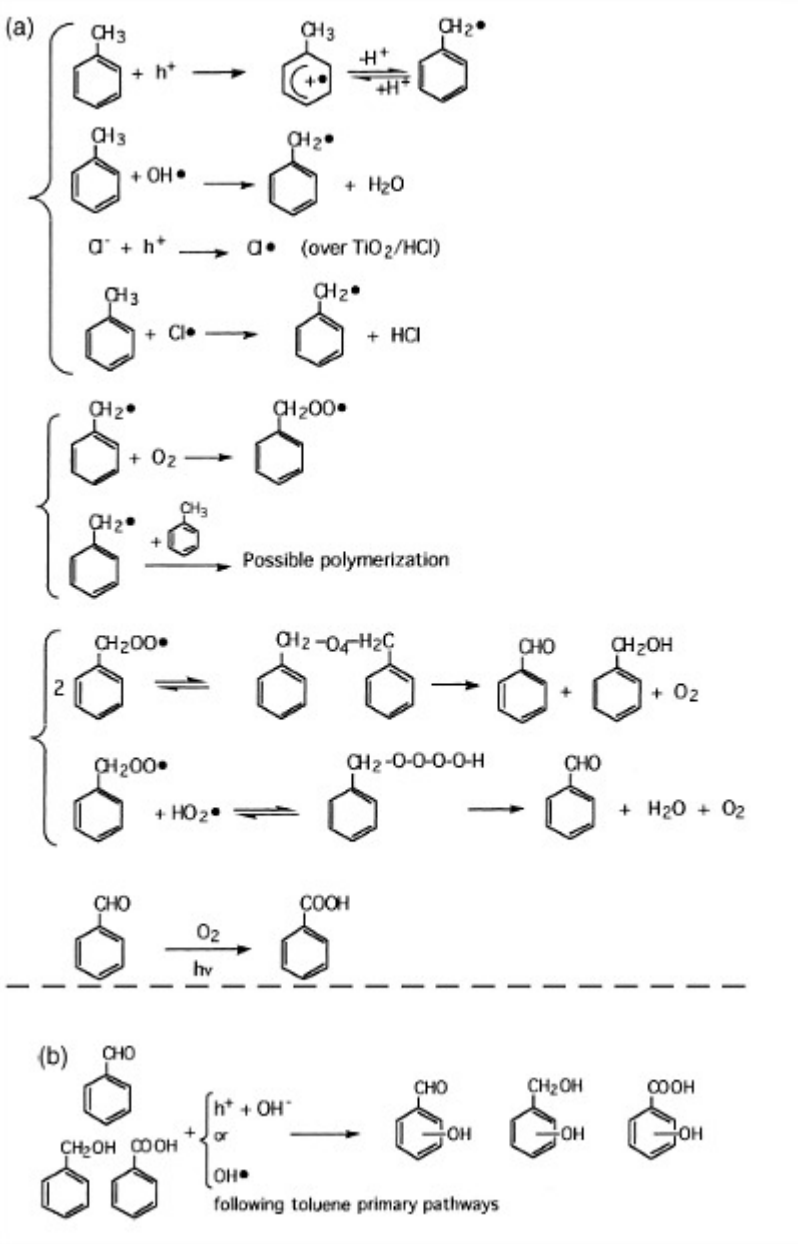

Figure 4.18: Possible pathways of toluene photo-oxidation as proposed by d'Hennezel *et al*.

The intermediates compete with the toluene molecule for active sites and are responsible for the loss of activity or deactivation and discolouration[65] of TiO_2 catalysts observed after toluene photo-oxidation.

4.10.1. Deactivation of immobilized TiO_2 thin film

The deactivation of TiO_2 photocatalysts can occur either as a reversible[179] or irreversible[180] deactivation and the aim of photocatalyst regeneration is to remove deactivating species without causing irreversible loss of

activity to the photocatalyst. Figure 4.19 is a simple schematic of toluene photo-oxidation showing the primary intermediates.

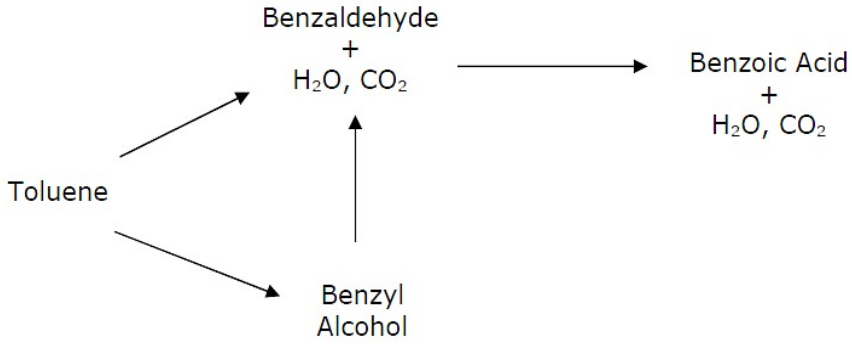

Figure 4.19: Pathway of toluene photo-oxidation showing the primary intermediates.

Previous studies have shown the amount and chemical composition of adsorbed deactivating species can determine if deactivation will be reversible or irreversible, the surface morphology of the photocatalyst also plays an important role[181]. Surfaces with a high amount of defects and irregularities like an immobilized thin film experience stronger adsorption and have lower removal rates of deactivating species, this may hamper the regeneration process and lead to irreversible deactivation. The regeneration of deactivated catalysts from toluene photo-oxidation is widely reported in the literature[66, 67] and was therefore not a focus of this investigation[67].

Due to the low illuminated catalyst surface area per unit reactor volume compared to reactors of other configurations[182], toluene degradation rate proceeded moderately with around 50% degradation achieved after a reaction time of 3 hours. Upon UV illumination, adsorbed toluene molecules desorb from the surface resulting in an increase in measured concentration. This is followed by a steady rate of degradation which later declines as a result of gradual loss of activity of the immobilized TiO_2 catalyst film due to strong binding of intermediate species on the catalyst surface[183]. Figure 4.20 shows the reducing activity of the immobilized TiO_2 catalyst which indicates catalyst deactivation. Unlike single-pass reactors, catalyst deactivation in batch reactors is concealed

by the concentration gradients in the reactor over the reaction time. The effect of deactivation on toluene photo oxidation was investigated as previously demonstrated by You *et al*.[66] by carrying out repeated runs of the same experimental conditions using the same photocatalytic impeller after flushing the reactor with fresh air. Reduced activity of the TiO_2 catalyst film becomes evident after the second run with almost total loss of activity on the fourth run.

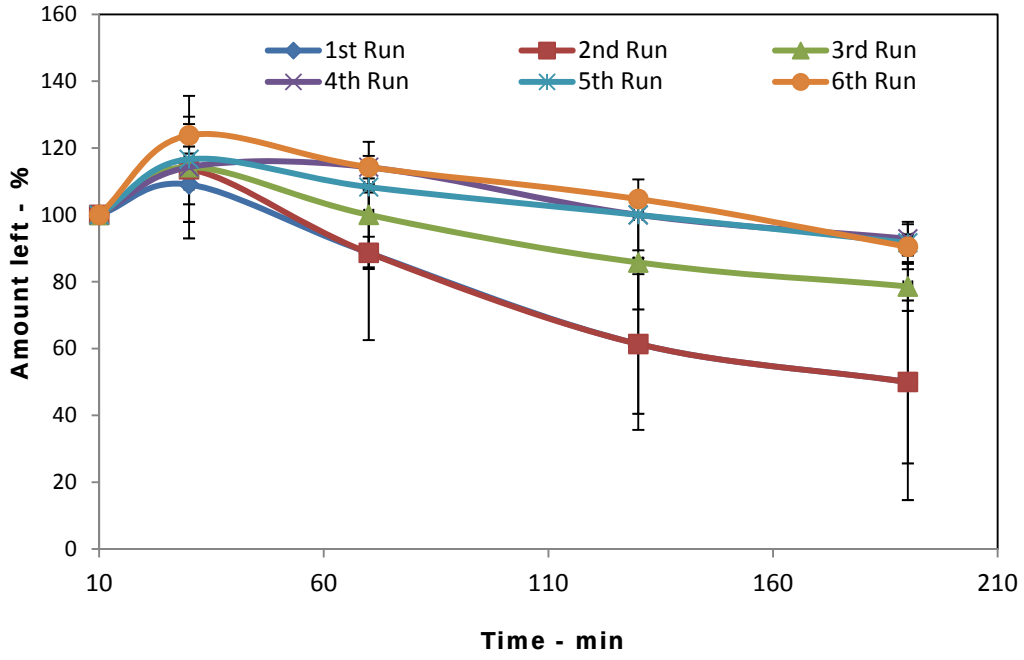

Figure 4.20: Photo-oxidation of toluene vapour showing loss of catalyst activity with repeated runs. The error bars are the standard deviations from the mean value of repeated experiments.

4.10.2. Langmuir-Hinshelwood kinetics

The rate of gas phase photo-oxidation of several VOCs including toluene have been previously shown to obey the Langmuir-Hinshelwood rate equation[78] (4.11), the accuracy of this model is based on the adsorption of a single reactant to the surface and the assumption that there is little or no competing adsorption by intermediate products.

$$-r = k\,K_{ads}\,[\text{Toluene}]/1 + K_{ads}\,[\text{Toluene}] \qquad (4.11)$$

At the low concentrations used in this study, between 2 ppm and 11 ppm, adsorption of toluene onto the photocatalytic impellers was marginal and reduced activity due to deactivation was noticeable after the first 6 hours. First-order kinetics was observed for the disappearance of toluene within this concentration and a linear plot of the double reciprocal of rate versus concentration verified the suitability of the Langmuir-Hinshelwood rate equation in modelling the photocatalytic reaction rates (fig. 4.21) with calculated apparent rate constant k of 0.0118 s^{-1} and a Langmuir adsorption coefficient K_{ads} of 0.3316 dm^3 ppm^{-1}.

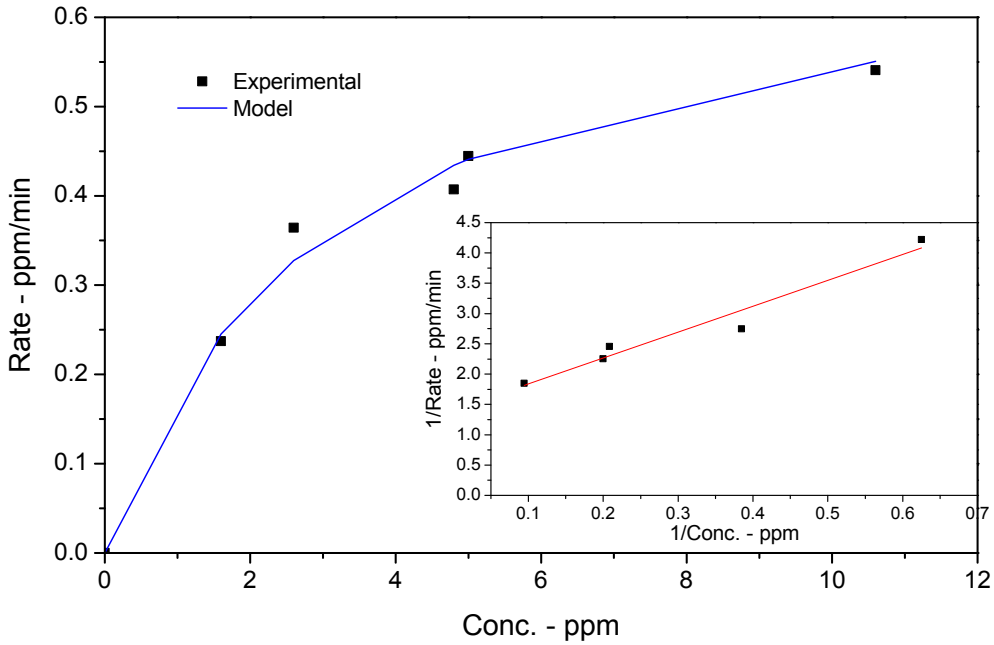

Figure 4.21: Comparison of toluene experimental and model degradation rates. Inset is the double reciprocal plot of rate versus concentration.

4.10.3. Influence of mass transfer on toluene photo-oxidation

The observed heterogeneous photocatalytic degradation of the toluene vapour occured at the boundary of the diffusion domain and was first-order. For photocatalytic reactions that obey the Langmuir-Hinshelwood rate equation, the heterogeneous second Damköhler number[184](4.12) is a representation of the ratio of the heterogeneous reaction rate to the radial diffusion rate. A Damköhler number above unity indicates toluene

diffusion time scale is greater than toluene reaction time scale hence, the overall process is mass transfer limited.

$$Da_{II} = \text{Reaction rate/Diffusive mass transfer rate} \quad (4.12)$$

For the reactor used in this study which is characterized by a radial flow aided by the impellers within the reactor, the dimensionless second Damköhler number was derived using the equation adapted by Gorges *et al*.[185] as follows:

$$Da_{II} = k/[(\beta a/K_{ads}) + \beta a C_b] \quad (4.13)$$

Where k is the apparent rate constant, K_{ads} is the Langmuir adsorption coefficient obtained from the slope of the double reciprocal linear plot in fig. 4.21 where $1/k$ is the intercept and $1/kK_{ads}$ equals the slope, C_b is the bulk toluene concentration, a is the interfacial area per unit volume of the reactor while β is the mass transfer coefficient such that

$$Sh \equiv \beta dh/D_s \quad (4.14)$$

dh and D_s are the reactor hydraulic diameter (0.094 m) and diffusivity of toluene in air respectively, Sh is the Sherwood number computed from Froessling equation (4.15)

$$Sh = 2 + 0.55Re^{0.5}Sc^{0.3} \quad (4.15)$$

Where Re and Sc are the dimensionless Reynolds (1.418) and Schmidt (17) numbers respectively. Table 4.1. shows the Damköhler number at different bulk concentrations, the results shows $Da_{II} < 1$ for all bulk concentrations indicating toluene photo-oxidation within the PIR reactor is reaction controlled. An increase in Da_{II} as bulk concentration decreases is observed, this is consistent with previous studies[185] and Fick's first law hence, mass transfer limitations are greater at lower bulk concentrations of toluene photo-oxidation in the reactor.

Table 4.1: Damköhler number of toluene degradation at different bulk concentrations.

C_b (ppm)	Damköhler no. (Da_{II})
10.6	0.2
5.0	0.3
4.8	0.3
2.6	0.4
1.6	0.4

4.10.4. Photonic efficiency of toluene photo-oxidation in the PIR reactor

In gas phase heterogeneous photocatalysis, typical quantum yields (φ) for reactions involving TiO_2 catalysts may exceed 50% under low UV illumination[80], this low efficiency has been previously attributed to mass transfer limitations, slow oxygen scavenging and charge-carrier recombination[64, 85, 186]. For toluene photo-oxidation in the PIR reactor, photonic efficiency (ζ) (4.16) which takes into consideration the photons incident on the photocatalyst and is therefore a lower limit of φ was correlated with mass transfer limitation and catalyst deactivation through the Damköhler number and reduced rates of reaction through loss of catalyst activity respectively (Table 4.2).

$$\zeta = \text{Reaction rate/Incident photon rate} \qquad (4.16)$$

Table 4.2: Damköhler number of toluene degradation at different bulk concentrations.

C_b (ppm)	Rate (ppm/s)	Photonic Efficiency (%)	Da_{II}
4.4	2.04E-04	2.0	0.3
4.4	2.04E-04	2.0	0.3
1.4	2.78E-05	0.3	0.5
1.4	9.26E-06	0.1	0.5
1.2	9.26E-06	0.1	0.5

Incident photon rate for the UV-LED array was 9.98E-7 Einsteins L^{-1} s^{-1}, reaction rates for toluene photo-oxidation were determined using the same photocatalytic impellers for five different 3 hour experiments. T he immobilized catalyst deactivated with each experiment and was reused for subsequent experiments and different bulk concentrations were used to vary the diffusion flux of toluene. The efficiency of photon utilization during toluene photo-oxidation in the PIR reactor showed a steady reduction as reaction rate reduced due to severe catalyst deactivation with increasing Da_{II} values indicating diffusional resistance also contributing to the low photonic efficiencies. The observed photonic efficiency showed equivalent values at both experiments of C_b = 4.4 ppm because the effects of deactivation becomes significant after the first 6 hours. At C_b = 1.4 ppm, toluene photo-oxidation rate is slower for the latter experiment hence, a lower photonic efficiency. After 12 hour of continuous toluene photo-oxidation, the immobilized catalyst is deactivated and this is indicated by the stagnating photo-oxidation rates and photonic efficiency at C_b = 1.4 ppm and 1.2 ppm.

4.11. Conclusion

A novel photocatalytic reactor based on a stirred tank configuration has been described; this reactor employs the use of photocatalytic impellers to aid the mass transport of gaseous organic compounds during photocatalytic reactions. Experiments involving toluene vapour photo-oxidation showed the reactor configuration is susceptible to catalyst deactivation even at low concentrations if treated for prolonged periods. In gas-solid heterogeneous photocatalysis, mass transfer of the reactants from the bulk to the catalyst surface is the single most important process especially in the photo-oxidation of VOCs which deactivate TiO_2 catalysts. Ultimately, this chapter shows the efficiency of photon utilization during the photo-oxidation of toluene in the PIR reactor is a function of the reaction rate which is affected by any limitations in mass diffusion of toluene to the immobilized catalyst and the simultaneous deactivation process. For the designed reactor used in this study, toluene photo-oxidation was reaction limited and the deactivation of the immobilized

catalyst further decreased the photo-oxidation rate of toluene vapour. The primary concern in the design of future immobilized reactors will be overcoming these limitations or adequately accounting for their effects.

CHAPTER V

5. CONCLUSION, CONTRIBUTION AND RECOMMENDATION FOR FUTURE WORK

5.1. Conclusion

Technological and industrial advances have led to large scale urbanization, industrialization and economic progress for many nations. This progress however, has had significant negative impacts on the environment particularly in the pollution of water and air. The increasing activities and expansion of the global oil and gas industry which is a major source of pollution to air and water has drawn a lot of focus to oil and gas activities as a source of pollution. Public awareness on the effects of environmental pollution especially from industries has also increased rapidly because of the cost in terms of public health, environmental degradation and social wellbeing. This has led to the regulation of the activities of the oil and gas industry with regard to emissions/effluent discharge to air and water and the implementation of measures for environmental protection by governments.

Volatile organic compounds (VOCs) which make up a significant amount of the emissions of the oil and gas industry have characteristics which make them suitable for degradation and mineralisation through heterogeneous photocatalysis. The majority of emissions from this industry however, are fugitive emissions with only a limited amount from point sources. Scale up of laboratory scale photocatalytic reactors and treatment systems such as have been designed in this research work can only have applications in VOC treatment from point sources.

Nevertheless, the application of semiconductor photocatalysis in the mineralization of aqueous and gaseous pollutants continues to remain a promising technology for environmental remediation. The goal of this project has been the improvement of the efficiency of this process in two ways; investigating the factors that influence photonic efficiency and the design of a highly efficient photoreactor. Even though outcomes show the

technique of CPI does not offer any advantage when applied alone, its application along with pH adjustments has been demonstrated to positively enhance photonic efficiency of photocatalytic oxidation reactions in a range of low duty cycles in a way which cannot be achieved by reducing UV intensity under continuous illumination.

To date, there is not yet a full scale deployment of photoreactor units for treatment of organic waste streams in industry. Catalyst deactivation by aromatic VOCs which can only be overcome by regenerating the catalyst through physical and chemical methods also affect the efficiency of the process. If semiconductor photocatalysis as a viable treatment method is to be commercialized, the practical and economic feasibility of the process has to be demonstrated. In order to do this, the design of photoreactors that are highly efficient in photon utilization is particularly essential. The use of UV-LEDs as sources of UV illumination in the design of such reactors is a first step because of their high energy efficiency and flexibility in design of reactors of different configurations.

5.2. Contribution

The research work which has been carried out and reported in this thesis has made a number of significant contributions to the understanding of the photonic efficiency of heterogeneous semiconductor photocatalysis as a whole.

5.2.1. A unique experimental approach

First among many contributions in this thesis is the study in chapter 2 which first showed experimentally in a closed loop and in one study that CPI under equivalent photon absorption by the catalyst does not provide any advantage over continuous UV illumination. The results of this study are published in the journal of catalysis[100], indicating the novelty of the controlled experimental design of the experiments and the relevance of the study.

5.2.2. Optimizing photonic efficiency

In chapter 3, an investigation of the combined effects of pH, duty cycle and role of oxidizing species on photonic efficiency is carried out. The results of this study outlines how photonic efficiency can be optimized under CPI through the harmonization of interaction between catalyst surface and reactants, duty cycle of illumination and oxidizing species. This study is published in the chemical engineering journal (Appendix D.2) indicating the importance of the findings in the study.

5.2.3. A new limitation for the Langmuir-Hinshelwood rate model

The Langmuir-Hinshelwood rate equation is suitable for predicting reaction rates of most photocatalytic reactions using the initial rates method despite the shortcomings[187] of this method. As a result of this, it is widely applied to photocatalytic reactions and a modified L-H model by Chen *et al*.[89] was adapted for photocatalytic reactions under CPI. The theoretical study in chapter 3 reports the limitations of this model's accuracy to reactions under a single duty cycle. When a range of duty cycles is involved, the model is unable to produce a good fit for experimental data.

5.2.4. Re-thinking photoreactor design

A Photocatalytic Impeller Reactor (PIR) is a reactor in which mass transfer of reactants within the reactor is aided by a photocatalytic impeller acting as an immobilized photocatalyst. This novel photoreactor configuration is first conceptualized, designed and introduced in chapter 4 of this research. The results of its evaluation are promising and show the potential which novel reactor designs like the PIR reactor can have in overcoming the limitations of immobilized reactor configurations.

5.2.5. Photonic efficiency as a function of mass transfer and deactivation rate

In the evaluation of the PIR reactor, the correlation of photonic efficiency of toluene photo-oxidation with mass transfer limitations and rate of loss of catalyst activity through catalyst deactivation is shown. This is important especially for understanding the low photonic efficiencies which characterize VOC treatment using heterogeneous photocatalysis.

5.2.6. Review of a body of knowledge

A review of the literature before and during this research work show the vast majority of irradiation sources used in photocatalysis studies to be artificial, usually in the form of UV lamps. A few studies have utilized lasers while there is an increase in the use of UV-LEDs. Artificial lighting sources in the form of UV-LEDs have been used all through this research work and this has led to a review journal paper titled 'UV-LED sources for heterogeneous photocatalysis' highlighting the present situation of UV-LEDs as irradiation sources being written. The review will be another major contribution of this thesis as the importance of UV-LEDs going forward in the field of photocatalysis and all advantages they offer will be made available in a single paper.

5.3. Recommendations for future work

The objectives of this research have largely been met but looking forward, there are several recommendations necessary for future work in this area of research and to the research community in the field of semiconductor photocatalysis

5.3.1. The future of controlled periodic illumination

Although the initial hypothesis which controlled periodic illumination was based on had the primary aim of enhancement of photonic efficiency, this is however not possible when it is applied alone. This technique can find applications in other areas of photocatalysis such as investigating its use in inhibiting catalyst deactivation in gas-solid photocatalysis.

5.3.2. Photocatalytic reaction rate modelling

The use of the Langmuir-Hinshelwood rate equation for the correlation of photocatalytic rates of reactions under controlled periodic illumination is inadequate; the modified L-H model fails to predict rates when a range of illumination duty cycle is used. This makes the development of rate models or the modification of the L-H model similar to the work by Mehrvar *et al*.[187] to accurately fit experimental data relevant for future CPI studies.

5.3.3. Photoreactor design

The photoreactor designed in this study used temporary materials such as PMMA and silicone seals, this was necessary for flexibility, adaptability and easy maintenance. In order to accurately assess the performance of the Photocatalytic Impeller Reactor (PIR) configuration, permanent and durable materials such as stainless steel and glass should be employed in the design of future reactors of this configuration.

REFERENCES

1. Hill MK. Understanding Environmental Pollution. Cambridge, UK: Cambridge University Press, 2010.

2. Mason CF. Water Pollution Biology. In: Harrison RM (ed). Pollution: Causes, Effects and Control. Cambridge, UK: The Royal Society of Chemistry, 2001:82.

3. Rao CS. Environmental Pollution Control Engineering. New Delhi, India: New Age International (P) Limited, 2006.

4. UN Web Services Section, Department of Public Information. United Nations Day 2011.

5. WHO Global Health Observatory. Urban population growth <http://www.who.int/gho/urban_health/situation_trends/urban_population_growth_text/en/index.html>. Accessed July 8. 2012.

6. Misaelides P. Application of natural zeolites in environmental remediation: A short review. Microporous and Mesoporous Materials. 2011; 144:15-18.

7. Scottish Environment Protection Agency. Pollution Control <http://www.sepa.org.uk/water/water_regulation/regimes/pollution_control.aspx>. Accessed July 8. 2012.

8. Yarón B, Calvet R, Prost R. Soil Pollution: Processes and Dynamics. Germany: Springer, 1996.

9. Mani D, Misra SG. Soil Pollution. New Delhi: APH Publishing Corporation, 2009.

10. Salameh E, Harahsheh S. Eutrophication processes in arid climates. In: Ansari AA, Jill SS, Lanza GR, Rast W (eds). Eutrophication: Causes, Consequences and Control. Springer, 2011:69.

11. Harrison RM. Air pollution: Sources, Concentrations and Measurements. In: Harrison RM (ed). Pollution: Causes, Effects and Control. Cambridge, UK: The Royal Society of Chemistry, 2001:169.

12. Agarwal SK. Air Pollution. New Delhi, India: A P H Publishing Corporation, 2009.

13. Harrison RM. Sources of Air pollution. In: World Health Organization (ed). Air Quality Guidelines: Global Update 2005: Particulate Matter, Ozone, Nitrogen Dioxide and Sulphur Dioxide. Germany: Druckpartner Moser, 2006:9.

14. The Economist. Let them have fuel <http://www.economist.com/node/21543199>. Accessed July 8. 2012.

15. The New York Times. As Oil Industry Fights a Tax, It Reaps Subsidies <http://www.nytimes.com/2010/07/04/business/04bptax.html?_r=2>. Accessed July 8. 2010.

16. UK Trade and Investment. The UK Oil and Gas industry <http://www.ukti.gov.uk/investintheuk/sectoropportunities/oilgas/item/280103.html>. Accessed July 8. 2012.

17. Cowling EB. Acid precipitation in historical perspective. Environmental Science and Technology. 1982; 16:110A-123A.

18. Dincer I, Rosen MA. Energy, environment and sustainable development. Applied Energy. 1999; 64:427-440.

19. Lacis AA, Schmidt GA, Rind D, Ruedy RA. Atmospheric CO_2: Principal control knob governing Earth's temperature. Science. 2010; 330:356-359.

20. Dincer I. Energy and environmental impacts: Present and future perspectives. Energy Sources. 1998; 20:427-453.

21. Wun-Cheng Wang. Volatile Organic Compounds in the Environment. Fredericksburg, USA: American Society for Testing and Materials, 1996.

22. United States Environmental Protection Agency. Volatile Organic Compounds Emissions <http://cfpub.epa.gov/eroe/index.cfm?fuseaction=detail.viewInd&lv=list.listbyalpha&r=219697&subtop=341>. Accessed 24.12. 2010.

23. Passant N. Speciation of UK emissions of non-methane volatile organic compounds. AEA Technology Report ENV-0545, Culham, Abingdon, United Kingdom. 2002; .

24. Wood F. Photocatalytic Destruction of Volatile Organic Compounds Generated by the Oil and Gas Industry. The Robert Gordon University. 2008.

25. Passant NR. Source, Inventories and Control Strategies for VOCs. In: Hestter RE, Harrison RM (eds). Volatile Organic Compounds in the Atmosphere. Cambridge, UK: The Royal Society of Chemistry, 1995:51.

26. Alberici MR, Jardim FW. Photocatalytic destruction of VOCs in the gas-phase using titanium dioxide. Applied Catalysis B: Environmental. 1997; 14:- 55.

27. An Alternate Approach to VOC Speciation Reporting. Proceedings of the 12th Annual Emission Inventory Conference: Emission Inventories - Applying New Technologies, 2003.

28. U.S Environmental Protection Agency. Ground-level Ozone <http://www.epa.gov/glo/>. Accessed September 23. 2011.

29. Scottish Environment Protection Agency (SEPA). Benzene, toluene, ethylbenzene, xylenes (BTEX) <http://apps.sepa.org.uk/spripa/Pages/SubstanceInformation.aspx?pid=999>. Accessed 01/24. 2014.

30. Crump KS. Risk of benzene-induced leukemia: A sensitivity analysis of the pliofilm cohort with additional follow-up and new exposure estimates. Journal of Toxicology and Environmental Health, Part A Current Issues. 1994; 42:219-242.

31. ChemSystems. The Future Of Benzene And Para-Xylene After Unprecedented Growth In 2010 <http://www.chemsystems.com/about/cs/news/items/PPE%20PCMD%20Aromatics%202011.cfm>. Accessed 01/24. 2011.

32. Cardelino C, Chameides W. An observation-based model for analyzing ozone precursor relationships in the urban atmosphere. J Air Waste Management Association. 1995; 45:161-180.

33. Atkinson R. Atmospheric chemistry of VOCs and NOx. Atmospheric Environment. 2000; 34:2063-2101.

34. Goldstein AH, Galbally IE. Known and unexplored organic constituents in the earth's atmosphere. Environmental Science and Technolnology. 2007; 41:1514-1521.

35. Scottish Environment Protection Agency. Ambient Air Quality <http://www.sepa.org.uk/air/ambient_air_quality.aspx>. Accessed July 8. 2012.

36. Environment Agency. Directives <http://www.environment-agency.gov.uk/business/regulation/31865.aspx>. Accessed 12.28. 2011.

37. Scottish Environment Protection Agency. Pollution Prevention and Control (Scotland) Regulation <http://www.sepa.org.uk/air/process_industry_regulation/pollution_prevention__control/legislation.aspx>. Accessed December 25. 2012.

38. European Comission. The IPPC directive <http://ec.europa.eu/environment/air/pollutants/stationary/ippc/summary.htm>. Accessed 12,25. 2011.

39. Reid DA. European Union environmental law and policy in relation to oil and gas. In: Gao Z (ed). Environmental Regulation of Oil and Gas. London, UK: Kluwer law International Ltd, 1998:180.

40. Khan FI, Kr. Ghoshal A. Removal of volatile organic compounds from polluted air. Journal of Loss Prevention in the Process Industries. 2000; 13:527-545.

41. Farhataziz, Ross AB. Selective Specific Rates of Reactions of Transients in Water and Aqueous Solutions. Part III. Hydroxyl Radical and Perhydroxyl Radical and their Radical Ions. National Standard Reference Data Series. 1977; 59.

42. Hoigné J, Bader H. Rate constants of reactions of ozone with organic and inorganic compounds in water—II: Dissociating organic compounds. Water Research. 1983; 17:185-194.

43. Andreozzi R, Caprio V, Insola A, Marotta R. Advanced oxidation processes (AOP) for water purification and recovery. Catalysis Today. 1999; 53:51-59.

44. Linsebigler LA, Lu G, Yates TJ. Photocatalytic on TiO_2 surfaces: Principles, mechanisms, and selected results. Chemical Reviews. 1995; 95:735-758.

45. Fujishima A, Zhang X. Titanium dioxide photocatalysis: Present situation and future approaches. Comptes Rendus Chimie. 2006; 9:750-760.

46. Hashimoto K, Irie H, Fujishima A. TiO_2 photocatalysis: A historical overview and future prospects. Japanese Journal of Applied Physics. 2005; 14:8269-8285.

47. Fujishima A, Honda K. Photolysis-decomposition of water at the surface of an irradiated semiconductor. Nature. 1972; 238:37-38.

48. Hoffmann MR, Martin ST, Choi W, Bahnemann DW. Environmental applications of semiconductor photocatalysis. Chemical Reviews. 1995; 95:69-96.

49. Ollis D. Kinetic Disguises in Heterogeneous Photocatalysis. Topics in Catalysis. 2005; 35:217-223.

50. Yaron P. Photocatalytic treatment of air: from basic aspects to reactors. In: De Lasa H, Serrano-Rosales B (eds). Advances in Chemical Engineering: Photocatalytic Technologies. USA: Elsevier Inc., 2009:289.

51. Fox AM, Dulay TM. Heterogeneous photocatalysis. Chemical Reviews. 1993; 93:341-357.

52. McCullagh C, Skillen N, Adams M, Robertson PKJ. Photocatalytic reactors for environmental remediation: A review. Journal of Chemical Technology & Biotechnology. 2011; 86:1002-1017.

53. Fujishima A, Rao TN, Tryk DA. Titanium dioxide photocatalysis. Journal of Photochemistry and Photobiology C: Photochemistry Reviews. 2000; 1:1-21.

54. Qiu R, Song L, Mo Y, Zhang D, Brewer E. Visible light induced photocatalytic degradation of phenol by polymer-modified semiconductors: Study of the influencing factors and the kinetics. Reaction Kinetics and Catalysis Letters. 2008; 94:183-189.

55. Wang X, Tang S, Zhou C, Liu J, Feng W. Uniform TiO_2–PANI composite capsules and hollow spheres. Synthetic Metals. 2009; 159:1865-1869.

56. Yao-Hsuan T, Chien-Sheng K, Chia-Hung H, Yuan-Yao L, Po-Wen C, Chia-Liang C, Ming. Visible-Light-Responsive Nano-TiO_2 with Mixed Crystal Lattice and its Photocatalytic Activity. Nanotechnology. 2006; 17:2490.

57. Henglein A. Photochemistry of colloidal cadmium sulfide. 2. effects of adsorbed methyl viologen and of colloidal platinum. Journal of Physical Chemistry. 1982; 86:2291-2293.

58. Ohtani B, Prieto-Mahaney OO, Li D, Abe R. What is degussa (evonik) P25? crystalline composition analysis, reconstruction from isolated pure particles and photocatalytic activity test. Journal of Photochemistry and Photobiology A. 2010; 216:179-182.

59. Mills A, Le Hunte S. An overview of semiconductor photocatalysis. Journal of Photochemistry and Photobiology A. 1997; 108:1-35.

60. Mao-Xiang J, Xue-Qin J, Wang-Xing L, Dong-Hong L, Zhou W. Preparation and photocatalytic activity of mesoporous TiO_2 microspheres. Micro and Nanosystems. 2009; 1:12-16.

61. Muktha B, Madras G, Row TNG, Scherf U, Patil S. Conjugated polymers for photocatalysis. Journal of Physical Chemistry. 2007; 111:7994-7998.

62. Lewandowski M, Ollis DF. Photocatalytic oxidation of gas-phase aromatic contaminants. In: Ramamurthy V, Schanze KS (eds). Semiconductor Photochemistry and Photophysics. New York, USA: Marcel Dekker Inc., 2005:238.

63. Ollis FD. Photocatalytic purification and remediation of contaminated air and water. Comptes Rendus de l'Académie des Sciences - Series IIC - Chemistry. 2000; 3:405-411.

64. Ollis DF, Al-Ekabi H, Eds. Photocatalytic Purification and Treatment of Water and Air. New York, USA: Elsevier, 1993.

65. Maira AJ, Yeung KL, Soria J. Gas-phase photo-oxidation of toluene using nanometer-size TiO_2 catalysts. Applied Catalysis B: Environmental. 2001; 29:327-336.

66. You Y, Chung K, Kim Y, Kim J, Seo G. Deactivation and regeneration of titania catalyst supported on glass fiber in the photocatalytic degradation of toluene. Korean Journal of Chemical Engineering. 2003; 20:58.

67. Cao L, Gao Z, Suib SL, Obee TN, Hay SO, Freihaut JD. Photocatalytic oxidation of toluene on nanoscale TiO_2 catalysts: Studies of deactivation and regeneration. Journal of Catalysis. 2000; 196:253-261.

68. Sauer ML, Ollis DF. Catalyst deactivation in Gas–Solid photocatalysis. Journal of Catalysis. 1996; 163:215-217.

69. Bhagwat, C., Dhar, V. Journal Indian Chemical Society. 1932, pp.335.

70. Doede CM, Walker CA. Photochemical engineering. Chemical Engineering. 1955; 62:159-178.

71. Yang R, Zhang Y, Zhao R. An improved model for analyzing the performance of photocatalytic oxidation reactors in removing volatile organic compounds and its application. Journal of Air and Waste Management Association. 2004; 54:1516-1524.

72. Mo J, Zhang Y, Xu Q, Lamson JJ, Zhao R. Photocatalytic purification of volatile organic compounds in indoor air: A literature review. Atmospheric Environment. 2009; 43:2229-2246.

73. Cassano EA, Martin AC, Brandi JR, Alfano MO. Photoreactor analysis and design: Fundamentals and applications. Industrial and Engineering Chemistry Research. 1995; 34:2155-2201.

74. Cassano AE, Silveston PL, Smith JM. Photochemical reaction engineering. Industrial and Engineering Chemistry. 1967; 59:18–38.

75. Cassano AE, Alfano OM. Reaction engineering of suspended solid heterogeneous photocatalytic reactors. Catalysis Today. 2000; 58:167-197.

76. Jo M, Rene ER, Kim S, Park H. An analysis of synergistic and antagonistic behavior during BTEX removal in batch system using response surface methodology. Journal of Hazardous Materials. 2008; 152:1276-1284.

77. Chen X, Zhang G, Zhang Q, Chen H. Mass concentrations of BTEX inside air environment of buses in changsha, china. Building and Environment. 2011; 46:421-427.

78. Boulamanti AK, Korologos CA, Philippopoulos CJ. The rate of photocatalytic oxidation of aromatic volatile organic compounds in the gas-phase. Atmospheric Environment. 2008; 42:7844-7850.

79. Grela AM, Colussi JA. Kinetics of Stochastic Charge Transfer and Recombination Events in Semiconductor Colloids. Relevance to Photocatalysis Efficiency. Journal of Physical Chemistry. 1996; 100:18214-18221.

80. Cornu JGC, Colussi AJ, Hoffmann RM. Quantum yields of the photocatalytic oxidation of formate in aqueous TiO_2 suspensions under continuous and periodic illumination. Journal of Physical Chemistry B. 2001; 105:1351-1354.

81. Ohko Y, Hashimoto K, Fujishima A. Kinetics of Photocatalytic Reactions Under Extremely Low-Intensity UV Illumination on Titanium Dioxide Thin Films. Journal of Physical Chemistry A. 1997; 101:8057-8062.

82. Disdier J, Herrmann J, Pichat P. Platinum/titanium Dioxide Catalysts. A Photoconductivity Study of Electron Transfer from the Ultraviolet-Illuminated Support to the Metal and of the Influence of Hydrogen. Journal of the Chemical Society, Faraday Transactions 1. 1983; 79:651-660.

83. Jiang Z, Wang H, Huang H, Cao C. Photocatalysis enhancement by electric field: TiO_2 thin film for degradation of dye X-3B. Chemosphere. 2004; 56:503-508.

84. Sczechowski JG, Koval CA, Noble RD. Evidence of critical illumination and dark recovery times for increasing the photoefficiency of aqueous heterogeneous photocatalysis. Journal of Photochemistry and Photobiology A. 1993; 74:273-278.

85. Upadhya S, Ollis FD. Simple photocatalysis model for photoefficiency enhancement via controlled, periodic illumination. Journal of Physical Chemistry B. 1997; 101:2625-2631.

86. Buechler JK, Noble DR, Koval AC, Jacoby AW. Investigation of the effects of controlled periodic illumination on the oxidation of gaseous trichloroethylene using a thin film of TiO_2. Industrial and Engineering Chemistry Research. 1999; 38:892-896.

87. Stewart G, Fox AM,. The effect of dark recovery time on the photoefficiency of heterogeneous photocatalysis by TiO_2 suspended in non-aqueous media. Research on Chemical Intermediates. 1995; 21:933-938(6).

88. Mehta DS, Saxena K, Dubey SK, Shakher C. Coherence characteristics of light-emitting diodes. Journal of Luminescence. 2010; 130:96-102.

89. Chen H, Ku Y, Irawan A. Photodecomposition of o-cresol by UV-LED/TiO_2 process with controlled periodic illumination. Chemosphere. 2007; 69:184-190.

90. Dias M, Azevedo E. Photocatalytic Decolorization of Commercial Acid Dyes using Solar Irradiation. Water, Air, & Soil Pollution. 2009; 204:79-87.

91. Fox Group Optoelectronics, FoxUV LEDs, 360nm 5mm round, Available online. Last accessed 12.08.2011. URL: http://www.thefoxgroupinc.com/index.php?%20%20option=com_content&view=article&id=74&Itemid=68. FoxUV™ LEDs, 360nm 5mm round <http://www.thefoxgroupinc.com/index.php?%20%20option=com_content&view=article&id=74&Itemid=68>. Accessed 12/08. .

92. Guettaï N, Ait Amar H. Photocatalytic oxidation of methyl orange in presence of titanium dioxide in aqueous suspension. part I: Parametric study. Desalination. 2005; 185:427-437.

93. Cornu CJG, Colussi AJ, Hoffmann MR. Time scales and pH dependences of the redox processes determining the photocatalytic efficiency of TiO_2 nanoparticles from periodic illumination experiments in the stochastic regime. The Journal of Physical Chemistry B. 2003; 107:3156-3160.

94. Ollis FD, Pelizzetti E, Serpone N. Photocatalyzed destruction of water contaminants Environmental Science and Technology. 1991; 25:1522-1529.

95. Rashed MN, El-Amin AA. Photocatalytic degradation of methyl orange in aqueous TiO_2 under different solar irradiation sources. International Journal of Physical Sciences. 2007; 2:073-081.

96. Curcó D, Giménez J, Addardak A, Cervera-March S, Esplugas S. Effects of radiation absorption and catalyst concentration on the photocatalytic degradation of pollutants. Catalysis Today. 2002; 76:177-188.

97. Chen Y, Wang K, Lou L. Photodegradation of dye pollutants on silica gel supported TiO_2 particles under visible light irradiation. Journal of Photochemistry and Photobiology A. 2004; 163:281-287.

98. Konstantinou IK, Albanis TA. TiO_2-assisted photocatalytic degradation of azo dyes in aqueous solution: Kinetic and mechanistic investigations: A review. Applied Catalysis B: Environmental. 2004; 49:1-14.

99. Marugán J, Hufschmidt D, Sagawe G, Selzer V, Bahnemann D. Optical density and photonic efficiency of silica-supported TiO2 photocatalysts. Water Research. 2006; 40:833-839.

100. Tokode OI, Prabhu R, Lawton LA, Robertson PKJ. Effect of controlled periodic-based illumination on the photonic efficiency of photocatalytic degradation of methyl orange. Journal of Catalysis. 2012; 290:138-142.

101. Brown GT, Darwent JR. Methyl orange as a probe for photooxidation reactions of colloidal titanium dioxide. Journal of Physical Chemistry. 1984; 88:4955-4959.

102. Chen LC, Chou TC. Photodecolorization of methyl orange using silver ion modified TiO_2 Industrial & Engineering Chemistry Research as photocatalyst. Industrial & Engineering Chemistry Research. 1994; 33:1436-1443.

103. Barka N, Qourzal S, Assabbane A, Ait-Ichou Y. Kinetic modeling of the photocatalytic degradation of methyl orange by supported TiO_2. Journal of Environmental Science and Engineering. 2010; 4:1-5.

104. Chen LC, Chou TC. Kinetics of photodecolorization of methyl orange using titanium dioxide as catalyst. Industrial & Engineering Chemistry Research. 1993; 32:1520-1527.

105. Buechler KJ, Zawistowski TM, Noble RD, Koval CA. Investigation of the mechanism for the controlled periodic illumination effect in TiO_2 photocatalysis. Industrial & Engineering Chemistry Research. 2001; 40:1097-1102.

106. Sczechowski JG, Koval CA, Noble RD. A taylor vortex reactor for heterogeneous photocatalysis. Chemical Engineering Science. 1995; 50:3163-3173.

107. Herrmann JM. Heterogeneous photocatalysis: State of the art and present applications in honor of pr. RL burwell jr.(1912–2003), former head of ipatieff laboratories, northwestern university, evanston (ill). Topics in Catalysis. 2005; 34:49-65.

108. Gerischer H, Heller A. Photocatalytic oxidation of organic molecules at TiO_2 particles by sunlight in aerated water. Journal of The Electrochemical Society. 1992; 139:113-118.

109. Rauf MA, Marzouki N, Körbahti BK. Photolytic decolorization of rose bengal by UV/H_2O_2 and data optimization using response surface method. Journal of Hazardous Materials. 2008; 159:602-609.

110. Sharma S, Ameta R, Malkani R, Ameta SC. Photocatalytic degradation of rose bengal using semiconducting zinc sulphide as the photocatalyst. Journal of the Serbian chemical society. 2013; 78:897-905.

111. Suttiponparnit K, Jiang J, Sahu M, Suvachittanont S, Charinpanitkul T, Biswas P. Role of surface area, primary particle size, and crystal phase on titanium dioxide nanoparticle dispersion properties. Nanoscale Research Letters. 2011; 6:27.

112. Siffert B, Metzger J. Study of the interaction of titanium dioxide with cellulose fibers in an aqueous medium. Colloids and Surfaces. 1991; 53:79-99.

113. Guo H, Lin K, Zheng Z, Xiao F, Li S. Sulfanilic acid-modified P25 TiO_2 nanoparticles with improved photocatalytic degradation on congo red under visible light. Dyes and Pigments. 2012; 92:1278-1284.

114. Kormann C, Bahnemann DW, Hoffmann MR. Photolysis of chloroform and other organic molecules in aqueous TiO_2, suspensions. Environmental Science and Technology. 1991; 25:494-500.

115. Kumar S, Davis AP. Heterogeneous photocatalytic oxidation of nitrotoluenes. Water Environment Research. 1997; 69:1238-1245.

116. Choi W, Hoffmann M, R. Photoreductive mechanism of CCl_4 degradation on TiO_2 particles and effects of electron donors. Environmental Science and Technology. 1995; 29:1646–1654.

117. Lewis NS. Chemical control of charge transfer and recombination at semiconductor photoelectrode surfaces. Inorganic Chemistry. 2005; 44:6900-6911.

118. Hou W, Ku Y. Photocatalytic decomposition of gaseous isopropanol in a tubular optical fiber reactor under periodic UV-LED illumination. Journal of Molecular Catalysis A: Chemical. 2013; 374–375:7-11.

119. Jamali A, Vanraes R, Hanselaer P, Van Gerven T. A batch LED reactor for the photocatalytic degradation of phenol. Chemical Engineering and Processing: Process Intensification. 2013; 71:43-50.

120. Baccaro ALB, Gutz IGR. Novel photoelectrocatalytic approach aiming at the digestion of water samples, estimation of organic matter content and stripping analysis of metals in a special UV-LED irradiated cell with a TiO_2-modified gold electrode. Electrochemistry Communications. 2013; 31:28-30.

121. Wang Z, Liu J, Dai Y, Dong W, Zhang S, Chen J. Dimethyl sulfide photocatalytic degradation in a light-emitting-diode continuous reactor: Kinetic and mechanistic study. Industrial & Engineering Chemistry Research. 2011; 50:7977-7984.

122. Venkataramani S, Davitt KM, Xu H. Semiconductor ultra-violet light-emitting diodes for flash photolysis. Journal of Neuroscience Methods. 2007; 160:5-9.

123. Natarajan TS, Natarajan K, Bajaj CH, Tayade JR. Energy Efficient UV-LED Source and TiO_2 Nanotube Array-Based Reactor for

Photocatalytic Application. Industrial & Engineering Chemistry Research. 2011; 50:7753.

124. Ishibashi K, Fujishima A, Watanabe T, Hashimoto K. Quantum yields of active oxidative species formed on TiO_2 photocatalyst. Journal of Photochemistry and Photobiology A. 2000; 134:139-142.

125. Carraway ER, Hoffman AJ, Hoffmann MR. Photocatalytic oxidation of organic acids on quantum-sized semiconductor colloids. Environmental Science and Technology. 1994; 28:786–793.

126. Mao Y, Schoeneich C, Asmus KD. Identification of organic acids and other intermediates in oxidative degradation of chlorinated ethanes on titania surfaces en route to mineralization: A combined photocatalytic and radiation chemical study. Journal of Physical Chemistry. 1991; 95:10080–10089.

127. Ge M, Guo C, Zhu X. Photocatalytic degradation of methyl orange using ZnO/TiO_2 composites. Frontiers of Environmental Science & Engineering in China. 2009; 3:271-280.

128. Prevot AB, Basso A, Baiocchi C. Analytical control of photocatalytic treatments: Degradation of a sulfonated azo dye. Analytical and bioanalytical chemistry. 2004; 378:214-220.

129. Bahnemann W, Muneer M, Haque M. Titanium dioxide-mediated photocatalysed degradation of few selected organic pollutants in aqueous suspensions. Catalysis Today. 2007; 124:133-148.

130. Gude K, Gun'ko VM, Blitz JP. Adsorption and photocatalytic decomposition of methylene blue on surface modified silica and silica-titania. Colloids and Surfaces A: Physicochemical and Engineering Aspects. 2008; 325:17-20.

131. Akpan UG, Hameed BH. Parameters affecting the photocatalytic degradation of dyes using TiO_2-based photocatalysts: A review. Journal of Hazardous Materials. 2009; 170:520-529.

132. Li S, Cai S, Zheng F. Self assembled TiO_2 with 5-sulfosalicylic acid for improvement its surface properties and photodegradation activity of dye. Dyes and Pigments. 2012; 95:188-193.

133. Gratzel M. Heterogeneous Photochemical Electron Transfer. Boca Raton, FL: CRC Press, 1989.

134. Brett CA, Oliveira-Brett AM. Electrochemistry: Principles, Methods and Applications. London: Oxford University Press, 1993.

135. Szczepankiewicz SH, Moss JA, Hoffmann MR. Electron traps and the stark effect on hydroxylated titania photocatalysts. Journal of Physical Chemistry B. 2002; 106:7654–7658.

136. Lawless D, Serpone N, Meisel D. Role of hydroxyl radicals and trapped holes in photocatalysis. A pulse radiolysis study. Journal of Physical Chemistry. 1991; 95:5166–5170.

137. Serpone N, Lawless D, Khairutdinov R. Subnanosecond relaxation dynamics in TiO_2 colloidal sols (particle sizes rp = 1.0-13.4 nm). relevance to heterogeneous photocatalysis. Journal of Physical Chemistry. 1995; 99:16655-16661.

138. Tunesi S, Anderson M. Influence of chemisorption on the photodecomposition of salicylic acid and related compounds using suspended titania ceramic membranes. Journal of Physical Chemistry. 1991; 95:3399.

139. Tang WZ, Huang CP. Photocatalyzed oxidation pathways of 2,4-dichlorophenol by CdS in basic and acidic aqueous solutions. Water Research. 1995; 29:745-756.

140. Interaction of hydrogen atoms and hydroxyl radicals with 5-halogen uracils. Proceedings of the National Academy of Sciences of the United States of America, 1966.

141. Moser J, Punchihewa S, Infelta PP, Graetzel M. Surface complexation of colloidal semiconductors strongly enhances interfacial electron-transfer rates. Langmuir. 1991; 7:3012-3018.

142. Robertson PKJ, Lawton LA, Munch B, Rouzade J. Destruction of cyanobacterial toxins by semiconductor photocatalysis. Chemical Communications. 1997; :393-394.

143. Ollis DF. Kinetics of liquid phase photocatalyzed reactions: An illuminating approach. The Journal of Physical Chemistry B. 2005; 109:2439-2444.

144. Xu Y, Langford CH. Variation of langmuir adsorption constant determined for TiO_2-photocatalyzed degradation of acetophenone under different light intensity. Journal of Photochemistry and Photobiology A. 2000; 133:67-71.

145. Emeline AV, Ryabchuk V, Serpone N. Factors affecting the efficiency of a photocatalyzed process in aqueous metal-oxide dispersions: Prospect of distinguishing between two kinetic models. Journal of Photochemistry and Photobiology A. 2000; 133:89-97.

146. Smith YR, Kar A, Subramanian V. Investigation of physicochemical parameters that influence photocatalytic degradation of methyl orange over TiO_2 nanotubes. Industrial & Engineering Chemistry Research. 2009; 48:10268-10276.

147. Emeline A, Rudakova A, Ryabchuk V, Serpone N. Photostimulated reactions at the surface of wide band-gap metal oxides (ZrO_2 and TiO_2): Interdependence of rates of reactions on pressure-

concentration and on light intensity. The Journal of Physical Chemistry B. 1998; 102:10906-10916.

148. Salinaro A, Emeline AV, Zhao J, Hidaka H, Ryabchuk VK, Serpone N. Terminology, relative photonic efficiencies and quantum yields in heterogeneous photocatalysis. part II: Experimental determination of quantum yields. Pure and applied chemistry. 1999; 71:321-335.

149. Bouchy M, Zahraa O. Photocatalytic reactors. International Journal of Photoenergy. 2003; 5:191-197.

150. Shan AY, Ghazi TIM, Rashid SA. Immobilisation of titanium dioxide onto supporting materials in heterogeneous photocatalysis: A review. Applied Catalysis A: General. 2010; 389:1-8.

151. Liou P, Chen S, Wu JC. Photocatalytic CO_2 reduction using an internally illuminated monolith photoreactor. Energy & Environmental Science. 2011; 4:1487-1494.

152. Sauer ML, Hale MA, Ollis DF. Heterogenous photocatalytic oxidation of dilute toluene-chlorocarbon mixtures in air. Journal of Photochemistry and Photobiology A. 1995; 88:169-178.

153. Paschoalino M, Jardim W. Indoor air disinfection using a polyester supported TiO_2 photo-reactor. Indoor Air. 2008; 18:473-479.

154. Prieto O, Fermoso J, Irusta R. Photocatalytic degradation of toluene in air using a fluidized bed photoreactor. International Journal of Photoenergy. 2007; 2007.

155. Peill NJ, Hoffmann MR. Development and optimization of a TiO_2-coated fiber-optic cable reactor: Photocatalytic degradation of 4-chlorophenol. Environmental Science and Technology. 1995; 29:2974-2981.

156. Ray AK, Beenackers AA. Development of a new photocatalytic reactor for water purification. Catalysis Today. 1998; 40:73-83.

157. Ranade V, V. Computational Flow Modeling for Chemical Reactor Engineering. California: Academic Press, 2002.

158. Esteban Duran J, Taghipour F, Mohseni M. CFD modeling of mass transfer in annular reactors. International Journal of Heat and Mass Transfer. 2009; 52:5390-5401.

159. Nallasamy M. Turbulence models and their applications to the prediction of internal flows: A review. Computers & Fluids. 1987; 15:151-194.

160. Ansys Fluent 12.0 Theory Guide. RNG κ- ε model 2009.

161. Ansys Fluent 12.0 Theory Guide. Single Rotating Reference Frame (SRF) Modeling 2009.

162. Turchi CS, Ollis DF. Comment. photocatalytic reactor design: An example of mass-transfer limitations with an immobilized catalyst. Journal of Physical Chemistry. 1988; 92:6852-6853.

163. Chang HT, Wu N, Zhu F. A kinetic model for photocatalytic degradation of organic contaminants in a thin-film TiO_2 catalyst. Water Research. 2000; 34:407-416.

164. Alphonse P, Varghese A, Tendero C. Stable hydrosols for TiO_2 coatings. Journal of Sol-Gel Science and Technology. 2010; 56:250-263.

165. Yoldas BE. Hydrolysis of titanium alkoxide and effects of hydrolytic polycondensation parameters. Journal of Materials Science. 1986; 21:1087-1092.

166. Oskam G, Nellore A, Penn RL, Searson PC. The growth kinetics of TiO_2 nanoparticles from titanium(IV) alkoxide at high Water/Titanium ratio. Journal of Physical Chemistry B. 2003; 107:1734–1738.

167. Vorkapic D, Matsoukas T. Reversible agglomeration: A kinetic model for the peptization of titania nanocolloids. Journal of Colloid and Interface Science. 1999; 214:283-291.

168. Isley SL, Lee Penn R. Relative brookite and anatase content in sol-gel-synthesized titanium dioxide nanoparticles. Journal of Physical Chemistry B. 2006; 110:15134–15139.

169. Valtierra J, Cardenas M, Reyes C, Calixto S. Formation of smooth and rough TiO_2 thin films on fiberglass by sol-gel method. Journal of Mexican Chemical Society. 2006; 50:8-13.

170. Brinker CJ, hurd AJ. Fundamentals of sol-gel dip-coating. Journal de Physique III France. 1994; 4:1231-1242.

171. Alam MJ, Cameron DC. Preparation and characterization of TiO_2 thin films by sol-gel method. Journal of Sol-Gel Science and Technology. 2002; 25:137–145.

172. Huang J, Liu Y, Lu L, Li L. The photocatalytic properties of amorphous TiO_2 composite films deposited by magnetron sputtering. Research on Chemical Intermediates. 2012; 38:487-498.

173. The Intelligent Ink and Pen Company. RZ PhotoCat pen 2010.

174. Flitney B. Which elastomer seal materials are suitable for use in biofuels? Sealing Technology. 2007; 2007:8-11.

175. Halmann MM. Photo Degradation of Water Pollutants. CRC Press, 1996.

176. d'Hennezel O, Pichat P, Ollis DF. Benzene and toluene gas-phase photocatalytic degradation over H_2O and HCL pretreated TiO_2: By-products and mechanisms. Journal of Photochemistry and Photobiology A. 1998; 118:197-204.

177. Bianchi CL, Gatto S, Pirola C. Photocatalytic degradation of acetone, acetaldehyde and toluene in gas-phase: Comparison between nano and micro-sized TiO_2. Applied Catalysis B: Environmental. 2014; 146:123-130.

178. Nakajima A, Obata H, Kameshima Y, Okada K. Photocatalytic destruction of gaseous toluene by sulfated TiO_2 powder. Catalysis Communications. 2005; 6:716-720.

179. Piera E, Ayllón JA, Doménech X, Peral J. TiO_2 deactivation during gas-phase photocatalytic oxidation of ethanol. Catalysis Today. 2002; 76:259-270.

180. González-Garcıa N, Ayllón JA, Doménech X, Peral J. TiO_2 deactivation during the gas-phase photocatalytic oxidation of dimethyl sulfide. Applied Catalysis B: Environmental. 2004; 52:69-77.

181. Carneiro JT, Moulijn JA, Mul G. Photocatalytic oxidation of cyclohexane by titanium dioxide: Catalyst deactivation and regeneration. Journal of Catalysis. 2010; 273:199-210.

182. Ray AK, Beenackers AA. Novel photocatalytic reactor for water purification. AIChE J. 1998; 44:477-483.

183. Ardizzone S, Bianchi C, Cappelletti G, Naldoni A, Pirola C. Photocatalytic degradation of toluene in the gas phase: Relationship between surface species and catalyst features. Environmental Science and Technology. 2008; 42:6671-6676.

184. Clark MM. Transport Modeling for Environmental Engineers and Scientists. John Wiley & Sons, 2012.

185. Gorges R, Meyer S, Kreisel G. Photocatalysis in microreactors. Journal of Photochemistry and Photobiology A. 2004; 167:95-99.

186. Lewis NS. Progress in understanding electron-transfer reactions at semiconductor/liquid interfaces. The Journal of Physical Chemistry B. 1998; 102:4843-4855.

187. Mehrvar M, Anderson WA, Moo-Young M, Reilly PM. Non-linear parameter estimation for a dynamic model in photocatalytic reaction engineering. Chemical Engineering Science. 2000; 55:4885-4891.

APPENDIX A

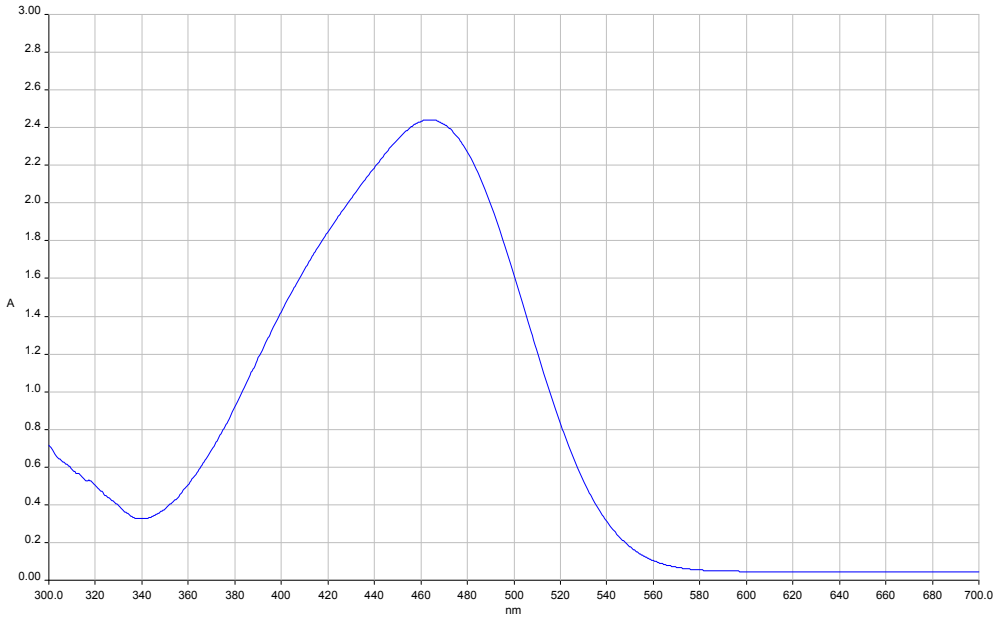

A.1: Methyl orange UV/Vis absorption spectra with a peak at 462 nm

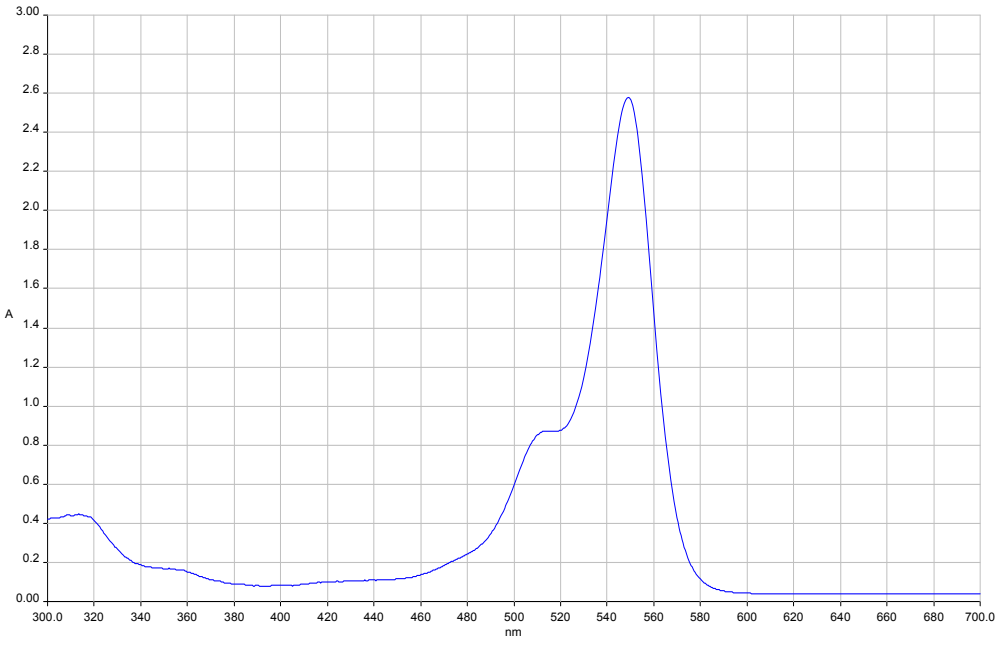

A.2: Rose bengal UV/Vis absorption spectra with peak at 548 nm.

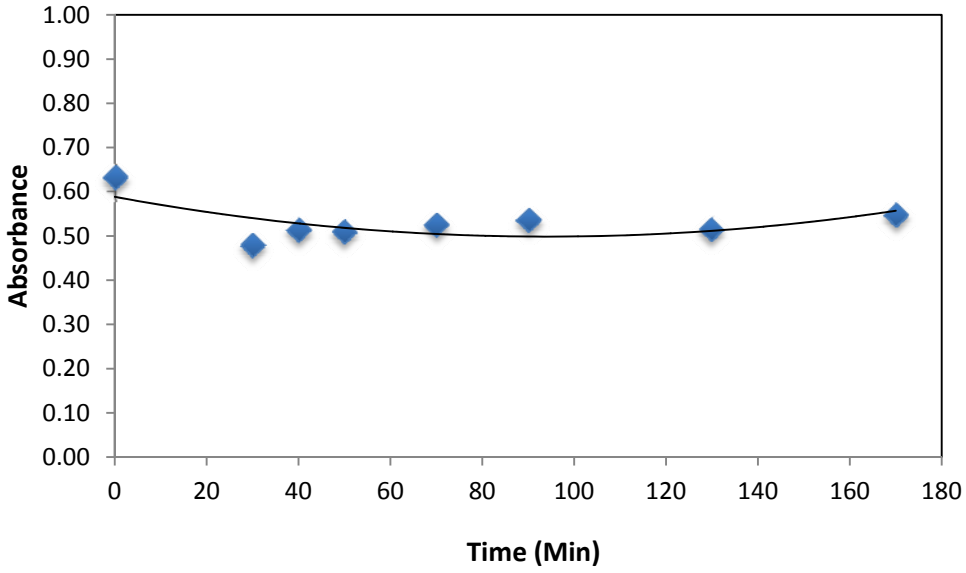

A.3: TiO_2 control experiment for methyl orange

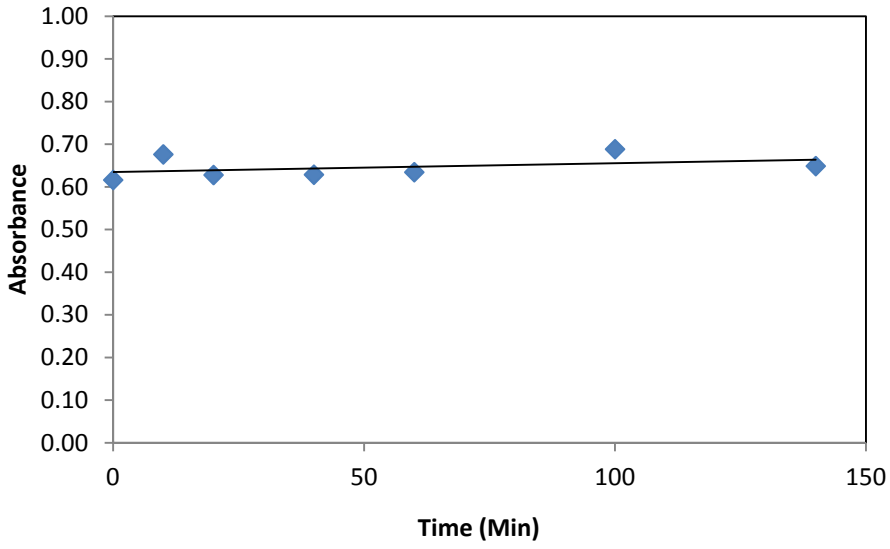

A.4: Ultra Violet (UV) illumination control experiment for methyl orange

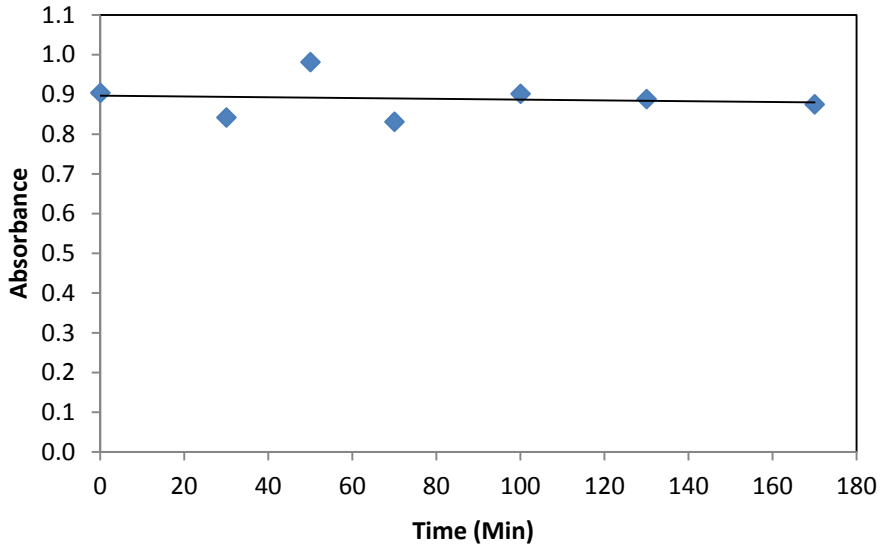

A.5: TiO_2 control experiment for rose bengal.

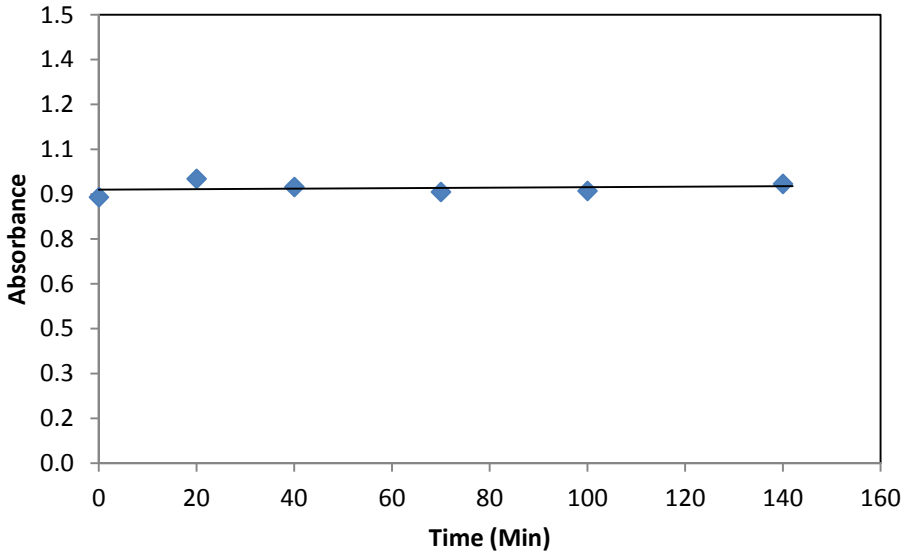

A.6: Ultra Violet (UV) control for rose bengal dye

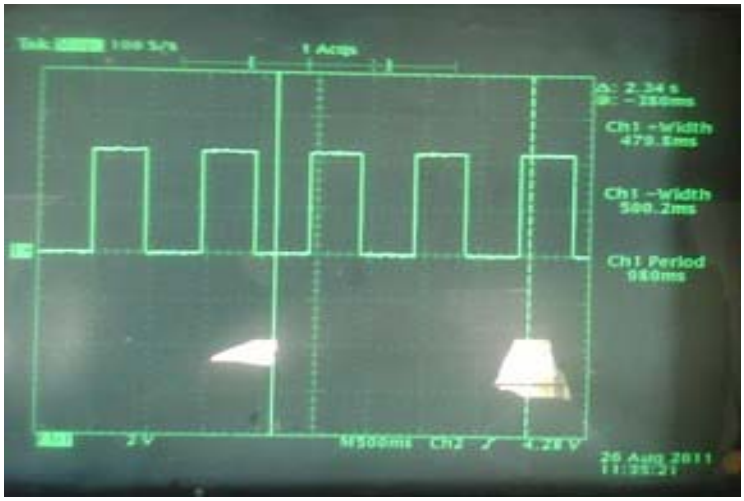

A.7: Oscilloscope generated square wave showing T_{on} and T_{off}

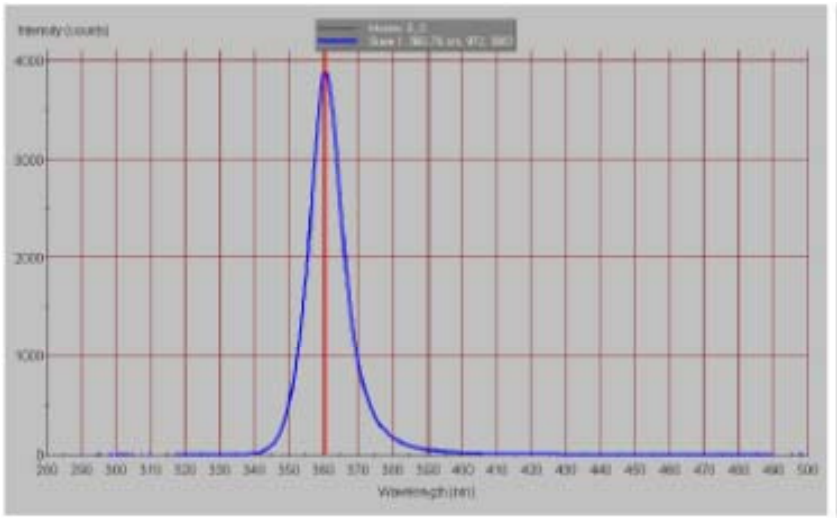

A.8: Emission spectra of FoxUV™ LEDs from the manufacturer.

APPENDIX B

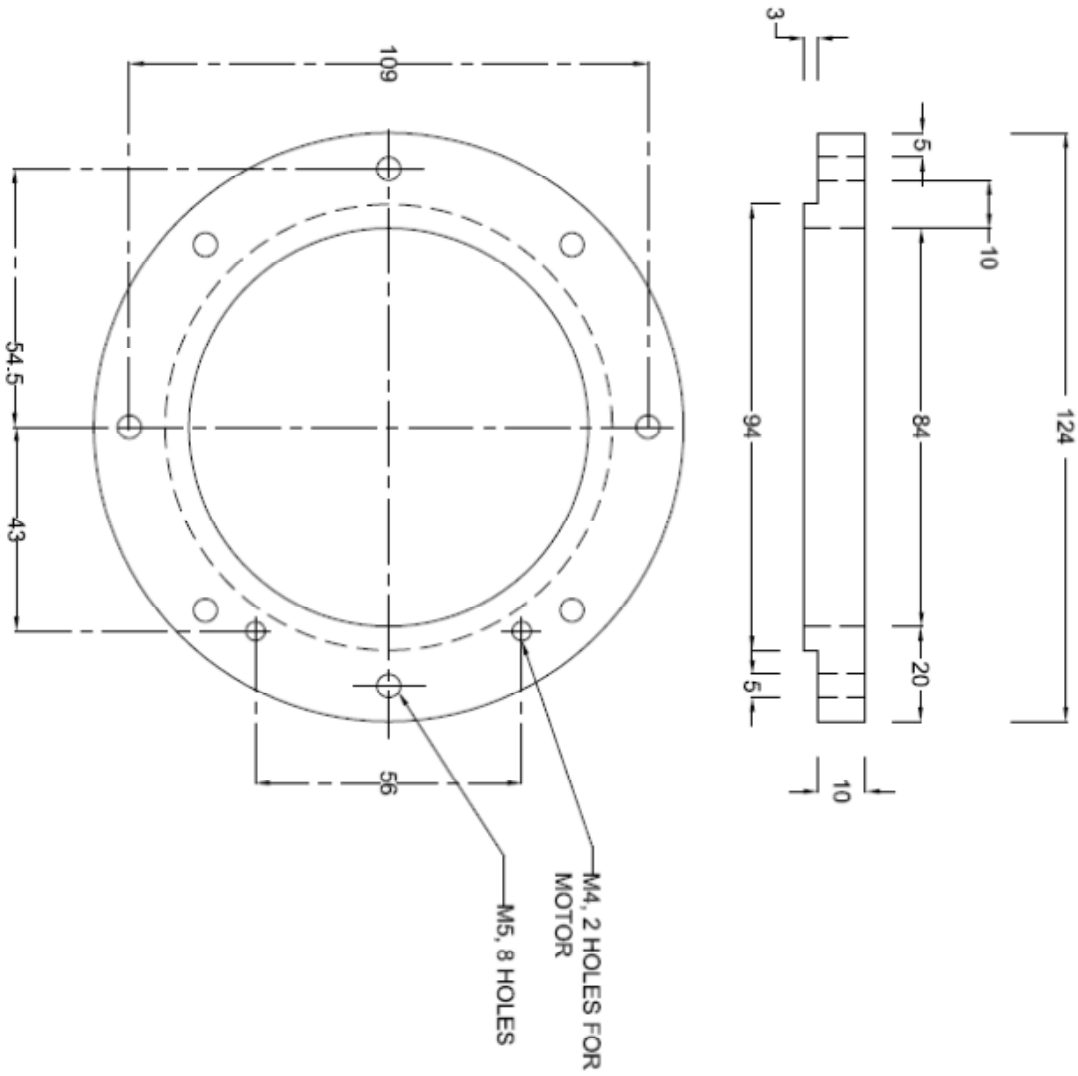

B.1: Assembly plates.

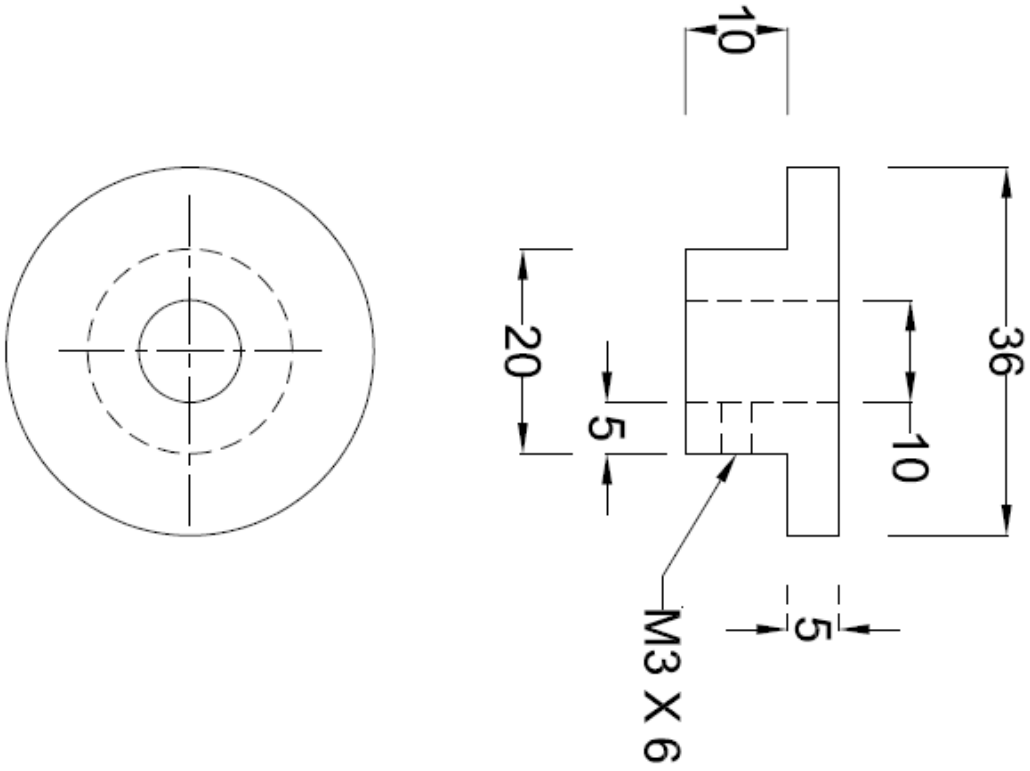

B.2: Impeller disc.

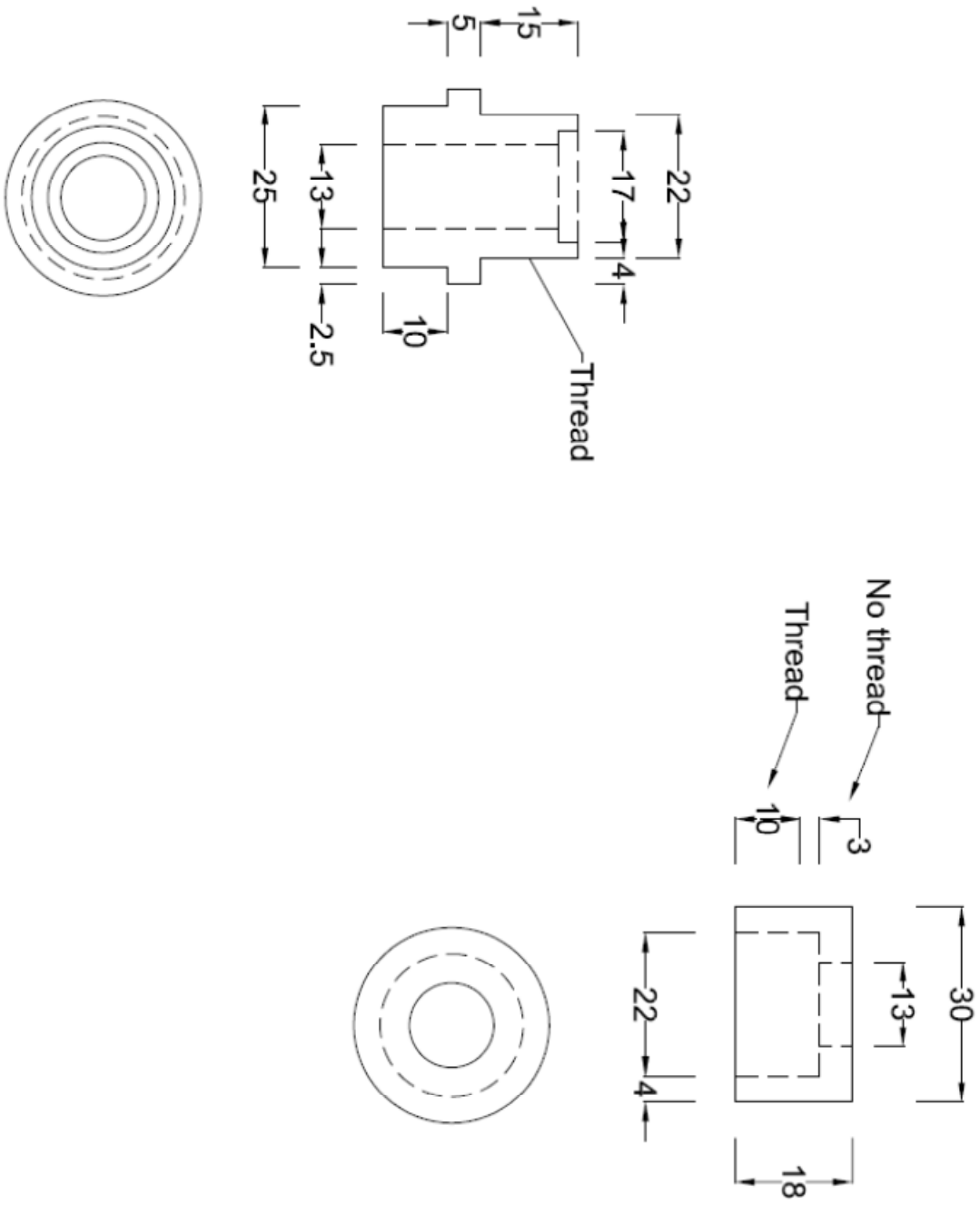

B.3: Sampling port.

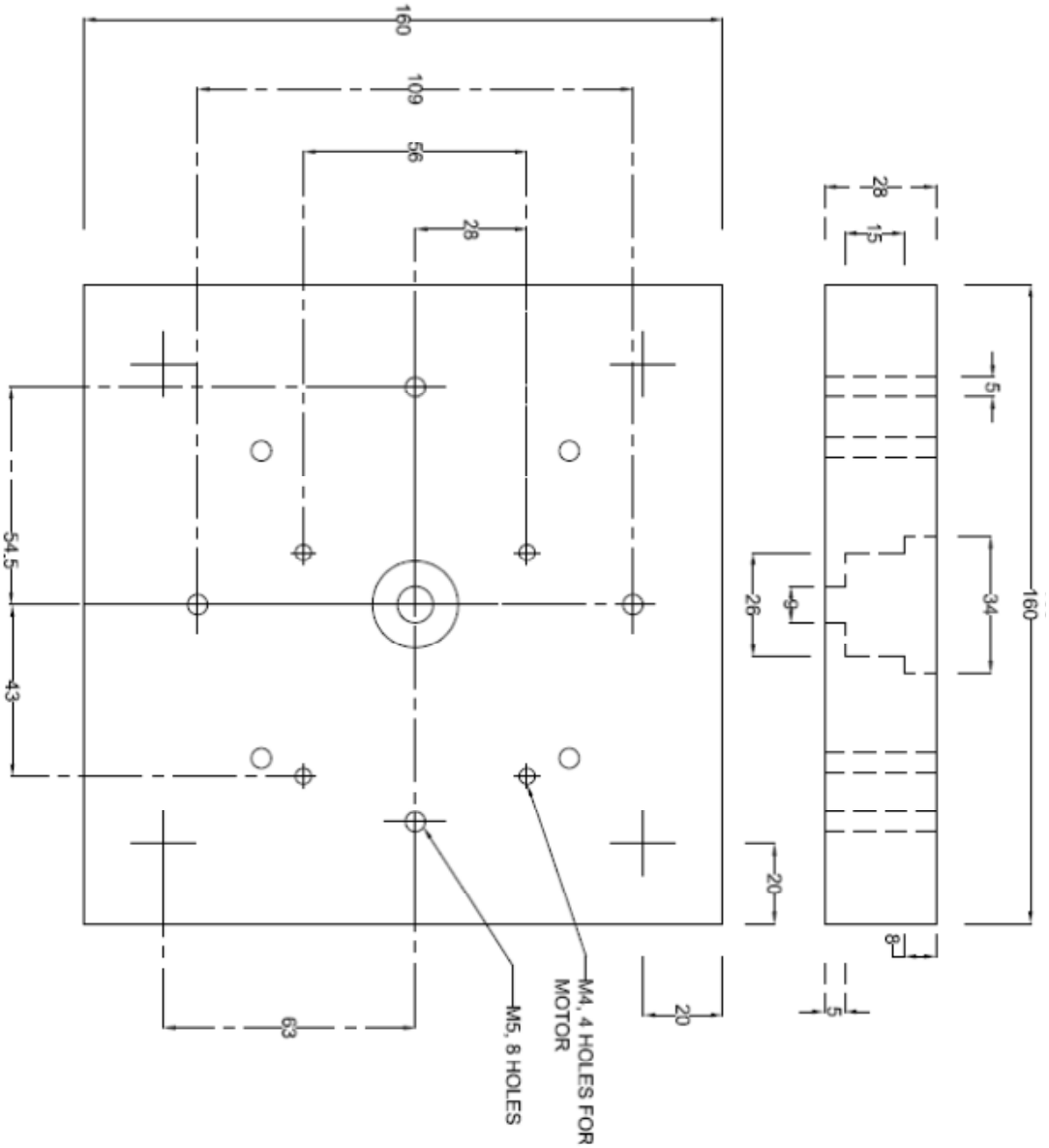

B.4: Bottom cover.

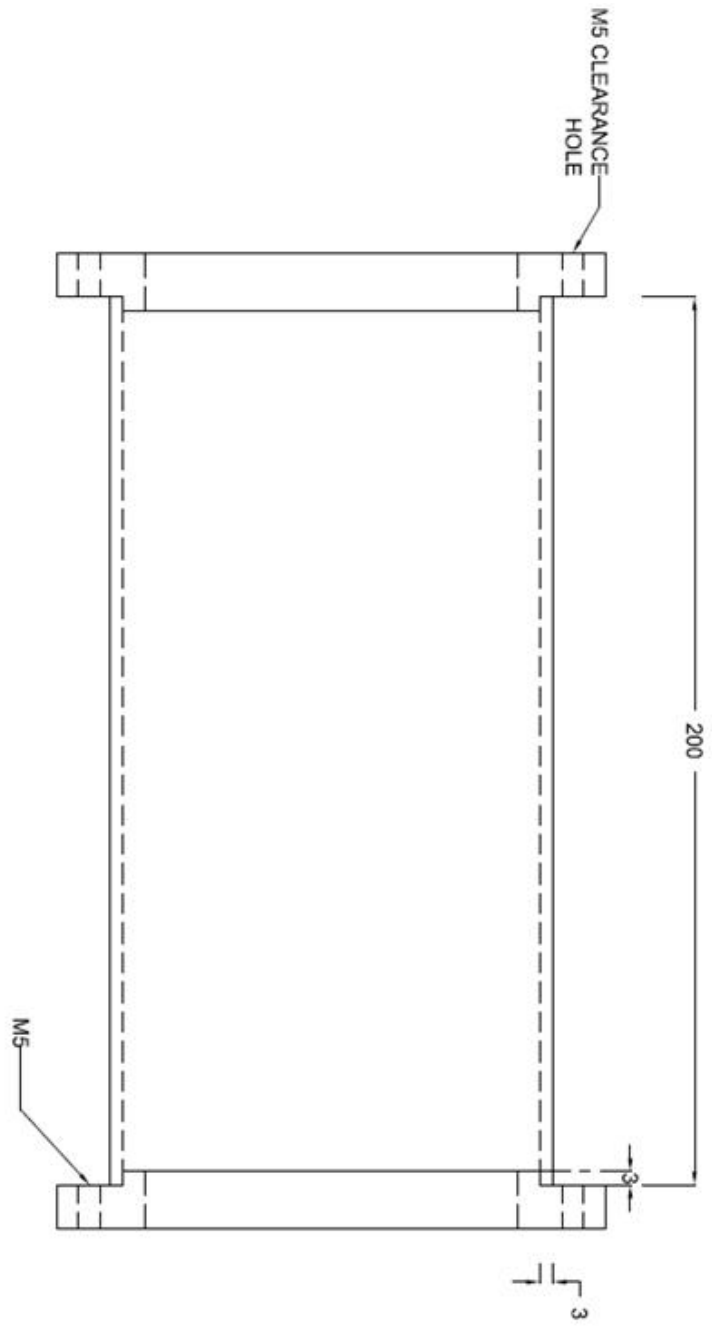

B.5: Subassembly.

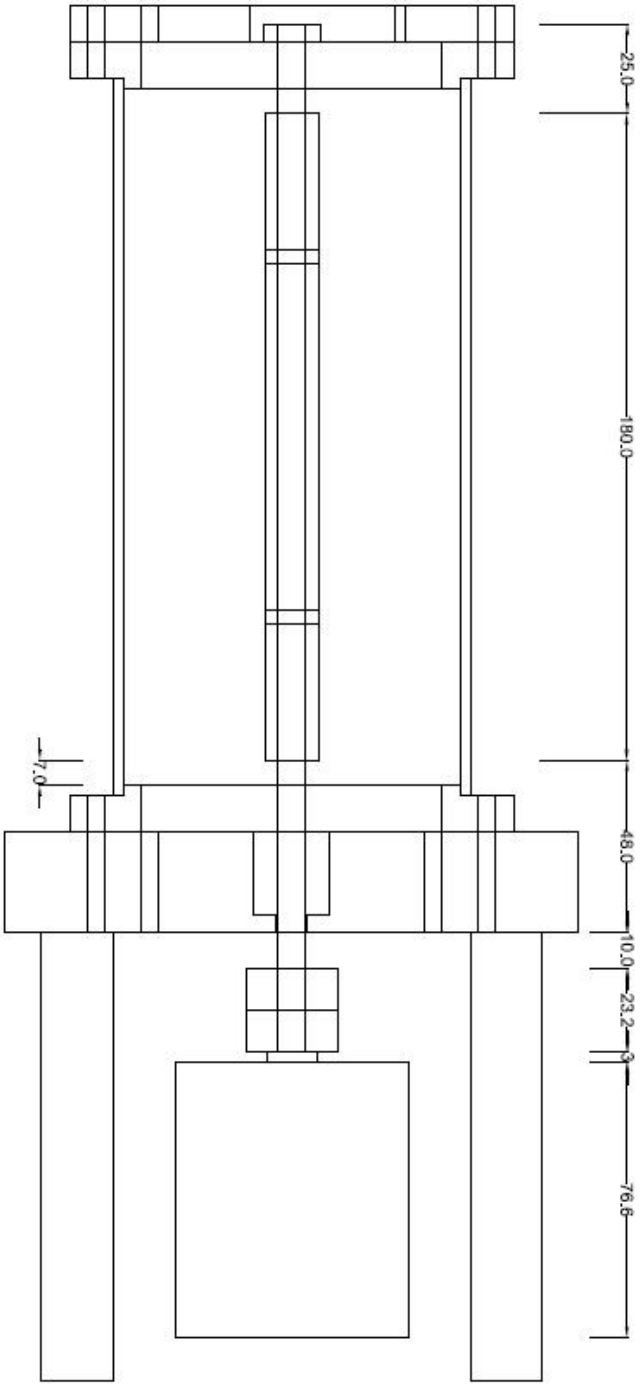

B.6: Assembly.

APPENDIX C

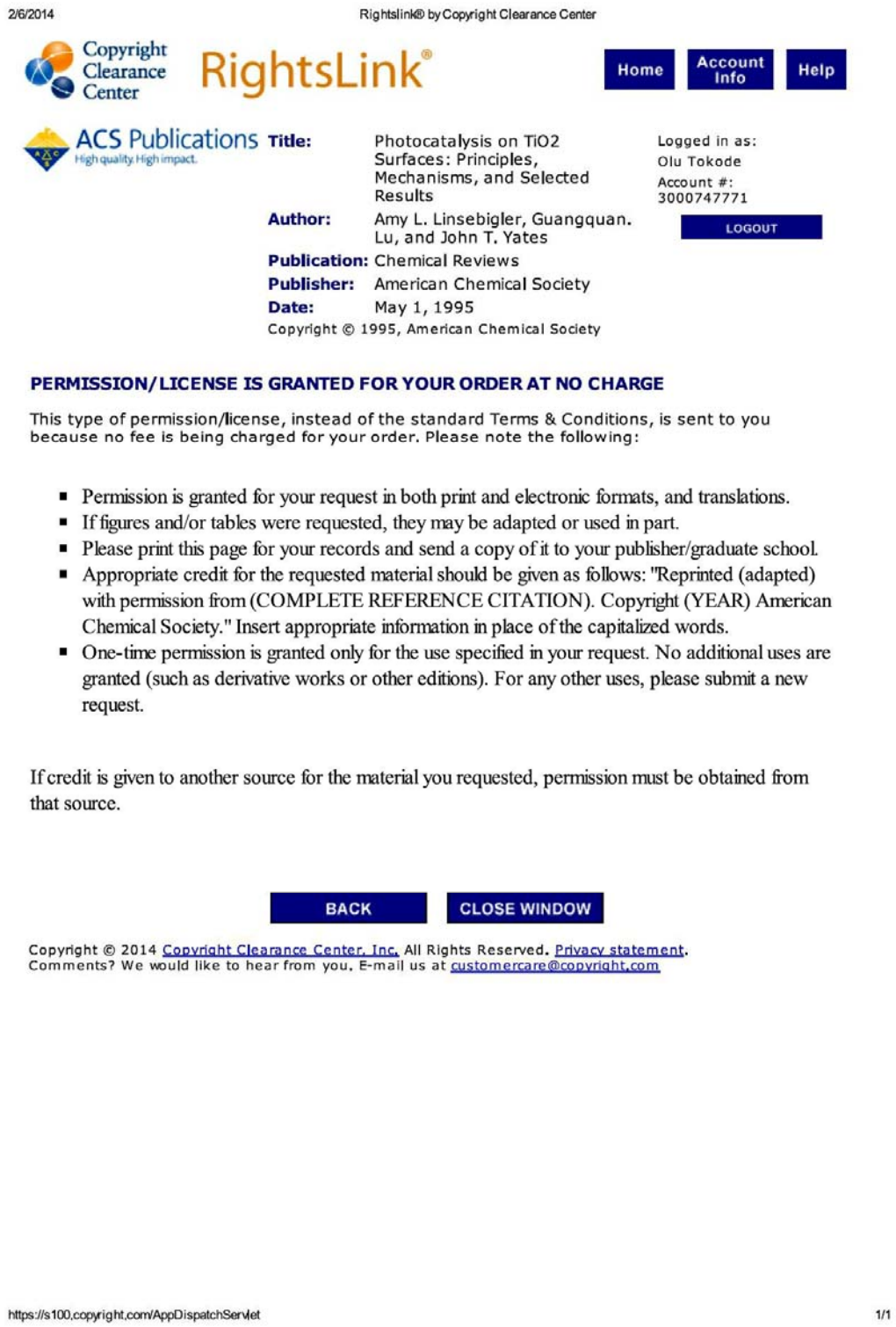

2/6/2014 Rightslink® by Copyright Clearance Center

Copyright Clearance Center RightsLink®

Home | Account Info | Help

ACS Publications High quality. High impact.

Title: Photocatalysis on TiO2 Surfaces: Principles, Mechanisms, and Selected Results

Author: Amy L. Linsebigler, Guangquan. Lu, and John T. Yates

Publication: Chemical Reviews

Publisher: American Chemical Society

Date: May 1, 1995

Copyright © 1995, American Chemical Society

Logged in as: Olu Tokode
Account #: 3000747771

LOGOUT

PERMISSION/LICENSE IS GRANTED FOR YOUR ORDER AT NO CHARGE

This type of permission/license, instead of the standard Terms & Conditions, is sent to you because no fee is being charged for your order. Please note the following:

- Permission is granted for your request in both print and electronic formats, and translations.
- If figures and/or tables were requested, they may be adapted or used in part.
- Please print this page for your records and send a copy of it to your publisher/graduate school.
- Appropriate credit for the requested material should be given as follows: "Reprinted (adapted) with permission from (COMPLETE REFERENCE CITATION). Copyright (YEAR) American Chemical Society." Insert appropriate information in place of the capitalized words.
- One-time permission is granted only for the use specified in your request. No additional uses are granted (such as derivative works or other editions). For any other uses, please submit a new request.

If credit is given to another source for the material you requested, permission must be obtained from that source.

BACK | CLOSE WINDOW

Copyright © 2014 Copyright Clearance Center, Inc. All Rights Reserved. Privacy statement.
Comments? We would like to hear from you. E-mail us at customercare@copyright.com

https://s100.copyright.com/AppDispatchServlet 1/1

C.1: Permission/License for figures 1.4 and 1.5a

RightsLink®

Home | Account Info | Help

Chapter: Photocatalytic Treatment of Air: From Basic Aspects to Reactors
Book: Advances in Chemical Engineering, Volume 36
Author: Yaron Paz
Publisher: Elsevier
Date: 2009
Copyright © 2009, Elsevier

Logged in as:
Olu Tokode
LOGOUT

Order Completed

Thank you very much for your order.

This is a License Agreement between Olu Tokode ("You") and Elsevier ("Elsevier"). The license consists of your order details, the terms and conditions provided by Elsevier, and the payment terms and conditions.

Get the printable license.

License Number	3323091271758
License date	Feb 06, 2014
Licensed content publisher	Elsevier
Licensed content publication	Elsevier Books
Licensed content title	Advances in Chemical Engineering, Volume 36
Licensed content author	Yaron Paz
Licensed content date	2009
Number of pages	48
Type of Use	reuse in a thesis/dissertation
Portion	figures/tables/illustrations
Number of figures/tables/illustrations	3
Format	both print and electronic
Are you the author of this Elsevier chapter?	No
Will you be translating?	No
Title of your thesis/dissertation	Photocatalytic destruction of volatile organic compounds from the oil and gas industry
Expected completion date	Jul 2014
Estimated size (number of pages)	156
Elsevier VAT number	GB 494 6272 12
Permissions price	0.00 GBP
VAT/Local Sales Tax	0.00 GBP / 0.00 GBP
Total	0.00 GBP

ORDER MORE... CLOSE WINDOW

C.2: Permission/License for figures 1.3 and 1.7.

Copyright Clearance Center RightsLink®

Home | Account Info | Help

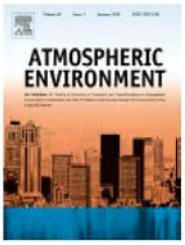

Title: Photocatalytic purification of volatile organic compounds in indoor air: A literature review

Author: Jinhan Mo,Yinping Zhang,Qiujian Xu,Jennifer Joaquin Lamson,Rongyi Zhao

Publication: Atmospheric Environment

Publisher: Elsevier

Date: May 2009

Logged in as:
Olu Tokode

LOGOUT

Order Completed

Thank you very much for your order.

This is a License Agreement between Olu Tokode ("You") and Elsevier ("Elsevier"). The license consists of your order details, the terms and conditions provided by Elsevier, and the payment terms and conditions.

Get the printable license.

License Number	3323100941724
License date	Feb 06, 2014
Licensed content publisher	Elsevier
Licensed content publication	Atmospheric Environment
Licensed content title	Photocatalytic purification of volatile organic compounds in indoor air: A literature review
Licensed content author	Jinhan Mo,Yinping Zhang,Qiujian Xu,Jennifer Joaquin Lamson,Rongyi Zhao
Licensed content date	May 2009
Licensed content volume number	43
Licensed content issue number	14
Number of pages	18
Type of Use	reuse in a thesis/dissertation
Portion	figures/tables/illustrations
Number of figures/tables/illustrations	2
Format	both print and electronic
Are you the author of this Elsevier article?	No
Will you be translating?	No
Title of your thesis/dissertation	Photocatalytic destruction of volatile organic compounds from the oil and gas industry
Expected completion date	Jul 2014
Estimated size (number of pages)	156
Elsevier VAT number	GB 494 6272 12
Permissions price	0.00 GBP
VAT/Local Sales Tax	0.00 GBP / 0.00 GBP
Total	0.00 GBP

ORDER MORE... CLOSE WINDOW

C.3: Permission/License for figures 1.6b and 1.8.

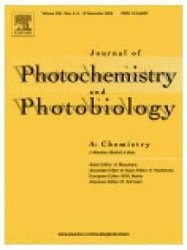

Title:	Evidence of critical illumination and dark recovery times for increasing the photoefficiency of aqueous heterogeneous photocatalysis
Author:	Jeffrey G. Sczechowski,Carl A. Koval,Richard D. Noble
Publication:	Journal of Photochemistry and Photobiology A: Chemistry
Publisher:	Elsevier
Date:	September 1993

Order Completed

Thank you very much for your order.

This is a License Agreement between Olu Tokode ("You") and Elsevier ("Elsevier"). The license consists of your order details, the terms and conditions provided by Elsevier, and the payment terms and conditions.

Get the printable license.

License Number	3323150108334
License date	Feb 06, 2014
Licensed content publisher	Elsevier
Licensed content publication	Journal of Photochemistry and Photobiology A: Chemistry
Licensed content title	Evidence of critical illumination and dark recovery times for increasing the photoefficiency of aqueous heterogeneous photocatalysis
Licensed content author	Jeffrey G. Sczechowski,Carl A. Koval,Richard D. Noble
Licensed content date	September 1993
Licensed content volume number	74
Licensed content issue number	2–3
Number of pages	6
Type of Use	reuse in a thesis/dissertation
Portion	figures/tables/illustrations
Number of figures/tables/illustrations	1
Format	both print and electronic
Are you the author of this Elsevier article?	No
Will you be translating?	No
Title of your thesis/dissertation	Photocatalytic destruction of volatile organic compounds from the oil and gas industry
Expected completion date	Jul 2014
Estimated size (number of pages)	156
Elsevier VAT number	GB 494 6272 12
Permissions price	0.00 GBP
VAT/Local Sales Tax	0.00 GBP / 0.00 GBP
Total	0.00 GBP

ORDER MORE... CLOSE WINDOW

C.4: Permission/License for figure 2.2.

Copyright Clearance Center RightsLink®

Home | Account Info | Help

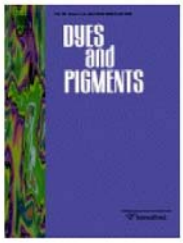

Title: Sulfanilic acid-modified P25 TiO2nanoparticles with improved photocatalytic degradation on Congo red under visible light

Author: Hong-xu Guo,Kai-li Lin,Zi-shan Zheng,Fei-bin Xiao,Shun-xing Li

Publication: Dyes and Pigments

Publisher: Elsevier

Date: March 2012

Logged in as:
Olu Tokode
Account #:
3000747771

LOGOUT

Order Completed

Thank you very much for your order.

This is a License Agreement between Olu Tokode ("You") and Elsevier ("Elsevier"). The license consists of your order details, the terms and conditions provided by Elsevier, and the payment terms and conditions.

Get the printable license.

License Number	3323170488169
License date	Feb 06, 2014
Licensed content publisher	Elsevier
Licensed content publication	Dyes and Pigments
Licensed content title	Sulfanilic acid-modified P25 TiO2nanoparticles with improved photocatalytic degradation on Congo red under visible light
Licensed content author	Hong-xu Guo,Kai-li Lin,Zi-shan Zheng,Fei-bin Xiao,Shun-xing Li
Licensed content date	March 2012
Licensed content volume number	92
Licensed content issue number	3
Number of pages	7
Type of Use	reuse in a thesis/dissertation
Portion	figures/tables/illustrations
Number of figures/tables/illustrations	1
Format	both print and electronic
Are you the author of this Elsevier article?	No
Will you be translating?	No
Title of your thesis/dissertation	Photocatalytic destruction of volatile organic compounds from the oil and gas industry
Expected completion date	Jul 2014
Estimated size (number of pages)	156
Elsevier VAT number	GB 494 6272 12
Permissions price	0.00 GBP
VAT/Local Sales Tax	0.00 GBP / 0.00 GBP
Total	0.00 GBP

ORDER MORE... CLOSE WINDOW

C.5: Permission/License for figure 3.1.

Copyright Clearance Center RightsLink®

Home | Account Info | Help

Title: Photodecomposition ofo-cresol by UV-LED/TiO2process with controlled periodic illumination
Author: Hua-Wei Chen,Young Ku,Agus Irawan
Publication: Chemosphere
Publisher: Elsevier
Date: September 2007
Copyright © 2007, Elsevier

Logged in as:
Olu Tokode
Account #:
3000747771
LOGOUT

Order Completed

Thank you very much for your order.

This is a License Agreement between Olu Tokode ("You") and Elsevier ("Elsevier"). The license consists of your order details, the terms and conditions provided by Elsevier, and the payment terms and conditions.

Get the printable license.

License Number	3323170951151
License date	Feb 06, 2014
Licensed content publisher	Elsevier
Licensed content publication	Chemosphere
Licensed content title	Photodecomposition ofo-cresol by UV-LED/TiO2process with controlled periodic illumination
Licensed content author	Hua-Wei Chen,Young Ku,Agus Irawan
Licensed content date	September 2007
Licensed content volume number	69
Licensed content issue number	2
Number of pages	7
Type of Use	reuse in a thesis/dissertation
Portion	figures/tables/illustrations
Number of figures/tables/illustrations	1
Format	both print and electronic
Are you the author of this Elsevier article?	No
Will you be translating?	No
Title of your thesis/dissertation	Photocatalytic destruction of volatile organic compounds from the oil and gas industry
Expected completion date	Jul 2014
Estimated size (number of pages)	156
Elsevier VAT number	GB 494 6272 12
Permissions price	0.00 GBP
VAT/Local Sales Tax	0.00 GBP / 0.00 GBP
Total	0.00 GBP

ORDER MORE... CLOSE WINDOW

C.6: Permission/License for figure 3.2.

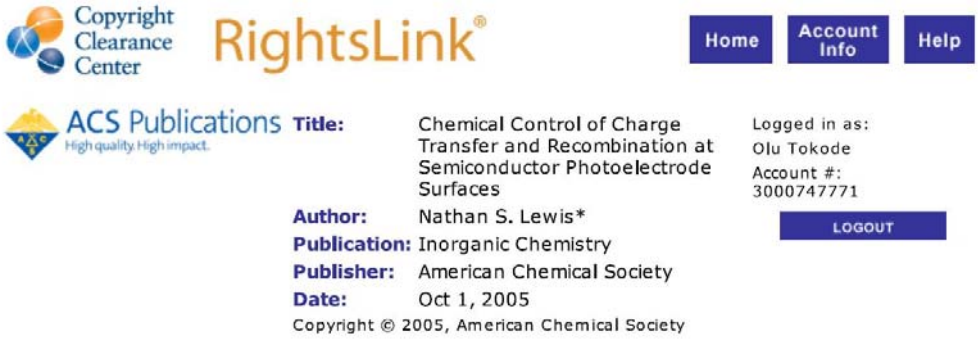

PERMISSION/LICENSE IS GRANTED FOR YOUR ORDER AT NO CHARGE

This type of permission/license, instead of the standard Terms & Conditions, is sent to you because no fee is being charged for your order. Please note the following:

- Permission is granted for your request in both print and electronic formats, and translations.
- If figures and/or tables were requested, they may be adapted or used in part.
- Please print this page for your records and send a copy of it to your publisher/graduate school.
- Appropriate credit for the requested material should be given as follows: "Reprinted (adapted) with permission from (COMPLETE REFERENCE CITATION). Copyright (YEAR) American Chemical Society." Insert appropriate information in place of the capitalized words.
- One-time permission is granted only for the use specified in your request. No additional uses are granted (such as derivative works or other editions). For any other uses, please submit a new request.

If credit is given to another source for the material you requested, permission must be obtained from that source.

BACK CLOSE WINDOW

C.7: Permission/License for figure 3.3.

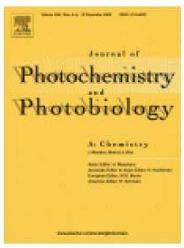

Title:	Benzene and toluene gas-phase photocatalytic degradation over H2O and HCL pretreated TiO2: by-products and mechanisms
Author:	Olga d'Hennezel,Pierre Pichat,David F Ollis
Publication:	Journal of Photochemistry and Photobiology A: Chemistry
Publisher:	Elsevier
Date:	13 November 1998

Order Completed

Thank you very much for your order.

This is a License Agreement between Olu Tokode ("You") and Elsevier ("Elsevier"). The license consists of your order details, the terms and conditions provided by Elsevier, and the payment terms and conditions.

Get the printable license.

License Number	3323200501673
License date	Feb 06, 2014
Licensed content publisher	Elsevier
Licensed content publication	Journal of Photochemistry and Photobiology A: Chemistry
Licensed content title	Benzene and toluene gas-phase photocatalytic degradation over H2O and HCL pretreated TiO2: by-products and mechanisms
Licensed content author	Olga d'Hennezel,Pierre Pichat,David F Ollis
Licensed content date	13 November 1998
Licensed content volume number	118
Licensed content issue number	3
Number of pages	8
Type of Use	reuse in a thesis/dissertation
Portion	figures/tables/illustrations
Number of figures/tables/illustrations	1
Format	both print and electronic
Are you the author of this Elsevier article?	No
Will you be translating?	No
Title of your thesis/dissertation	Photocatalytic destruction of volatile organic compounds from the oil and gas industry
Expected completion date	Jul 2014
Estimated size (number of pages)	156
Elsevier VAT number	GB 494 6272 12
Permissions price	0.00 GBP
VAT/Local Sales Tax	0.00 GBP / 0.00 GBP
Total	0.00 GBP

C.8: Permission/License for figure 4.18.

APPENDIX D

Effect of controlled periodic based illumination on the photonic efficiency of photocatalytic degradation of methyl orange

Oluwatosin I. Tokode, Radhakrishna Prabhu, Linda A Lawton and Peter K. J. Robertson.

Abstract

The use of controlled periodic illumination with UV-LEDs for enhancing photonic efficiency of photocatalytic decomposition processes in water has been investigated using methyl orange as a model compound. The impact of the length of light and dark time periods (T_{ON}/T_{OFF} times) on photo-degradation and photonic efficiency using a UV-LED illuminated photoreactor has been studied. The results have shown an inverse dependency of the photonic efficiency on duty cycle and a very little effect on T_{ON} or T_{OFF} time periods, indicating no effect of rate limiting steps through mass diffusion or adsorption/desorption in the reaction. For this reactor, the photonic efficiency under controlled periodic illumination (CPI) matches to that of continuous illumination, for the same average UV light intensities. Furthermore, under CPI conditions, the photonic efficiency is inversely related to the average UV light intensity in the reactor, in the millisecond time regime. This is the first study that has investigated the effect of controlled periodic illumination using UV-LED sources. The results not only enhances the understanding of the effect of periodic illumination on photocatalytic processes but also provides a greater insight to the potential of these light sources in photocatalytic reactions.

D.1: Abstract for journal paper published in *J. Catal.*

The effect of pH on the photonic efficiency of the destruction of methyl orange under controlled under periodic illumination with UV-LED sources

Oluwatosin Tokode, Radhakrishna Prabhu, Linda A Lawton and Peter K. J. Robertson.

Abstract

The nature of photon interaction and reaction pH can have significant impacts on semiconductor photocatalysis. This paper describes the effect of pH on the photonic efficiency of photocatalytic reactions in the aqueous phase using TiO_2 catalysts. The reactor was irradiated using periodic illumination with UV-LEDs through control of the illumination duty cycle (γ) through a series of light and dark times (T_{on}/T_{off}). Photonic efficiencies for methyl orange degradation were found to be comparable at high γ irrespective of pH. At lower γ, pH effects on photonic efficiency were very distinct across acidic, neutral and alkaline pH indicating an effect of complementary parameters. The results suggest photonic efficiency is greatest as illumination time, T_{on} approaches interfacial electron-transfer characteristic time which is within the range of this study or charge-carrier lifetimes upon extrapolation and also when electrostatic attraction between surface-trapped holes, $\{Ti^{IV}OH^{\bullet}\}^{+}_{ads}$ and substrate molecules is strongest.

D.2: Abstract for journal paper published in *Chem. Eng. J.*

Mathematical modelling of quantum yield enhancements of methyl orange photo-oxidation in aqueous TiO_2 suspensions under controlled periodic UV-LED illumination

Oluwatosin Tokode, Radhakrishna Prabhu, Linda A Lawton and Peter K. J. Robertson.

Abstract

Quantum yields of the photocatalytic degradation of methyl orange under Controlled Periodic Illumination (CPI) have been modelled using existing models. A modified Langmuir-Hinshelwood (L-H) rate equation was used to predict the degradation reaction rates of methyl orange at various duty cycles and a simple photocatalytic model was applied in modelling quantum yield enhancement of the photocatalytic process due to the CPI effect. A good agreement between the modelled and experimental data was achieved for quantum yield modelling while the limitations of the L-H model in predicting photocatalytic rates of periodically illuminated TiO_2 suspensions resulted in a divergent trend from the experimental data.

D.3: Abstract for journal paper published in *Appl. Catal. B*

A photocatalytic impeller reactor for gas phase heterogeneous photocatalysis

Oluwatosin Tokode, Radhakrishna Prabhu, Linda A Lawton and Peter K. J. Robertson.

Abstract

A novel photocatalytic reactor based on a stirred tank configuration has been described. This reactor employs the use of photocatalytic impellers to aid the mass transport of gaseous organic compounds during photocatalytic reactions. Experiments involving toluene vapour photo-oxidation showed the reactor configuration is susceptible to catalyst deactivation even at low concentrations if treated for prolonged periods. For this reactor, the reactive time scale exceeds the diffusive time scale hence, toluene photo-oxidation was mass reaction limited. The dependency of photonic efficiency of the reaction on mass transfer and catalyst deactivation was observed when correlated with the Damköhler number and deactivation induced reduction reaction rates respectively, the results show an inverse variation with Damköhler number and proportionality to reaction rates.

D.4: Abstract for journal paper submitted to *Environ. Sci. Technol.*

UV LED sources for heterogeneous photocatalysis

Oluwatosin Tokode, Radhakrishna Prabhu, Linda A. Lawton and Peter K. J. Robertson.

Abstract

This review presents an overview of the application of UV LED sources in heterogeneous photocatalysis within the context of artificial UV sources. The feasibility of UV LEDs as a source of UV irradiation in heterogeneous photocatalysis was first demonstrated almost a decade ago however, for the most part, photocatalytic experimental setups utilize artificial light sources in the form of conventional UV lamps to initiate the desired photocatalytic transformations. A look at all sources of UV irradiation used in heterogeneous photocatalysis is taken with a focus on the growing importance of solid state lighting devices such as UV LEDs. UV LEDs have higher external quantum efficiency, a lifetime of over 100000 hours, are small in size and produce directional UV light which can be of the desired wavelength. In recent times, these UV LED sources have become widely applied in several studies in the research literature and are fast becoming a viable alternative to conventional UV lamps.

D.5: Abstract for journal paper to be submitted to *Appl. Catal. B*